

Energy Performance of Buildings: Modeling of Dynamic Summer Behavior

Alessandro Prada



UNIVERSITÀ DEGLI STUDI DI TRENTO
Dipartimento di Ingegneria Civile
e Ambientale

2012

Doctoral thesis in **Environmental Engineering**, 24th cycle

Faculty of Engineering, **University of Trento**

Academic year 2011/2012

Supervisor: **Prof. Paolo Baggio**, **University of Trento**

University of Trento

Trento, Italy

31st January 2012

*"Cum autem omnium rerum simulatio vitiosa est,
tollit enim iudicium veri idque adulterat"*

*"E come poi la simulazione è in ogni cosa colpevole,
toglie difatti il discernimento del vero e lo adultera"*

(Cicero de Amictia).

Acknowledgements

First and foremost, I offer my gratitude to my supervisor, Prof. Paolo Baggio, for his warm encouragement and thoughtful guidance. I also owe my gratitude to Piercarlo, Marco and Andrea for inspiring me by the interesting discussions and conversations we had in the meetings. I also greatly appreciate the revisions suggested me by Prof. Anna Magrini.

During this work I have collaborated with Francesca and Giovanni for whom I have great regard, and I wish to extend my warmest thanks to all those who have helped me with my work.

A special acknowledgement goes to my office mates during these years Elisa, Maurizio and Daniele who have been supportive in every way.

In recognition of all your help and support, I would like to mention all the Doctoral School in Environmental Engineering and, in particular, the secretariat who has been very helpful throughout the three years.

Last but not least, a special thanks to Giulia for providing the support that made this work possible.

Contents

List of Figures	xiii
List of Tables	xv
List of Symbol	xx
Introduction	1
I Weather data for energy simulation	5
1 Evaluation of the Typical Reference Year for Italian cities	7
1.1 Introduction	7
1.2 Weather data sources for Italian cities	8
1.3 Literature Review	10
1.4 Raw Data Analysis	12
1.5 Procedure	16
1.6 Results	19
1.7 Comparison with other Italian weather sources	23
1.8 Summarizing	26
2 Solar radiation models	29
2.1 Decomposition models	29
2.2 Projection models	33
2.3 Experimental activity	35
2.4 Results and comparison	36
2.4.1 Statistical indicators	37
2.4.2 Enhanced Statistical indicators	40
2.5 Several parameters influence on model deviations	45

2.5.1	Sky condition effects	45
2.5.2	Season effects	46
2.6	Summarizing	47
3	Sensitivity of cooling demand to weather data	49
3.1	Test Cases	50
3.2	Dynamic simulation	52
3.3	Quasi steady state method	53
3.4	Weather data preprocessing	55
3.5	Results	57
3.6	Real vs synthetic trend of weather data	61
3.7	Procedure of sensitivity analysis	62
3.8	Differential sensitivity analysis	64
3.8.1	DSA of cooling demand	64
3.8.2	DSA of loss utilization factor	68
3.9	Factorial Method	70
3.9.1	FM of cooling demand	71
3.9.2	FM of loss utilization factor	73
3.10	Conclusions	75
II	Analysis of building envelope issues	77
4	Monte Carlo method for the uncertainty analysis of the heat transfer	79
4.1	Overview	80
4.2	Probability Density Function for input/output data	81
4.2.1	Normal or Gaussian distribution	82
4.2.2	Lognormal distribution	82
4.2.3	Weibull distribution	83
4.3	Monte Carlo Method	83
4.3.1	Generating Sample Data	85
4.4	Dynamical model of heat transfer through envelope	85
4.4.1	Conduction Transfer Functions	88
4.5	Error classification in thermophysical properties	91
4.6	Uncertainty in thermophysical properties	93
4.6.1	Thermal conductivity	93
4.6.2	Specific Mass	94
4.6.3	Specific Heat	94

4.6.4	Thickness	95
4.7	Test Cases	96
4.7.1	Wall typologies	96
4.7.2	Cities and climate	98
4.7.3	Thermophysical properties distributions	99
4.8	Summarizing	101
5	Results of Monte Carlo simulations	103
5.1	Postprocessing of output data	104
5.2	Monthly distribution curves for heat gains of South facing walls .	106
5.2.1	Perturbation of Specific Mass and Specific Heat	108
5.2.2	Perturbation of Conductivity	111
5.2.3	Perturbation of Thickness	112
5.2.4	Perturbation of all the thermophysical properties	115
5.3	Annual heat gains	117
5.4	Relation between input and annual heat gains	119
5.5	Influence of external conditions	123
5.6	Conclusions	129
	Conclusions and future developments	131
	Appendix	135
	A Rank of historical series	137
	B Model responses for Factorial Method	139
	C Mean and Standard deviations of model predictions	143
	D Adimensional fractiles of model predictions	155
	Bibliography	175

List of Figures

1.1	Relationship between different weather variables. (Guan [52]) . . .	9
1.2	Anomalous dry bulb temperature in Trento Sud recording (July 2003)	13
1.3	Interpolation of missing values in historical series.	15
1.4	Cumulative probability for primary variables in July in Trento Sud.	18
1.5	Smooth transition between July and August in Trento Sud reference year.	19
1.6	Test reference year obtained from Trento Sud historical series. . .	20
1.7	Hourly global solar irradiation for Palermo	25
1.8	Direct Normal solar irradiation for Palermo.	26
2.1	Pyranometers used in the experimental test	36
2.2	Comparison between models provisions and measures using Erbs method for vertical surface facing to South.	38
2.3	Mean Bias Error	39
2.4	Root Mean Square Error	40
2.5	Probability Density Function for measured and estimated data.	43
2.6	Influence of k_t class on percentage RMSE.	46
2.7	Influence of seasons on RMSE.	47
3.1	Reference building used in the analysis [4].	51
3.2	Scheme of type connection in TRNSYS [127] simulation.	53
3.3	MTD approximation by a Fourier series	56
3.4	July diffuse fraction in Milan	57
3.5	Monthly cooling demand as a function of the ratio of loss to gain	58
3.6	External DBT for Palermo in a typical summer period.	59
3.7	Deviation in monthly cooling demand as a function of the ratio of loss to gain	60
3.8	Deviation in Monthly loss utilization factor as a function of the ratio of loss to gain	60

3.9	Loss utilization factor with both real and MTD weather data . . .	61
3.10	Percentage sensitivity index as a function of the ratio of losses to gains.	67
4.1	Scheme of the Monte Carlo procedure adopted.	84
4.2	Solution strategies for unsteady heat transfer through envelope. .	87
4.3	CTF errors with different calculation procedure Qian et al. [112]	91
4.4	Thickness variability of insulation layer in a building retrofit . . .	96
4.5	Wall typologies used in Monte Carlo analysis.	98
4.6	Distribution curves of input data for expanded clay wall (Le). . .	101
5.1	Scheme of the uncertainty analysis of heat transfer through envelope.	105
5.2	Trento distribution curves of August heat gains due to ρ perturbation.	108
5.3	Palermo distribution curves of August heat gains due to ρ perturbation.	109
5.4	Trento distribution curves of August heat gains due to λ perturbation.	112
5.5	Palermo distribution curves of August heat gains due to λ perturbation.	113
5.6	Trento distribution curves of August heat gains due to l perturbation.	114
5.7	Palermo distribution curves of August heat gains due to l perturbation.	115
5.8	PDF curves of August heat gains due to a simultaneous variation of layer properties	116
5.9	Relations between clay block parameters (Mi) and annual heat gains in Palermo	121
5.10	Relations between stone parameters (Sw) and annual heat gains in Trento	122
5.11	Adimensional deviation of annual heat gains as a function of adimensional perturbation of inputs.	124
5.12	Adimensional deviation of annual heat losses as a function of adimensional perturbation of inputs.	125
5.13	Influence of external weather conditions on deviation in monthly heat losses.	127
5.14	Influence of external weather conditions on deviation in monthly heat gains.	128
6.1	Experimental activities on full scale building components	133

List of Tables

1.1	Meteorological stations analyzed in correlation analysis.	10
1.2	Pearson's correlation index for the three dataset analyzed.	11
1.3	Missing or rejected data in historical series of Palermo and Trento.	14
1.4	Average Pearson's index for Palermo and Trento dataset.	14
1.5	Eligible reference months from historical series of Palermo and Trento.	15
1.6	Degree days for historical series and for TRYs.	21
1.7	Design temperature for system sizing.	22
1.8	Monthly mean daily solar radiation [$MJ m^{-2}$].	23
1.9	Comparison of Pearson's index.	24
1.10	Comparison between different sources of monthly mean temperature.	24
1.11	Comparison between different sources of monthly mean daily solar radiation.	25
2.1	Location of weather stations used for the decomposition models.	30
2.2	Decomposition models used in the comparison.	32
2.3	Projection models used in the comparison.	34
2.4	Geographical coordinates of the experimental location.	35
2.5	Instruments used in experimental test.	35
2.6	Results of percentage MBE and RMSE for different couples of models.	41
2.7	Result of t-statistic and correlation index for different couples of models.	44
3.1	Construction characteristics of test buildings.	51
3.2	Climate classification of Italian cities	55
3.3	Effects of weather data perturbations	58

3.4	Monthly sensitivity indexes s for the mean outdoor temperature (T_M), for the amplitude of the external temperature (T_A) and for the max global solar radiation on the horizontal plane (Q_A)	64
3.5	Percentage sensitivity index for cooling demand.	66
3.6	Percentage sensitivity index for loss utilization factor.	69
3.7	Factorial design scheme for three variables analysis [84]	70
3.8	Results of factorial analysis for cooling demand in kWh	72
3.9	Results of factorial analysis of loss utilization factor for cooling.	74
4.1	Stratigraphy and layer thickness of the four test cases (Figure 4.5)	98
4.2	Climate features of the cities used in Monte Carlo simulations.	99
4.3	PDF parameters of thermophysical property distributions used in Monte Carlo simulations	100
5.1	Best fit distributions for August heat gains and February heat losses due to perturbation of input data	107
5.2	Value of $(f_{99\%} - f_{1\%})/E\{x\}$ due to uncertain ρ and c_p	110
5.3	Value of $(f_{99\%} - f_{1\%})/E\{x\}$ due to uncertain λ	111
5.4	Value of $(f_{99\%} - f_{1\%})/E\{x\}$ due to uncertain l	114
5.5	Value of $(f_{99\%} - f_{1\%})/E\{x\}$ due to all uncertain parameters	116
5.6	Best fit distributions for annual heat gains and heat losses due to perturbation of input data on wall facing South	118
5.7	Opening interval for annual heat gains distributions	119
5.8	Percentage of monthly hours with a sol-air temperature:	126
A.1	Rank of Trento historical series	137
A.2	Rank of Palermo historical series	138
B.1	Building cooling response for FM in Milan	139
B.2	Building cooling response for FM in Palermo	140
B.3	Building loss utilization factors for FM in Milan	140
B.4	Building loss utilization factors for FM in Palermo	141
C.1	Mean and Std Dev. for Le test case due to expanded clay properties perturbations	143
C.2	Mean and Std Dev. for Sw test case due to stone properties perturbations	145
C.3	Mean and Std Dev. for Mi test case due to insulation properties perturbations	147
C.4	Mean and Std Dev. for Mi test case due to clay block properties perturbations	149

C.5	Mean and Std Dev. for Me test case due to insulation properties perturbations	151
D.1	Adimensional fractiles for Le case due to expanded clay properties perturbations	155
D.2	Adimensional fractiles for Sw case due to stone properties perturbations	156
D.3	Adimensional fractiles for Me case due to clay block properties perturbations	157
D.4	Adimensional fractiles for Me case due to insulation properties perturbations	158
D.5	Adimensional fractiles for Mi case due to clay block properties perturbations	159
D.6	Adimensional fractiles for Mi case due to insulation properties perturbations	159

List of Symbol

Φ	Cumulative distribution function of variable daily means within the whole historical series of the calendar months
α	Solar altitude [<i>rad</i>]
α_w	Wall coefficient of absorption for solar radiation
φ_n	Phase lag of the <i>n</i> -th harmonic of dry bulb temperature [<i>rad</i>]
η_c	Loss utilization factor for cooling [–]
κ	Thermal diffusivity [$m^2 s^{-1}$]
λ	Thermal conductivity [$W m^{-1} K^{-1}$]
ω_n	Angular frequency of the <i>n</i> -th harmonic [$rad s^{-1}$]
θ	Temperature of the internal air node of the thermal zone [$^{\circ}C$]
θ_z	Zenith angle [<i>rad</i>]
ρ	Specific mass [$kg m^{-3}$]
τ	Time expressed in [<i>s</i>] or in [<i>h</i>]
ψ_n	Phase lag of the <i>n</i> -th harmonic of solar irradiation [<i>rad</i>]
A_n	Amplitudes of the <i>n</i> -th harmonic [$^{\circ}C$]
B_n	Amplitudes of the <i>n</i> -th harmonic [$W m^{-2}$]
CDD_{20}	Cooling Degree Days using $20^{\circ}C$ as a balance point

C_i	Internal heat capacitance of the thermal zone [$J K^{-1}$]
c_p	Specific heat [$J kg^{-1} K^{-1}$]
\overline{DBT}	Daily mean of dry bulb temperature [$^{\circ}C$]
DBT	Dry bulb temperature [$^{\circ}C$]
$DBT_{1\%}$	External design temperature for heating systems, computed as the 1% percentile [$^{\circ}C$]
$DBT_{99\%}$	External design temperature for cooling systems, computed as the 99% percentile [$^{\circ}C$]
DN	Direct normal solar irradiation [$W \cdot m^{-2}$]
$E\{x\}$	Mean value or first moment of a probability dis- tribution of x
E	Estimated value of solar radiation on tilted sur- face [$W m^{-2}$]
F	Cumulative distribution function of variable daily means within the whole historical series of the calendar month
F_S	Finkelstein-Schafer statistic
G_{ET}	Hourly extraterrestrial solar irradiance on a hor- izontal surface [$W \cdot m^{-2}$]
\overline{GSI}	Daily mean of solar irradiation [$W m^{-2}$]
GSI	Hourly global solar irradiance on a horizontal surface [$W \cdot m^{-2}$]
HDD_{20}	Heating Degree Days using $20^{\circ}C$ as a balance point
J	Rank order of variable daily means within the month of a specific year
K	Rank order of variable daily means within the month of a specific year
k_d	Ratio of diffuse to global irradiation ratio [—]

k_t	Clearness index [-]
l	Layer thickness [m]
M	Measured value of solar radiation on tilted surface [$W m^{-2}$]
MBE	Mean bias error
N	Total number of data series
n	Number of days for the month considered
p	The primary weather variables used for the calculation of test reference year
PDF	Probability Density function
\dot{q}	Heat flux [$W m^{-2}$]
\dot{q}_c	Convective heat exchanges with wall [W]
$Q_{h,nd}$	The energy need for heating [kWh]
$Q_{c,nd}$	The energy need for cooling [kWh]
Q_{gn}	The sum of internal and solar heat gains [kWh]
Q_{ht}	Thermal losses through the envelope and for ventilation [kWh]
\dot{q}_i	Internal convective heat gains [W]
\dot{q}_{sys}	Supplied or removed heat by the energy systems [W]
\dot{q}_v	Ventilation heat losses [W]
r	Pearson's index of the variable correlations
RH	Relative humidity [%]
$RMSE$	Root mean square error
s	Sensitivity index obtained with DSA approach
$s\%$	Percentage sensitivity index obtained with DSA approach

t	T-statistic
T_{solair}	Sol-air temperature [$^{\circ}C$]
U	Thermal transmittance [$W m^{-2} K^{-1}$]
$Var\{x\}$	Variance or second central moment of a probability distribution of x
WV	Wind velocity [$m \cdot s^{-1}$]

Introduction

Background

In Europe about one third of total annual energy consumption is used in both residential and commercial buildings. Besides, buildings use more energy than any other sector as such are a major contributor to CO_2 emissions. Therefore, it is estimated that substantial energy savings can be achieved through careful planning for energy efficiency. However, a considerable number of inefficient buildings will remain until they will be renovated. Consequently it is important to improve also the existing building stock.

One of the aims of the European Directives 2002/91/CE and 2010/31/EU is the increasing in building energy performance both for new buildings and major renovations. In many countries already a building regulation exists to ensure the reduction of energy needs for heating and for domestic hot water preparations. Hence, the interest in reducing summer energy demand has grown in the last few years, especially because of the widespread diffusion of low efficiency cooling systems such as split type units.

The summer behavior of buildings is mostly non-stationary and, therefore, the reliability of simple quasi steady state model predictions can not be taken for granted. Besides, this cooling demand interacts dynamically with occupants, climate features and system controls. Since detailed hourly energy simulations emulate the dynamic interaction between environment, building structure, occupants and indoor conditions, they have the potential to provide relevant information about the building summer behavior and to indicate the possible conservation measures for the reduction of energy consumptions. However, the detailed models require a better knowledge of properties and an increase of the number of input data. The main usages of detailed dynamic simulations can be listed as follows:

- to ensure that energy consumption meets mandatory provisions,
- to get energy efficiency awards, such as LEED certificate,

- to compare different design choices such as wall materials, windows, shapes and orientations,
- to compare alternatives energy systems and their integration with renewable energy sources,
- to develop energy efficient control strategies,
- to identify the system malfunction by comparing predicted and actual energy consumptions.

One of the limits for the application of enhanced simulation methods, that sometimes can undermine the reliability of their results, is the difficulty to gather reliable input data. Moreover, if dynamic simulation are used in order to compare different choices, decisions are often suboptimal because of the insufficient knowledge of data that has a large consequence on results. Consequently, AE (Architect-Engineer) community could believe these tools not suited to assess building energy performance with acceptable speed and robustness.

This thesis should increase in AE the capability to better predict the impact of input, in particular of weather data and of thermophysical properties, and therefore to make better decisions and to provide optimal solution with building simulation tools.

Aim and Objectives

The aim of the thesis is to investigate the reliability and applicability of energy simulation to Italian context. In fact, due to the particular climate and to the construction techniques, the use of the calculation procedure developed in the USA can not always be taken for granted.

In order to broaden the use of building simulation in the design process, it is essentially to clarify some aspects. For instance, one of the biggest objection versus the use of detailed procedure is: *"to what extent these methods are meaningful if input data are not reliable?"* This question usually refers to some initial issues that designers face:

- hourly weather data are not available for the city on which there is the building,
- are the weather data developed from airports measurements really representative of the urban context?
- the manufacturer of construction materials does not provide all the thermophysical properties required for the software,

- for existing buildings the design documentations are not available, hence the properties of the envelope are not known.

For this reason, the emphasis of this thesis is on the uncertainties of model predictions. In particular, the research is divided in two parts: the investigation of climate issues and the uncertainty analysis of heat transfer estimation, especially for massive wall.

The purpose of the research is to support AE in the choice of the characteristics to which the model predictions are more sensitive. Therefore AE have to carefully estimate these properties.

Research methodology

The research starts from a set of existing and proven concepts and calculation procedures. In addition to this, some experimental activities have been carried out with the purpose of investigate the uncertainties of solar radiation models. Besides, since the backbones of the thesis are the uncertainty and sensitivity analyzes, some codes have been developed with Matlab and Fortran. Consequently, uncertainty and sensitivity analyzes are expected to clarify the role of climate data and thermophysical properties.

For each parts of the thesis, the following steps are carried out:

- **literature review** for the analysis of the state of the art. In this phase, the designer available methods are investigated as well as the sources of input data;
- **quantification of uncertainties** of input data. The reliability of the data are investigated both by considering the measurement procedure and by checking the availability of product standard;
- **run of dynamic simulations** with suboptimal input data. This stage represents and models what happen when AE misestimates the input values;
- **postprocessing and summarizing** of simulation outcomes.

The results of sensitivity and uncertainty analyzes allow to know the robustness of simulation models and make AE aware if the wrong specifications can lead to uncertain results. In the next section, the outline of the research is reported.

Thesis outline

- **Chapter1** the thesis starts with the development of the Test Reference Year (TRYs) for two Italian cities. These datasets use historical series collected in urban sites and, consequently, more suitable for energy analyzes. Following on from this point, the representativeness of the new TRYs is verified. Moreover, critical points found in previous databases are highlighted such as the incorrect values of solar irradiation and the underestimation of the variable cross correlations;
- **Chapter2**, as the previous chapter, deals with the issues of uncertainties in weather data. In particular, it focuses mainly on the reliability of the calculation procedure for the postprocessing of solar irradiation. The outcomes of several combinations of diffuse fraction estimations and projection models are compared with experimental data collected by the author;
- **Chapter3**, in conclusion of this first part of the thesis, a sensitivity analysis is performed with the purpose of studying the influence of uncertain weather data on the dynamic building heat balance;
- **Chapter4** provides the theoretical basis and data research for the uncertainty analysis about the calculation of unsteady heat transfer through the envelope;
- **Chapter5** reports in details the results of Monte Carlo simulations and points out the different behavior of well insulated components with respect to non insulated walls. Moreover, some considerations are drawn about the dynamic thermal performance of the walls.
- **Conclusions** summarizes and concludes the research by highlighting the main results and future challenges in this domain.

Part I

Weather data for energy simulation

Chapter 1

Evaluation of the Typical Reference Year for Italian cities

The interest in building simulation has grown in the last few years due to the need to reduce building energy consumptions and CO_2 emissions in atmosphere. The evaluation of hourly energy consumption of building requires a collection of weather data representative of the climate features of the site. Moreover, a reliable set of weather data is essential to correctly design efficient and comfortable buildings and to analyze the effectiveness of the energy saving measures. The aim of this chapter is to clarify and to set up a complete procedure for the selection of typical reference year (TRY) for some Italian cities. Finally, considerations about cross correlations of weather variables and raw data analysis are proposed.

1.1 Introduction

One of the aims of the European Directives 2002/91/CE and 2010/31/EU is the increase in building energy performance for both new buildings and major renovations. Hence, in Italy, the interest in reducing summer energy demand has grown in the last few years, especially because of the widespread diffusion of low efficiency cooling systems, such as split type units. Since the evaluation of summer behavior of building is strictly connected with external climate, a collection of weather data representative of the climate features of the site is needed. Moreover, a reliable set of weather data is essential to correctly design efficient and comfortable buildings and to analyze the effectiveness of the energy saving measures. Detailed energy models are more suitable for the design of sustainable buildings. In fact, they can provide a better understanding of the performance of HVAC systems and the interaction between building and energy

systems. These dynamic simulations require hourly weather data in order to estimate building energy consumptions and energy production by renewable systems.

As reported in [73] hourly weather data for building energy simulation are classified in three types:

- Multi-year datasets, they include a substantial amount of information for a number of years;
- Typical year, it is a single year of hourly data selected to represent the typical trend in a multi-year dataset;
- Representative days: they are hourly data for some average days selected to represent typical climatic conditions.

Since a multi-year hourly simulation of a whole building is rather time-consuming, the typical reference year (TRY) approach is preferable. Starting from the first TRY, developed by Lund [80], several procedures have been developed to prepare typical weather data using historical series recorded in meteorological stations. As reported in Lund [81] a TRY should have three key features:

- True frequencies, TRY should be as near as possible to mean values over a long period of measurements;
- True sequences, the weather data must follow each other in a similar manner to the recorded data;
- True correlation, weather data are not independent variables but they are cross-correlated.

Besides, TRY for energy calculation must be representative of real conditions in urban area. In Italy only in the last twenty years, the regional environmental protection agencies (ARPA) have installed meteorological stations in urban sites as shown in [15]. Consequently, for the currently Italian TRY weather data, measurements collected in airports have been used in the past by Mazzarella [88]. But, by and large, the open field sites can have different climate variables with respect to urban sites. For instance, the urban heat island effect can cause shifts in minimum, maximum and average temperature [51].

1.2 Weather data sources for Italian cities

The Italian climate was investigated for building simulation in an earlier study in 1979 by the Institute of Atmospheric Physics (CNR). In this research, Maz-

zarella [88] used the data collected by the Aeronautical Meteorological Services in several Italian airports from 1951 to 1970. For the selection of the reference month, only the temperatures, recorded in three hourly intervals, were taken into account. Consequently relative humidity, wind velocity and number of solar hours per day were considered as secondary parameters. Besides, in most of the historical series there were missing periods of data and, with the purpose of overcoming this lack in measured data, empirical methods for data estimations were used. However, the possible interaction between weather variables (Figure 1.1) were not considered. Afterwards, in 1984, the hourly trend of solar irradiation were computed, starting from the daily number of hours of solar radiation, using an empirical correlation. For meteorological stations without solar measurements, the data collected in the closest station were used and, consequently, the cross-correlation between weather variables were lost. Another

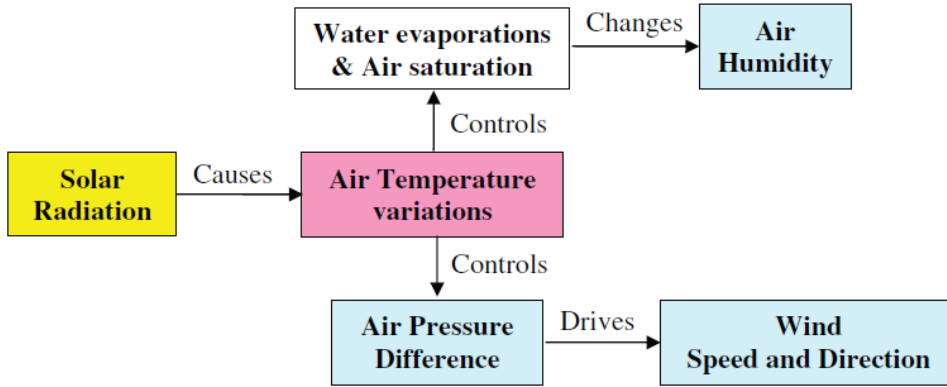


Figure 1.1: Relationship between different weather variables. (Guan [52])

source of hourly weather data for Italian cities is the technical standard UNI 10349 [1]. This document provides hourly trends of temperature and solar irradiation for a day representative of the whole month. Therefore, the synthetic day obtained through this standard is unable to supply a valid description of the true sequences and true frequencies of weather data. In order to analyze the trustworthiness of the De Giorgio [88] approximations, the relations among the weather variables are investigated by means of a correlation analysis. For the investigation of the two variable correlations, the Pearson's index is largely used:

$$r = \frac{\sum(X \cdot Y) - \sum X \cdot \sum Y/N}{\sqrt{\left(\sum X^2 - \frac{(\sum X)^2}{N}\right) \left(\sum Y^2 - \frac{(\sum Y)^2}{N}\right)}} \quad (1.1)$$

where X and Y are the two variables analyzed.

Although the thresholds to interpret the correlation can be different, it is believed that Pearson's correlation between -1 and -0.5 means a strong negative association, while a correlation between $+0.5$ and $+1$ indicates a strong positive association [53]. In this analysis the correlations between dry bulb temperature (DBT), global solar irradiation (GSI), relative humidity (RH) and wind velocity (WV) for three different datasets (Table 1.1) are investigated. In Table 1.2 the

Table 1.1: *Meteorological stations analyzed in correlation analysis.*

Name	Zone	Latitude	Longitude	Elevation	Period
Palermo	Urban	38°.1311N	13°.3270E	50	2002 - 2010
Trento Sud	Urban	46°.0231N	11°.1369E	185	1984 - 2011
Roncafort	Semiurban	46°.1039N	11°.0986E	201	2003 - 2007

Pearson's correlation values are reported for the coincident periods of measurements. These results show good agreement with previous studies [53] and supply evidence to the dependence among climate features. In particular, the key role of solar irradiation is highlighted from the values of Pearson's index. Indeed, solar radiation has Pearson's index close to either 0.5 or -0.5 for altogether, dry bulb temperature, relative humidity and wind velocity. Temperature has an high correlation with relative humidity because of the strong influence of temperature on vapor saturation pressure. Instead, the weak bond with temperature and wind velocity is due to the variation of atmospheric pressure that leads the air motion. As found by Guan et al. [53], in site placed in a valley (such as Trento) the variation of air temperature may have a much larger effect on the wind speed than in other location (such as Palermo).

Finally, the wind velocity affects the vapor partial pressure and, consequently, there is a strong correlation between wind velocity and relative humidity. It follows that, in order to consider the true correlation between weather variables as suggest by Lund [81], the same period of measurements must be used in the TRY preparation. Moreover, the difference in Pearson's index between two close meteorological stations such as Trento Sud and Roncafort, evidences that replacing missing data with measurements collected in a close meteorological station is not advisable.

1.3 Literature Review

One of the first dataset for building energy analysis is the test reference year [128] developed by the National Climatic Data Center (NCDC). In this docu-

Table 1.2: *Pearson's correlation index for the three dataset analyzed.*

	Station	2003	2004	2005	2006	2007
GSI-DBT	Palermo	0.508	0.518	0.517	0.528	0.534
	Trento Sud	0.565	0.483	0.479	0.486	0.534
	Roncafort	0.408	0.275	0.275	0.334	0.450
DBT-WV	Palermo	0.175	0.201	0.229	0.228	0.288
	Trento Sud	0.432	0.408	0.389	0.425	0.479
	Roncafort	0.149	0.021	-0.003	-0.123	-0.123
DBT-RH	Palermo	-0.500	-0.476	-0.493	-0.589	-0.643
	Trento Sud	-0.394	-0.405	-0.326	-0.470	-0.467
	Roncafort	-0.397	-0.190	-0.005	-0.284	-0.523
GSI-WV	Palermo	0.465	0.491	0.516	0.489	0.511
	Trento Sud	0.297	0.320	0.343	0.366	0.380
	Roncafort	0.171	0.115	0.097	0.099	-0.104
GSI-RH	Palermo	-0.586	-0.536	-0.571	-0.587	-0.554
	Trento Sud	-0.479	-0.559	-0.527	-0.578	-0.536
	Roncafort	-0.476	-0.146	-0.345	-0.420	-0.373
WV-RH	Palermo	-0.442	-0.462	-0.474	-0.458	-0.448
	Trento Sud	-0.573	-0.594	-0.601	-0.613	-0.596
	Roncafort	-0.514	-0.220	-0.568	-0.343	-0.201

ment weather data for 60 locations in the United States are available. However, basic data of TRY do not include any solar radiation. With the purpose of overcoming this deficiency, other works such as the weather year for energy calculations (IWEC [12] and IWEC2 [122]) and typical meteorological year (TMY [59], TMY2 [86] and TMY3 [134]) have been done.

Several approaches to develop and format a typical weather year have been reported in literature such as Lund and Eidorff [82], Pissimanis et al. [107], Festa and Ratto [48], Marion and Urban [86], Lund [81], Wilcox and Marion [134]. Most of them follow and modify the approach proposed by Hall et al. [59]. Almost all of these methods share the principle of preserving the actual trend of weather data and they agree that solar radiation is the primary parameter for the selection of the reference month. The main difference between them is the choice of the other primary weather variables for the selection of the reference month. In particular Pissimanis [107] uses the daily mean, maximum

and minimum values for altogether, air temperature, relative humidity, wind velocity and solar irradiation. Instead in [82] and [48] the daily means of air temperature, relative humidity, wind velocity and global solar irradiation are considered in addition to daily maximum of dry bulb temperature.

As reported by Harriman et al. [60], the selection of primary weather variables depends on the final use of the reference year. If the aim is the sizing of energy systems, the most important aspect will be the reliability of the extreme values. Consequently, the primary inputs become maximum and minimum values. Contrarily, with the aim of analyzing the energy requirements of buildings, it is important that TRY represents the climate conditions considered to be typical over a long time periods. Moreover, Bilbao et al. [18] highlights the influence of weather station characteristics on the choice of an appropriate method.

The method of EN ISO 15927-4 [6] is chosen for the development of a new TRY for some Italian cities. This methodology is similar to the ones proposed in NCDC's TRY [128]. The selection method is based on dry-bulb temperature, solar radiation, and humidity but not on wind speed. The monthly mean wind velocity is used as a secondary parameter. In fact, the month with the lowest deviation in the short list of selected months, with respect to the monthly mean velocity of the historical series, is selected as the month to be included in the typical reference year. However, the standard does not specify any criterion neither for the preprocessing and validations of raw data nor about the method to use for the smoothing of TRY data across monthly boundaries. Consequently the aim of this chapter is to clarify and to set up a complete procedure for the selection of TRY for some Italian cities. In particular two different historical series are treated:

- Palermo 2002-2010: a city in Southern Italy. Its climate is type 3A "Warm - Humid" for ASHRAE classification [8], and *Dfa* "Humid Subtropical" for Köppen classification [75] ;
- Trento 1984-2011: a city in Northern Italy. Its climate is type 4A "Mixed - Humid" for ASHRAE classification [8], and *Cfa* "Humid Continental" for Köppen classification [75].

1.4 Raw Data Analysis

Since every measurement is imperfect, some quality control tests must be performed before using the weather data. Any likely sources of problems related to weather measurements may be categorized like equipment errors or uncertainty caused by operation errors. The purpose of this quality control is to ensure that

data meet requirements for uncertainty, resolution and representativeness. The higher the accuracy in the whole observing system, the better will be the quality of data. However, once a datum from a measurement process is obtained, values can be only verified and the datum rejected or adjusted in order to get the quality required.

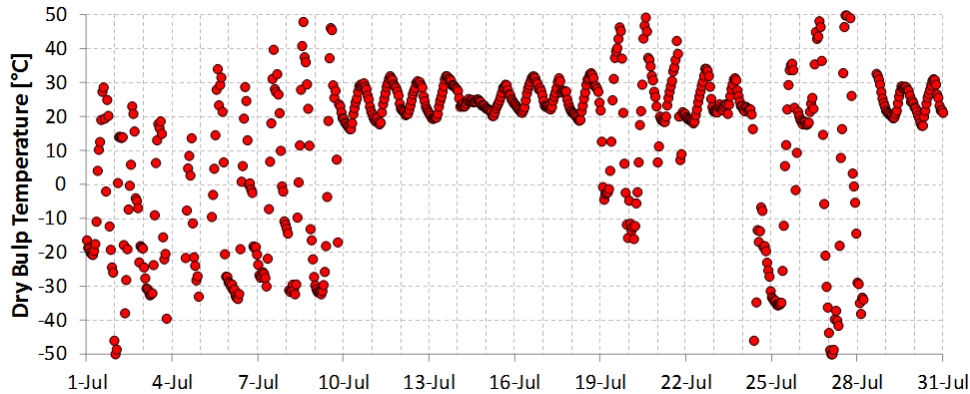


Figure 1.2: *Anomalous dry bulb temperature in Trento Sud recording (July 2003)*

For instance, in solar irradiation measures, errors may increase for the cosine response of the pyranometer in hours close to either sunrise or sunset. The cosine error is the sensor's response to the angle at which radiation strikes the sensing area. The more acute the angle of the sun, i.e. at sunrise and sunset, the greater the error will be. Cosine error is typically dealt with the exclusion of the recorded data at sunrise and sunset times. In particular, in order to limit also the cosine response errors, a maximum value of the clearness index, defined as Equation (1.2) is set to one in according with [38], [108] and [46]. Moreover, all the solar irradiation values before sunrise and after sunset hours are set to zero.

$$k_t = \frac{GSI}{G_{ET}} \quad (1.2)$$

where GSI is the hourly global solar irradiance on a horizontal surface,
 G_{ET} is the hourly extraterrestrial solar irradiance on a horizontal surface.

In this analysis the quality of all the weather variables is checked assuming

some empirical but reasonable criteria for the data discarding.

$$\begin{aligned}
0 &\leq GSI \leq G_{ET} \\
-20^{\circ}C &\leq DBT \leq 50^{\circ}C \\
0\% &\leq RH \leq 100\% \\
DBT(\tau) - DBT(\tau - 1h) &\leq 5^{\circ}C \\
RH(\tau) - RH(\tau - 1h) &\leq 30\%
\end{aligned} \tag{1.3}$$

Subsequently, data rejected are handled like missing values. The missing or rejected data as a percentage of the wall historical period for each parameter are reported in Table 1.3. Despite the short period of data recording, in Palermo there is an higher quality of raw data. Due to the upper-grade of the average

Table 1.3: *Missing or rejected data in historical series of Palermo and Trento.*

	City	DBT	GSI	RH	WV
Accepted	Trento	95.2%	95.6%	95.8%	93.2%
	Palermo	99.7%	99.7%	98.5%	99.5%
Missing or Rejected	Trento	4.8%	4.4%	4.2%	6.8%
	Palermo	0.3%	0.3%	1.5%	0.5%

cross-correlation of weather variables, measured by Pearson's index (Table 1.4), the gaps in weather data are not filled with measurements collected in a close station. Instead, the historical series are completed using suitable methods either of interpolation or estimation (Figure 1.3).

Table 1.4: *Average Pearson's index for Palermo and Trento dataset.*

City	GSI-DBT	DBT-WV	DBT-RH
Palermo	0.526	0.259	-0.545
Trento Sud	0.510	0.391	-0.414

City	GSI-WV	GSI-RH	WV-RH
Palermo	0.498	-0.575	-0.474
Trento Sud	0.328	-0.571	-0.563

Specifically, a linear interpolation is adopted in order to fill temperature, relative humidity and wind velocity gaps when the dimension of missing data are lower than 6 values. Otherwise, using the daily periodicity of weather variables,

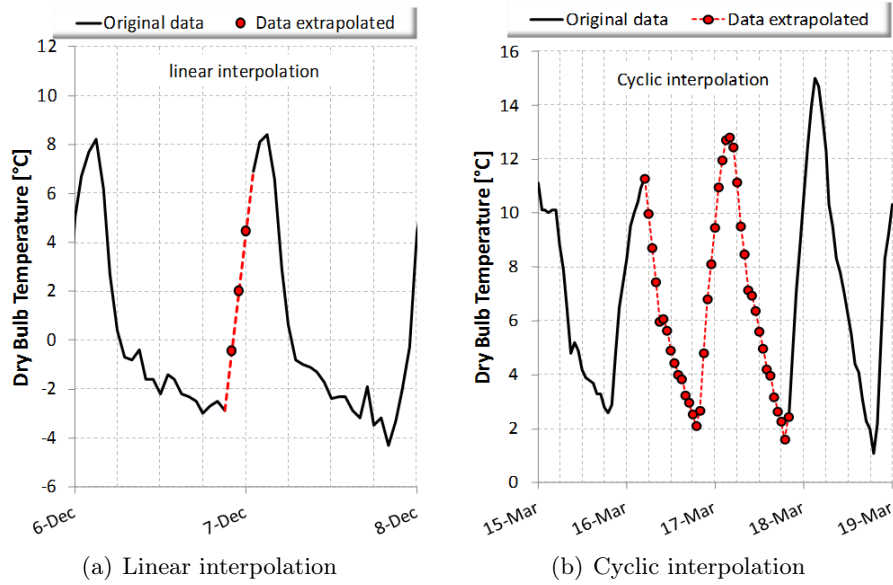


Figure 1.3: *Interpolation of missing values in historical series.*

a cyclic interpolation is chosen for data replacement. Besides, this approach is also adopted for filling solar irradiation gaps. In fact, a linear interpolation would give solar radiation either before sunrise or after sunset hours or solar irradiance greater than extraterrestrial solar irradiation.

Subsequently, in order to avoid the misrepresentation of reference month due to the excessive interpolation, months missing more than 20% of a weather variable are not taken into account for the analysis. Using these criterions, the eligible reference months for the two cities are reported in Table 1.5.

Table 1.5: *Eligible reference months from historical series of Palermo and Trento.*

	City	DBT	GSI	RH	WV
Eligible	Trento	308	310	318	307
	Palermo	106	107	103	106
Non eligible	Trento	28	26	18	29
	Palermo	2	1	5	2
Total	Trento	336	336	336	336
	Palermo	108	108	108	108

1.5 Procedure

Correct simulation of building performance depends not only on the appropriate mean values of the meteorological parameters, but also on the frequency distributions of individual parameters and on the cross correlations between them. For this reason, the use of long periods (at least ten years but preferably more) of hourly meteorological data is suggested in order to artificially construct a reference year. The reference year is, in fact, a year of hourly values of appropriate meteorological parameters representative of the long term climate. In this analysis the procedure of standard EN ISO 15927-4 [6] is used for the construction of a test reference year starting from a longer meteorological record.

In this method, the following hourly values of meteorological parameters should be considered:

1. dry-bulb air temperature (*DBT*);
2. global solar irradiance on a horizontal surface (*GSI*);
3. relative humidity (*RH*);
4. wind speed at a height of 10 m above ground level (*WV*).

In fact, heat transfer through building envelope and building heat balance are strictly connected with external air temperature and inward solar irradiation. Besides, relative humidity is the key climatic source of latent cooling demand of buildings. Instead, wind velocity influences only the convective heat transfer between wall external surfaces and air and it also affects air leakage through the building envelope. Although different weighting factors for the primary climatic parameters have been used in literature studies, in this work all the parameters have the same weight. Obviously, each climatic variable has a different influence on the heating and cooling demand (Section 2.4). However, the effects depend on buildings features [10, 49] and on the purpose for which the climatic data are used. For instance, the influence of the solar irradiation depends also on the glazed area and on the window orientations. Moreover, the relative humidity does not affect the heating requirements but can modify the heating capacity of heat pump, by increasing the defrost cycle number. Consequently, the use of the same weighting factors can be an acceptable compromise for all cases.

The procedure used can be divided in two main stages:

1. selection of the best month from the multi-year record for each calendar month;

2. adjustment of the hourly values in the selected months so that to provide a smooth transition when the different months are joined to form a year.

The two stages have to maintain correlations between the different variables within each month but also the mean value of individual variables and their frequency distribution. As suggested by the EN ISO 15927-4 [6], dry-bulb temperature, solar irradiation and relative humidity are taken as the primary parameters for selecting the “best” months to form the reference year, with wind speed as a secondary parameter. The following stages are necessary in order to construct a reference year:

Calculation of the daily means for each climatic parameter . The main climatic parameters, i.e. dry-bulb temperature, solar radiation and relative humidity, are generally indicated with p . The first step of the EN ISO 15927-4 [6] is the calculation of the daily means \bar{p} from the hourly values of p for each month and each year.

Calculation of the cumulative distribution function $\Phi(p, m, i)$. Secondly, all the values are sorted in increasing order. For each calendar month m , the cumulative distribution function $\Phi(p, m, i)$ of the daily means over all years in the data set is calculated (Figure 1.4):

$$\Phi(p, m, i) = \frac{K(i)}{N + 1} \quad (1.4)$$

where $K(i)$ is the rank order of the i th value of the daily means within that calendar month in the whole data set.

Calculation of the cumulative distribution function $F(p, y, m, i)$. Thirdly, all the values for the month m of the year y are sorted in increasing order. The cumulative distribution function of the daily means within each calendar month, $F(p, y, m, i)$, is:

$$F(p, y, m, i) = \frac{J(i)}{n + 1} \quad (1.5)$$

where $J(i)$ is the rank order of the i th value of the daily means within that month m and that year y .

Calculation of the Finkelstein-Schafer statistic . For each calendar month, the Finkelstein-Schafer statistic, $F_S(p, y, m)$, for each year y of the data set is:

$$F_S(p, y, m) = \sum_{i=1}^n |F(p, y, m, i) - \Phi(p, m, i)| \quad (1.6)$$

where n is the number of days in an individual month.

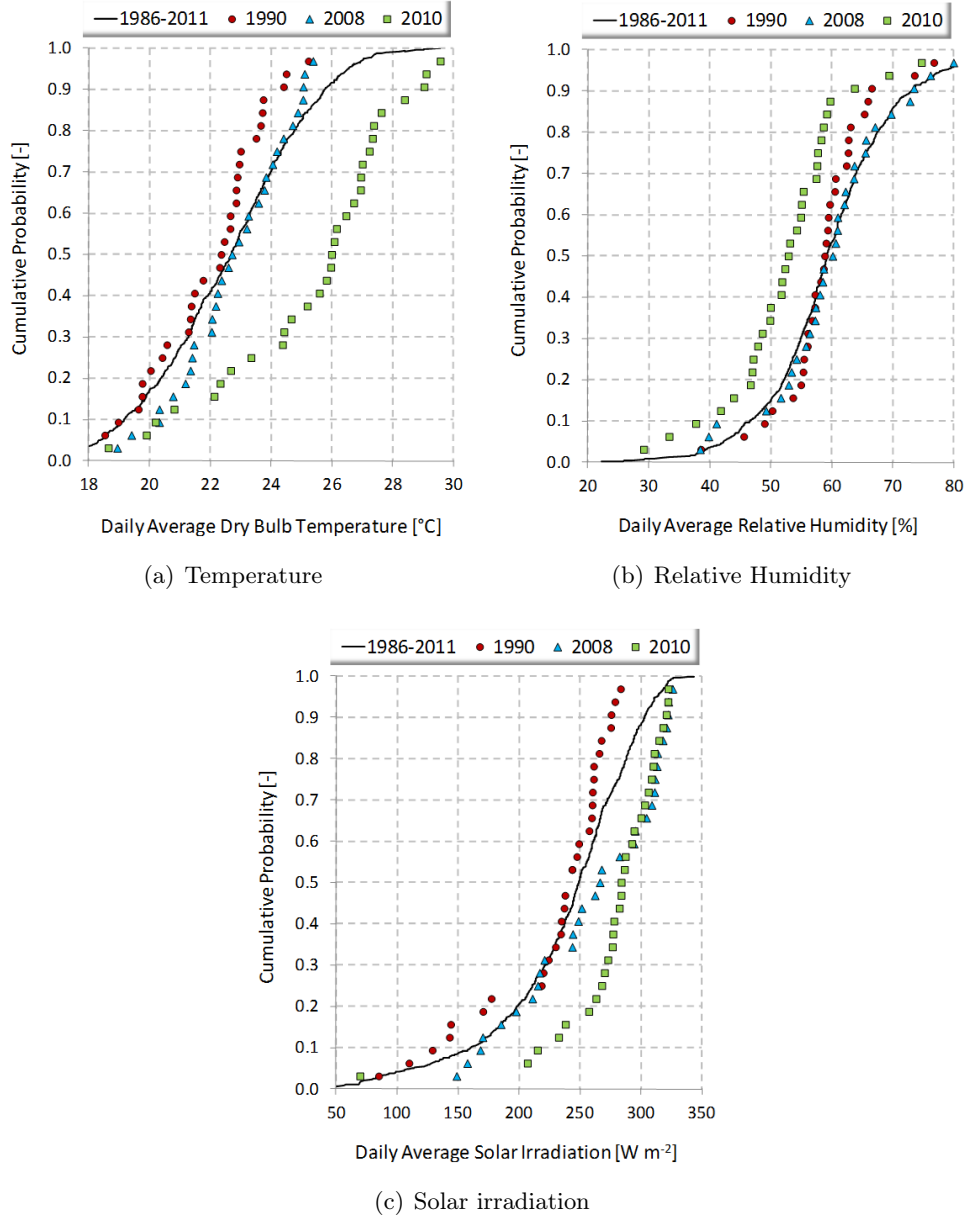


Figure 1.4: Cumulative probability for primary variables in July in Trento Sud.

Selection of the "best" month . For each calendar month m , the months are sorted in order of increasing size of $F_S(p, y, m)$. The previous stages are done for the main climatic parameter dry-bulb temperature, solar radiation and relative humidity. The separate ranks for the three climate parameters p are then added. For each calendar month, for the three

months with the lowest total ranking, the deviation of the monthly mean wind speed from the corresponding multi-year calendar-month mean is calculated. The month with the lowest deviation in wind speed is selected as the “best” month to be included in the reference year.

Smoothing of the transition between the reference months . To guarantee maximal probable frequencies, sequences and a true cross-correlation, the TRY contains months from a number of calendar years. The use of months from different years requires climatic data at the beginning and at the end of the month to be smoothed. The smoothing period adopted for this analysis is sixteen hours (eight per month). Data replaced do not represent actual physical data, but they avoid unphysical jump in the junction. Consequently, for temperature (Figure 1.5) and relative humidity the eight values of each month close to the junction are adjusted by means of a cubic spline interpolation.

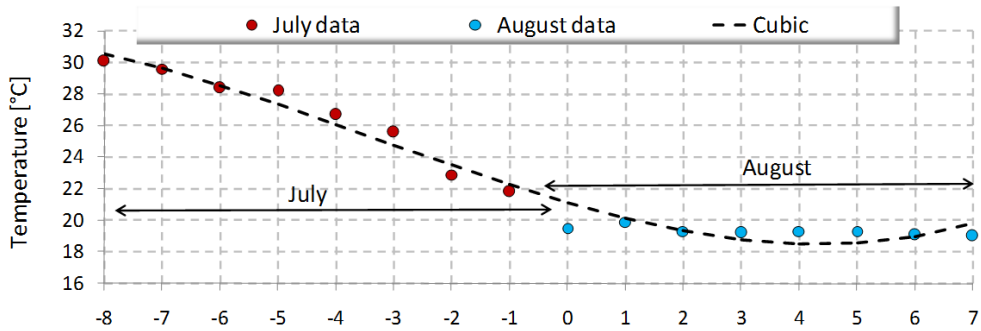
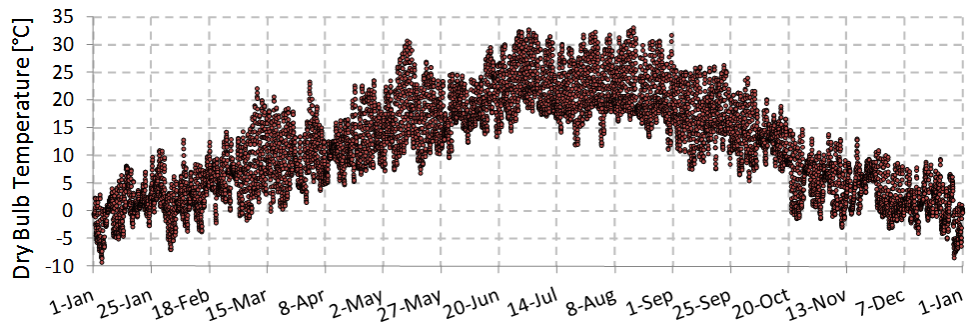


Figure 1.5: *Smooth transition between July and August in Trento Sud reference year.*

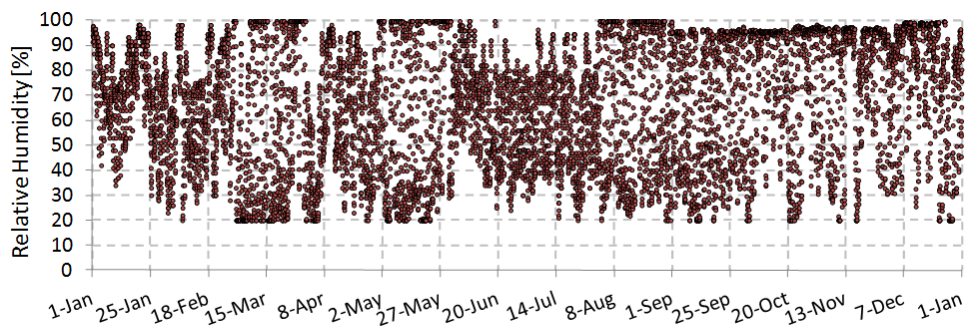
Since the TRY can be used for a multi-year simulation, also the transition between December and January is adjusted. Besides, the junction between two reference months is during the night and, then, no interpolation is performed for solar irradiation. Moreover, also for wind velocity no adjustments are done in the reference year, because of the large variability in hourly values.

1.6 Results

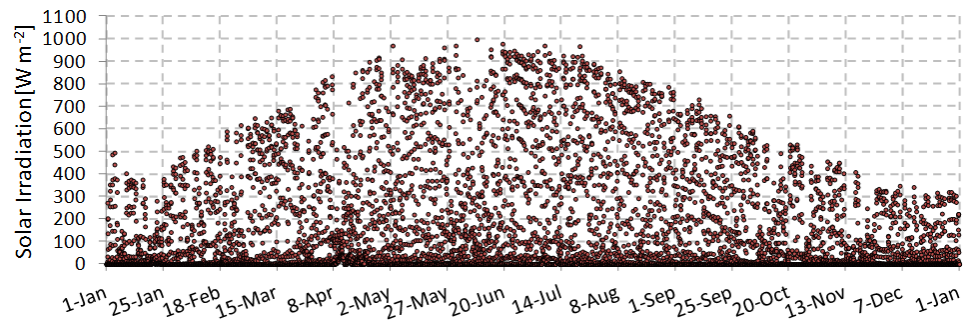
The final ranks of each month and the Finkelstein-Schafer statistics are reported in appendix A. Figure 1.6 shows the hourly trend of the Trento TRY for the four climate variable analyzed, i.e. dry bulb temperature, solar irradiance, relative humidity and wind velocity.



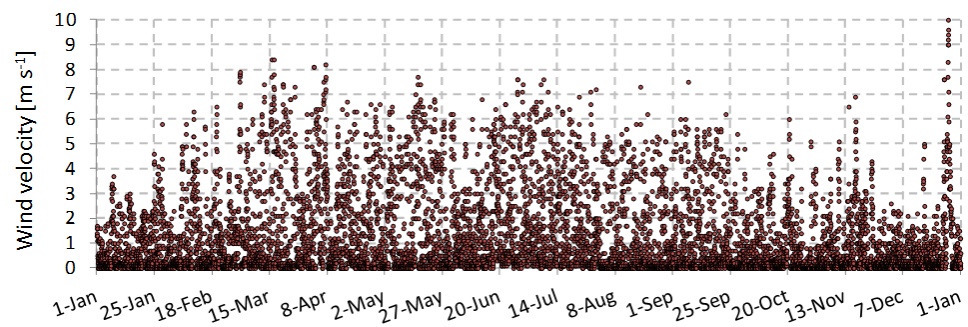
(a) Temperature



(b) Relative Humidity



(c) Solar irradiation



(d) Wind velocity

Figure 1.6: Test reference year obtained from Trento Sud historical series.

With the goal of assessing the representativeness of the TRY obtained and the conservation of the true frequencies and sequences, an analysis is herein presented. In the first test, the preservation of the annual degree days for heating and cooling is verified. In fact, since degree days are the sum of the temperature difference between internal setpoint and external temperature, they are strictly connected with heat losses/gains through the envelope. In degree day theory, the base temperature, or "balance point" of a building is the outside temperature at which internal setpoint is ensured without energy systems. No balance point is fixed for cooling degree day calculation instead, for heating degree days, an Italian decree [41] fixes the balance point in 20°C . Consequently, this standard neglects that the heating system has to supply only a part of the heat necessary to maintain the internal setpoint, i.e. 20°C . In fact, some heat comes from other sources such as the people and equipment in the building. However, the method of calculating an appropriate base temperature by subtracting the average internal heat gain from the building temperature is a sensible approximation.

In this analysis, the degree days refer to a balance point of 20°C for both heating and cooling calculation. The following Table 1.6 shows a good agreement between the average degree days of the historical series and those calculated using the TRY. The TRYs show deviation lower than 5% with respect to the mean degree days of the series. Only in Trento Sud CDD_{20} there is a bigger percentage error, also because the magnitude in Trento cooling degree days is very low.

Table 1.6: Degree days for historical series and for TRYs.

City	HDD ₂₀			CDD ₂₀		
	Series	TRY	Error	Series	TRY	Error
Trento	2763	2798	1.3%	219	197	-10.0%
Palermo	1027	994	-3.2%	696	704	1.2%

In the second test some considerations about extreme dry bulb temperature are done. Since TRYs are calculated with the final goal of energy analysis, it should be noticed that they have limitations in energy system sizing. In fact, in Table 1.7 the extreme and the design temperature, i.e. the 1% and 99% percentile, are reported. Results highlight the unfitness of TRY to the description of extreme phenomena, because of the selection procedure does not consider extreme temperature as primary weather variables. Consequently, TRYs do not preserve the 1% and 99% percentiles of the whole historical series. However, the fractiles 1% and 99% of TRY can be used with a good approximation in the

sizing of energy systems. In fact, an incomplete satisfaction of heating/cooling demand is still acceptable for a limited period.

Table 1.7: *Design temperature for system sizing.*

		Trento	Palermo
DBT_{min}	Series	-11.9	1.1
	TRY	-9.2	1.3
	Error	-22.7%	18.2%
DBT_{max}	Series	38.7	40.0
	TRY	33.2	36.2
	Error	-14.2%	-9.5%
DBT_{1%}	Series	-5.8	4.8
	TRY	-5.0	7.0
	Error	-13.8%	45.8
DBT_{99%}	Series	31.0	35.1
	TRY	30.5	32.3
	Error	-1.6%	-8.0%

Another test regards the preservation of the average trend of solar radiation. Because of the high insulation level and high mass of most opaque components, the main cooling loads are usually a result of solar radiation entering through the windows. Moreover, solar radiation is also an important heat gain in heating period. In Table 1.8 a comparison between the monthly average of daily solar radiation computed using the TRYs and mean values of the historical series is shown. The deviations are larger than those for monthly mean temperature however, they are in the satisfactory range between $\pm 10\%$. Consequently, also the true frequencies of solar irradiation are respected.

Finally, the preservation of the true correlation between weather variables is investigated. In Table 1.9 the average Pearson's index of the historical series and the one obtained with TRY are compared. Results clearly show that, despite the interpolation of weather data and the adjustment for the different month transitions, the true correlation is preserved for altogether, air temperature, relative humidity, wind velocity and solar irradiation.

In conclusion, this analysis highlights that the new Italian TRYs have the key features required for a test reference year [81]. In particular this selection procedure ensures the preservation of true sequences and frequencies of either temperature and solar irradiation and it also maintains the actual cross corre-

lation of weather variables. Instead, TRYs are not able to correctly represent the extreme weather conditions.

Table 1.8: *Monthly mean daily solar radiation [$MJ m^{-2}$].*

	Trento			Palermo		
	Series	TRY	Error	Series	TRY	Error
January	4.7	4.5	-5.6%	7.4	6.8	-8.2%
February	7.7	7.1	-8.8%	10.0	9.8	-2.1%
March	11.6	12.4	5.9%	14.7	14.5	-1.8%
April	14.3	14.6	1.7%	17.7	18.5	4.1%
May	17.8	19.1	6.9%	23.1	24.2	4.4%
June	19.7	19.3	-1.8%	25.1	24.7	-1.6%
July	20.6	22.3	7.7%	25.4	25.6	0.8%
August	18.0	17.8	-0.8%	22.1	22.4	1.2%
September	13.1	12.9	-1.7%	16.4	16.6	1.5%
October	8.2	7.9	-3.4%	12.1	11.1	-8.3%
November	5.0	4.8	-3.8%	8.9	8.7	-2.2%
December	3.6	3.7	1.6%	6.4	6.4	-0.3%

1.7 Comparison with other Italian weather sources

Even if the dynamic interaction between building and external climate thermal involves a large number of variables, the energy balance is mainly influenced by dry bulb temperature and solar irradiation. Since all building simulation programs require meteorological input data for their energy balances, the provisions of suitable weather data becomes critical.

In this section, it is investigated to what extent the procedure of selection of reference year affects the final hourly set of weather data. For this reason, a comparison between the possible sources of Italian weather data is required. In this comparison, the monthly mean values of standard UNI 10349 [1] are selected as benchmark. Table 1.10 shows the monthly mean values of external dry bulb temperature.

For Trento, the new TRY has lower values than the technical standard ¹ for winter and summer periods. Oppositely, the new Palermo TRY has generally

¹The reference monthly mean temperatures for Trento are not from UNI 10349 but from an erratum proposed in an internal document of the Energy Department of Trento Province [45]

higher external temperature than UNI 10349 [1994].

Table 1.9: *Comparison of Pearson's index.*

	Trento		Palermo	
	Series	TRY	Series	TRY
SI-DBT	0.510	0.512	0.526	0.555
DBT-WV	0.391	0.401	0.259	0.258
DBT-RH	-0.414	-0.433	-0.545	-0.552
GSI-WV	0.328	0.351	0.498	0.498
GSI-RH	-0.571	-0.570	-0.575	-0.567
WV-RH	-0.563	-0.570	-0.474	-0.435

Moreover, other sources are available for Palermo, i.e. De Giorgio [88] and IWECC [12] datasets. Also for these sources the deviation between monthly mean temperature are in the range of $\pm 10\%$.

Table 1.10: *Comparison between different sources of monthly mean temperature.*

	Trento		Palermo			
	UNI10349	TRY	UNI10349	TRY	DeGiorgio	IWECC
January	1.5	1.1	11.1	12.2	12.1	12.7
February	4.5	3.5	11.6	12.9	13.0	11.8
March	9.0	8.6	13.1	14.9	13.4	13.8
April	13.7	12.1	15.5	16.6	15.8	15.7
May	17.2	17.0	18.8	20.7	19.2	19.1
June	21.2	20.9	22.7	23.3	21.9	22.8
July	23.5	22.7	25.5	26.9	24.8	25.5
August	22.7	21.8	25.4	27.0	25.8	27.0
September	19.5	16.8	23.6	23.4	23.7	24.1
October	13.6	10.3	19.8	19.5	19.9	21.6
November	7.4	4.9	16.0	15.3	17.4	17.2
December	2.9	1.0	12.6	12.0	13.4	13.9

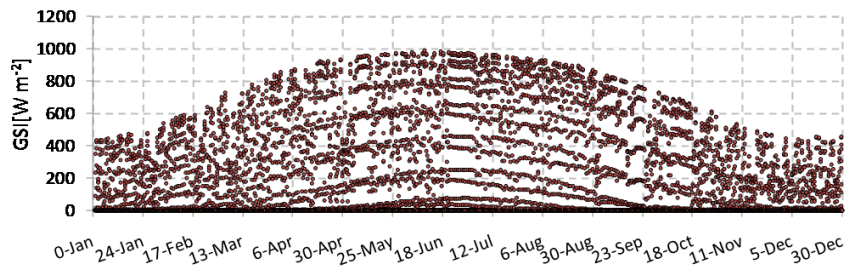
A similar comparison is performed for the monthly mean daily solar radiation. Table 1.11 clearly shows that UNI 10349 overestimates the solar radiation with respect to the new TRYs for both Trento and Palermo. Furthermore, also IWECC and De Giorgio give lower value than the technical standard UNI 10349.

In particular, there are very low values for De Giorgio dataset especially in winter months. This anomalous trend is highlighted in Figure 1.7 where both

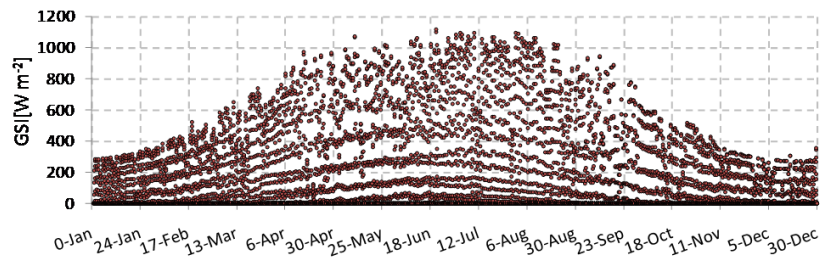
Table 1.11: Comparison between different sources of monthly mean daily solar radiation.

	Trento		Palermo			
	UNI10349	TRY	UNI10349	TRY	DeGiorgio	IWEC
January	4.9	4.5	7.7	6.8	5.7	7.5
February	8.4	7.1	11.1	9.8	8.3	10.9
March	13.7	12.4	15.7	14.5	12.7	15.0
April	17.7	14.6	20.8	18.5	17.4	20.2
May	20.9	19.1	25.2	24.2	21.9	23.5
June	23.2	19.3	27.9	24.7	23.7	26.2
July	24.6	22.3	27.9	25.6	24.3	26.4
August	20.2	17.8	25.2	22.4	21.6	23.8
September	15.5	12.9	19.6	16.6	15.8	17.8
October	9.4	7.9	13.5	11.1	10.2	13.2
November	5.5	4.8	9.3	8.7	6.5	7.7
December	4.1	3.7	6.9	6.4	4.8	6.5

the IWEC and De Giorgio trend of hourly solar irradiation are plotted.



(a) IWEC [12] solar irradiation for Palermo



(b) De Giorgio [88] solar irradiation for Palermo

Figure 1.7: Hourly global solar irradiation for Palermo

By comparing the De Giorgio trend, Figure 1.7 (b), with the new TRY, Figure 1.6(c), and the IWEC one, Figure 1.7(a), it can be seen that some errors rise up in the winter period where, for IWEC and TRY, the typical peak solar irradiation is about 400 Wm^{-2} while in De Giorgio is about 250 Wm^{-2} . Moreover, the shape of the curve in De Giorgio is very different from the other two sources.

Probably De Giorgio dataset is affected by errors due to a misconception of the weather file for the energy plus software (i.e. .epw weather file). In fact, the file requires the direct normal solar irradiation (DN) that is the amount of solar irradiation received by a surface always perpendicular to the sunbeams. In Figure 1.8 there is the DN trend obtained from De Giorgio dataset for Palermo. This graph clearly shows that the direct solar radiation on an horizontal plane is used in lieu of direct normal irradiation. The lower is the solar altitude the greater is the deviation between beam irradiation on an horizontal surface and direct normal irradiation. Consequently, the errors in De Giorgio solar irradiation are mainly in winter periods and in hours close to either sunrise and sunset.

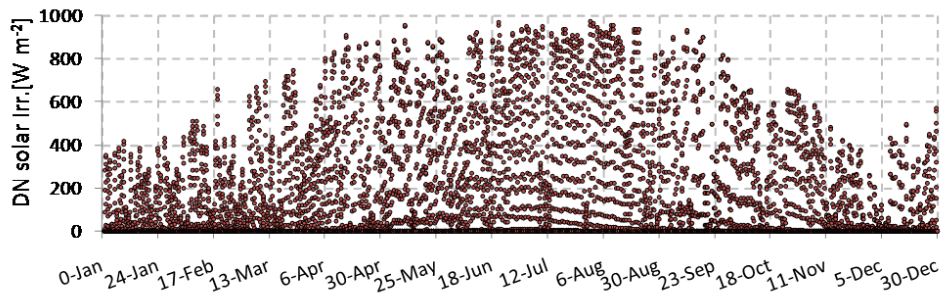


Figure 1.8: Direct Normal solar irradiation for Palermo.

1.8 Summarizing

In this chapter two test reference years (TRYs) for Italian cities are developed. The innovative point of this work is about the representativeness of these data and about the reliability of TRY for the evaluation of energy demand for building air conditioning. In fact, in the previous sources the cross correlation of weather data were often neglected. Moreover, some misconceptions in reference year constructions are highlighted by the comparison with the new TRYs. In the evaluation of typical weather variables, changes can be relevant. Consequently, the variability of weather input can lead to inaccuracy that could be cumulative

with the uncertainty in simulation model.

In the following sections, in order to assess to what extent the uncertainty of climate input can lead inaccuracy to cooling load predictions, a sensitivity analysis is carried out.

Chapter 2

Solar radiation models

The energy balance of a building is strictly connected with the solar irradiation. In order to compute the solar heat gains, a reliable estimation of the global irradiation incident on various inclined surfaces, starting from the measured data on a horizontal surface is essential. A variety of mathematical and empirical models have been proposed in the literature for both the decomposition of solar radiation in direct and diffuse components and for the projection of irradiation on tilted surfaces. However, no reliable pair of decomposition and projection models, which could be applied to worldwide stations, has been found.

In this chapter a briefly review of existing models is presented. Besides, with the aim of selecting the couple of procedure that produces less error in building simulation, the model expectations are compared to the actual solar irradiation measured during some experimental tests carried out in Trento. In this analysis, four statistical indicators are used for the rating of different model combinations.

2.1 Decomposition models

The first studies about the decomposition of global solar radiation in diffuse and direct parts were conducted by Liu and Jordan [77]. In this work, a relationship between daily diffuse and global solar radiation on clear days on a horizontal surface is proposed starting from measurements collected in meteorological station in the USA (Table 2.1). In particular, the diffuse fraction of solar irradiation k_d was correlated with the clearness index k_t that represents the portion of horizontal extraterrestrial radiation reaching the surface (Equation 1.2).

Table 2.1: *Location of weather stations used for the decomposition models.*

Model	City	Latitude	Longitude	Elevation	State
Liu et al. [77]	Blue Hill Ave	42°13'N	71°05'W	10	USA
Orgil et al. [100]	Toronto	43°48'N	79°23'W	106	CAN
Erbs et al. [44]	Fort Hood	31°07'N	97°46'W	280	USA
	Livermore	37°40'N	121°46'W	149	USA
	Raleigh	35°46'N	78°38'W	97	USA
	Maynard	42°46'N	71°26'W	50	USA
	Albuquerque	35°05'N	106°39'W	1619	USA
	Toronto	43°48'N	79°23'W	106	CAN
	Montreal	45°30'N	73°23'W	31	CAN
Spencer [120]	Alice Springs	23°49'S	133°53'E	576	AUS
	Mt Gambier	37°49'S	140°46'E	55	AUS
	Hobart	42°53'S	147°20'E	20	AUS
	Laverton	37°53'S	144°45'E	14	AUS
	Perth	31°57'S	115°51'E	15	AUS
Ma and Iqbal [83]	Goose Bay	53°24'N	60°25'W	35	CAN
	Trappes	48°46'N	2°00'E	168	FRA
	Carpentras	44°03'N	5°02'E	95	FRA
Hawladar [61]	Singapore	1°21'N	103°49'E	25	SIN
Muneer et al. [95]	New Delhi	28°36'N	77°12'E	210	IND
Reindl et al. [114]	Albany	42°39'N	73°35'W	60	USA
	Cape Canaveral	28°29'N	80°34'W	5	USA
	Copenhagen	55°41'N	12°34'E	10	DEN
	Hamburg	53°33'N	9°59'E	168	GER
	Valencia	39°28'N	0°22'E	15	SPA
	Oslo	59°54'N	10°45'E	5	NOR
Chandras. et al. [22]	Madras	13°04'N	80°16'E	8	IND
Chendo et al. [27]	Lagos	6°27'N	3°24'E	10	NIG
Lam and Li [76]	Hong Kong	22°50'N	114°11'E	306	CHI
de Miguel et al. [38]	Athens	37°58'N	23°42'E	107	GRE
	Lisboa	38°42'N	9°08'E	80	POR
	Coimbra	40°12'N	8°25'E	35	POR
	Evora	38°34'N	7°54'E	10	POR
	Faro	37°00'N	7°56'E	10	POR
	Oporto	41°08'N	8°36'E	100	POR
	Carpentras	44°03'N	5°02'E	95	FRA
	Pau	43°17'N	0°22'E	183	FRA
	Perpignan	42°41'N	2°53'E	42	FRA
	Madrid	40°24'N	3°42'E	664	SPA
	Sevilla	37°22'N	5°59'E	15	SPA
	Boland et al. [19]	Victoria	37°28'S	144°44'E	335
Oliveira et al. [99]	Saint Paul	23°33'N	46°38'W	760	BRA
Karatasou et al. [71]	Athens	37°58'N	23°42'E	107	GRE
Soares et al. [119]	Saint Paul	23°33'N	46°38'W	760	BRA

Following the Liu's approach [77], Orgill and Hollands [100] tried to correlate the hourly diffuse ratio k_d to the hourly clearness index k_t . In this study, four years of hourly data collected in Canadian meteorological stations were used.

Erbs et al. [44] followed the procedure of Orgill and Hollands [100] to develop a regression model using a dataset of 65 months covering five locations over the USA (Table 2.1). A similar research was carried out by Muneer et al. [95] for New Delhi. In a study for five Australian locations, Spencer [120] found a latitude effect on the diffuse ratio, consequently he proposed a new correlation.

On the other hand, Ma and Iqbal [83] and Skartveit and Olseth [118] used two predictors for their correlations: k_t and the solar elevation α .

Skartveit and Olseth [118] introduced then a new parameter: the hour-to-hour variability index. This parameter considers the variation of the clearness index of the previous and the following time interval. They used hourly data from several European stations discarding periods where a snow cover was present.

Reindl et al. [114] added two more significant predictors to the clearness index and the solar elevation, i.e. the external dry bulb temperature and the relative humidity. With these new parameters, they were able to reduce the standard error of Liu and Jordan [77] derived models. They used stepwise regression to reduce a set of 28 potential variables down to four significant predictors. In this study, the authors processed hourly data for several weather stations both in European and North American locations.

Oppositely, Boland et al. [19] asserted that the predictability is not relevantly improved when solar elevation is used as parameter. Moreover, they state that hourly time step is short enough for a reliable prediction. They also affirmed that the apparent solar time is a good second variable for the calculation of diffuse ratio.

During the last thirty years, several works have been done on the diffuse fraction estimation, most of them used the same correlation of previous researches. In these studies the authors try to adjust the correlation coefficients in order to adapt the formula to a specific climate [22, 27, 38, 61, 71, 76, 99, 119].

The above mentioned models were compared to each other on different locations. For instance Notton et al. [98] compared various models on Ajaccio, Jacovides et al. [69] use solar irradiation collected in Cyprus for the model validations and a similar work was done by Katiyar et al. [72] for Indian locations.

For the analysis of the applicability and reliability of empirical correlations in the Italian context, 17 models are implemented in this work (Table 2.2).

Table 2.2: *Decomposition models used in the comparison.*

Model	Parameters	Range	Relation
Orgill [100]	k_t	$0 \leq k_t < 0.35$	Linear
	k_t	$0.35 \leq k_t < 0.75$	Linear
	–	$0.75 \leq k_t$	Constant
Erbs [44]	k_t	$0 \leq k_t \leq 0.22$	Linear
	k_t	$0.22 < k_t \leq 0.8$	Quadratic
	–	$0.8 < k_t$	Constant
Spencer [120]	ϕ	$0 \leq k_t < 0.35$	Linear
	ϕ, k_t	$0.35 \leq k_t \leq 0.75$	Linear
	ϕ	$0.75 < k_t$	Linear
Hawlander [61]	–	$0 \leq k_t \leq 0.225$	Constant
	k_t	$0.225 < k_t < 0.775$	Quadratic
	–	$0.775 \leq k_t$	Constant
Muneer [95]	–	$0 \leq k_t < 0.175$	Constant
	k_t	$0.175 \leq k_t \leq 0.775$	Cubic
	–	$0.775 < k_t$	Constant
Reindl v1 [114]	k_t	$0 \leq k_t \leq 0.3$	Linear
	k_t	$0.3 < k_t < 0.78$	Linear
	–	$0.78 \leq k_t$	Constant
Reindl v2 [114]	$k_t, \sin(\alpha)$	$0 \leq k_t \leq 0.3$	Linear
	$k_t, \sin(\alpha)$	$0.3 < k_t < 0.78$	Linear
	$\sin(\alpha)$	$0.78 \leq k_t$	Linear
Reindl v3 [114]	$k_t, \sin(\alpha), DBT, RH$	$0 \leq k_t \leq 0.3$	Linear
	$k_t, \sin(\alpha), DBT, RH$	$0.3 < k_t < 0.78$	Linear
	$k_t, \sin(\alpha), DBT, RH$	$0.78 \leq k_t$	Linear
Chandrasekaran [22]	k_t	$0 \leq k_t \leq 0.24$	Linear
	k_t	$0.24 < k_t \leq 0.8$	Quartic
	–	$0.8 < k_t$	Constant
Chendo v1 [27]	k_t	$0 \leq k_t \leq 0$	Linear
	k_t	$0.3 < k_t \leq 0.3$	Linear
	–	$0.8 < k_t$	Constant
Chendo v2 [27]	$k_t, \sin(\alpha)$	$0 \leq k_t \leq 0$	Linear
	$k_t, \sin(\alpha)$	$0.3 < k_t \leq 0.3$	Linear
	$k_t, \sin(\alpha)$	$0.8 < k_t$	Linear
Lam - Li [76]	–	$0 \leq k_t \leq 0.15$	Constant
	k_t	$0.15 < k_t < 0.7$	Linear
	–	$0.7 \leq k_t$	Constant
de Miguel [37]	k_t	$0 \leq k_t \leq 0.21$	Linear
	k_t	$0.21 < k_t \leq 0.76$	Cubic
	–	$0.76 < k_t$	Constant
Boland [19]	k_t	$0 \leq k_t \leq 1$	Exponential
Oliveira [99]	–	$0 \leq k_t \leq 0.17$	Constant
	k_t	$0.17 < k_t \leq 0.75$	Quartic
	–	$0.75 < k_t$	Constant
Karatasou [71]	k_t	$0 < k_t \leq 0.75$	Cubic
	–	$0.75 < k_t$	Constant
Soares [119]	–	$0 \leq k_t \leq 0.17$	Constant
	k_t	$0.17 < k_t \leq 0.75$	Quartic
	–	$0.75 < k_t$	Constant

2.2 Projection models

Starting from the diffuse and beam irradiation on horizontal plane, a projection model is required for the estimation of solar irradiation on a tilted surface. While the projection of beam solar irradiance is based on trigonometric relations, for the diffuse fraction of solar irradiance the anisotropy of the sky and of the ground reflections have to be taken into account.

As reported in [93], the mathematical models for the calculation of solar irradiation on a slope surface can be divided in three categories:

- First generation: the simplest and earliest models based on strong assumptions (e.g. [67, 77, 83]);
- Second generation: these models differentiate the radiance distribution between clear and overcast skies (e.g. [20, 62, 74, 113, 117, 125]);
- Third generation: these models consider the anisotropy of the diffuse irradiation. Consequently, they decompose the diffuse irradiance in two components that are the circumsolar and background sky diffuse (e.g. [54, 92, 94, 104, 105, 106]).

The first model for the evaluation of solar radiation on tilted surface was developed by Hottel and Woertz [67] and modified by Liu and Jordan [77]. In these study the main assumption is the isotropic behavior of the sky. Consequently, also the diffuse irradiation can be evaluated using trigonometric relations.

Temps and Coulson [125] observed both an increased intensity of diffuse radiation near the horizons and in the circumsolar region of the sky. Therefore they introduced two corrective coefficients to the Liu and Jordan [77] model. Klucher [74] progressed the work of Temps and Coulson and, in order to obtain a better provision for part-overcast conditions, he adjusted the corrective coefficients. Moreover, Hay and Davies [62], Skartveit and Olseth [117] and Reindl et al. [113] followed the approach of Klucher and proposed different weighting factors for the circumsolar and uniform background diffuse components.

Ma and Iqbal [83] assumed that sky diffuse radiation, as well as the beam component, comes from the sun disc. Due to this strong assumption, this method provides reliable results only for clear sky conditions.

In Gueymard [54] the sky diffuse irradiance on a tilted surface is computed as a function of the radiance distribution in the sky. Moreover Gueymard assumed that the radiance of a partly cloudy sky can be estimated by means of a weighted sum of radiance for clear and overcast sky conditions.

Perez et al. [104] and Perez et al. [106] proposed a model based on a subdivision of the sky diffuse irradiance in three components, i.e the horizon brightness, the isotropic and the circumsolar irradiation.

Muneer [92] analyzed separately the shaded and sunlit surfaces and he distinguished between overcast and non overcast conditions. He defined a linear relationship between a vertical surface and horizontal diffuse irradiance. Besides using several data recorded in worldwide weather stations, he proposed four different slopes of this linear curve [93].

The above mentioned models were compared to each other on different locations. For instance, Loutzenhiser et al. [79] compared 7 radiation models using actual values of beam and diffuse horizontal irradiation in Switzerland. Similar studies were carried out by Chirarattananon et al. [29] using solar data collected in Bangkok and by Noorian et al. [97] with Tehran measurements.

In Gueymard [55] actual solar irradiance on a tilted surface is compared to predictions from 10 transposition models in combination with either optimal or suboptimal input data of horizontal irradiance. In particular suboptimal inputs deal with the misestimation of the diffuse over global solar irradiance on horizontal surface and with the uncertainty in the albedo representation.

Table 2.3: *Projection models used in the comparison.*

Model	Generation	Circumsolar Anisotropy	Horizons Anisotropy
Liu and Jordan [77]	First		
Bugler [20]	Second	X	
Temps and Coulson [125]	Second	X	X
Klucher [74]	Second	X	X
Hay and Davies [62]	Second	X	X
Ma and Iqbal [83]	First		
Skartveit and Olseth [117]	Second	X	X
Gueymard [54]	Third	X	X
Reindl et al. [113]	Second	X	X
Perez et al. [106]	Third	X	X
Muneer [92] Overcast Skies	Third	X	X
Muneer [92] Non Overcast Skies	Third	X	X

Finally, for the analysis of the applicability and reliability of empirical models

in the Italian context, 12 models are implemented and compared in this work (Table 2.3).

2.3 Experimental activity

In order to evaluate the robustness of various radiation models, a comparison between experimental measurements and the models expectations is carried out. The model provisions are obtained by combining 17 methods for the decomposition of the global irradiation in the beam and diffuse parts (Table 2.2) with 12 models for the projection of radiation on a tilted surface (Table 2.3).

The experimental tests are performed in the campus of the University of Trento. This site is located on the South side of the hill surrounding the city of Trento in North of Italy (Table 2.4). Since the annual average of direct normal solar radiation (DN) is 5.85 kWh m^2 [43], the location can be defined as relatively favorable for solar application [57].

Table 2.4: *Geographical coordinates of the experimental location.*

Site	Latitude	Longitude	Elevation
Mesiano - Trento	$46^\circ 03' 53'' N$	$11^\circ 08' 17'' E$	275 m a.s.l.

The data are collected and recorded every 10 minutes and they cover 6 months from June 2011 to November 2011. This period includes a range of different atmospheric conditions and solar positions.

Two pyranometers are used for the experimental test (Table 2.5). The global irradiance is obtained by a net radiometer $NR01$, instead, a $CMP6$ pyranometer provides measures on a vertical plane that faces to South direction (Figure 2.1).

Table 2.5: *Instruments used in experimental test.*

Parameter	Instruments	Manufacturer	Model	ISO 9060 class	Accuracy
GSI Vertical surf	Pyranometer	Kipp & Zonen	CMP6	First	$\pm 5\%$
GSI horizontal	Net radiometer	Hukseflux	NR01	Second	$\pm 10\%$
Ground reflection	Net radiometer	Hukseflux	NR01	Second	$\pm 10\%$
RH	capacitive	Rotronic	Hygroclip S	—	$\pm 0.8\%$
DBT	thermoreistance	Rotronic	Hygroclip S	—	$\pm 0.1^\circ C$

Other parameters such as temperature, relative humidity, wind velocity and ground albedo are also recorded. Consequently, the ground albedo is measured by means of a net radiometer and used in lieu of default values.



Figure 2.1: *Pyranometers used in the experimental test*

Further, the measurements is checked against quality control rules and, in addition to the criterion (1.3), all data points with albedo values beyond some acceptable limits (i.e. $0.1 \div 1$) are rejected. Although this quality control, some outliers arise whenever external obstacles provide shadow only for the tilted radiometer, or vice versa.

2.4 Results and comparison

In this study, with the purpose of investigating to what extent model predictions are accurate, several decomposition and projection models (Table 2.1 and Table 2.3) are implemented by means of the software MATLAB [87]. The accuracy of the different couples of decomposition and projection methods is assessed by the comparison against actual measured values. This analysis tries to reproduce what would be typical in building energy simulations. In fact, since Italian meteorological stations record only global horizontal solar irradiation, empirical methods have to be used to obtained the other solar data.

Figure 2.2 shows the comparison among four projection models using the decomposition procedure proposed by Erbs et al. [44]. These scatter graphs clearly indicate the error arising with a systematic underestimation of the simplified method, i.e. [77] and [125].

Besides, in each method the deviation between measured and predicted data

is held down for high solar irradiation that means clear sky conditions. Instead, the distance increases in the range of $200 \div 400 \text{ W m}^{-2}$ of solar irradiance. This could be expected because, for clear sky conditions, the sky diffuse irradiance is low and consequently the uncertainty in diffuse radiation models is limited. Moreover, since values of $200 \div 400 \text{ W m}^{-2}$ are typical of partial sky conditions or of low solar altitude, the uncertainties in model provisions increase.

2.4.1 Statistical indicators

The accuracy of the different couples of decomposition and projection methods is assessed by means of the widely used statistical indicators, i.e. the mean bias error (*MBE*) and the root mean square error (*RMSE*) [83].

The *MBE* provides information on the long-term performance of a model. A positive value represents the average amount of overestimation in the estimated values and vice versa. A drawback of this index arises from the compensation between overestimations and underestimations.

The second index proposed by Ma and Iqbal [83] is the *RMSE*. This parameter provides information about the short-term performance of the method by means of a term by term comparison. The smaller the *RMSE* value, the better is the model provisions. However, this test does not differentiate between under and overestimation and a few large errors can produce a significant increase in the *RMSE* index.

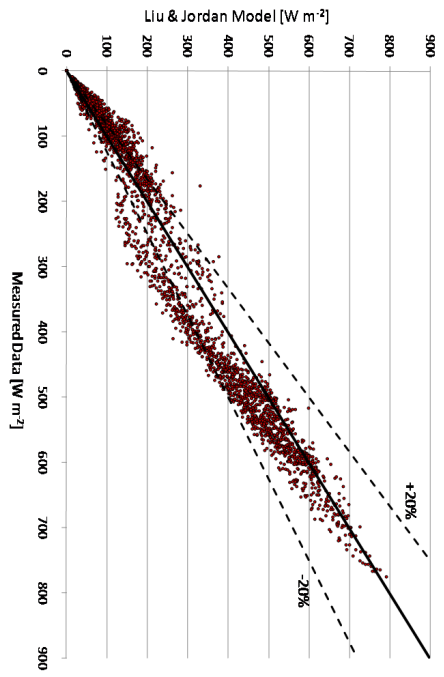
$$MBE = \frac{\sum_{i=1}^N M_i - E_i}{N} \quad (2.1)$$

$$RMSE = \sqrt{\frac{\sum_{i=1}^N (M_i - E_i)^2}{N}} \quad (2.2)$$

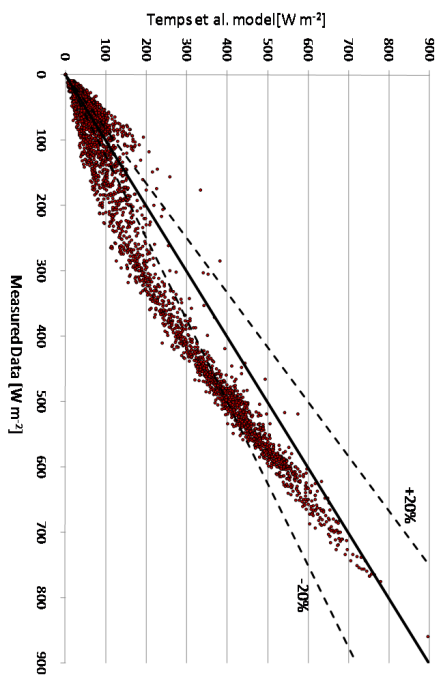
where M_i indicates the measured solar irradiation, E_i the model predictions and N the number of sample data.

Nevertheless, these statistical indexes can produce conflicting results. In fact, at the same time it is possible to have a large *RMSE* and small *MBE* that means a significant even scatter estimation about the measured data. Otherwise, simultaneously high *MBE* and low *RMSE* values indicate a consistently small over or underestimation.

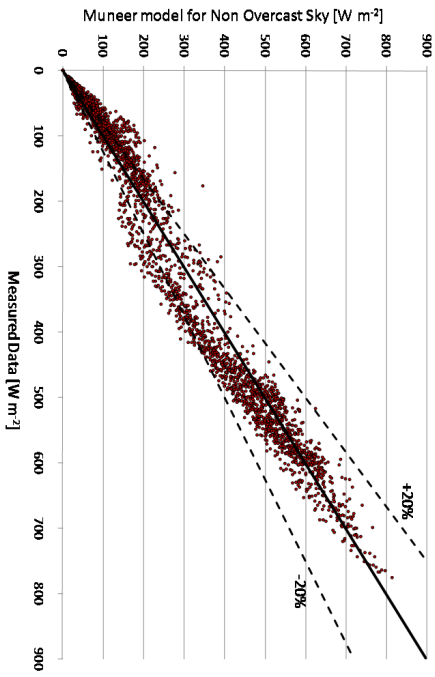
Graphical analysis of *MBE* and *RMSE* are reported respectively in Figure 2.3 and Figure 2.4. The *MBE* graph (Figure 2.3) shows that the early methods (i.e. first and second generations) usually underestimate the solar irradiation on vertical surface facing to South. This difference between measured and esti-



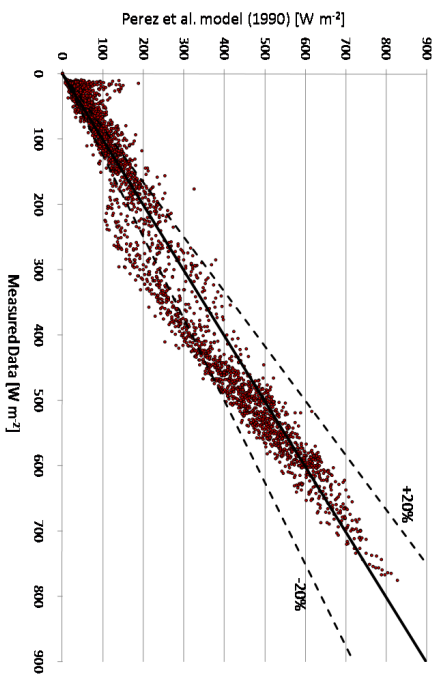
(a) Liu and Jordan [77]



(b) Temps and Coulson [125]



(c) Muneer [92]



(d) Perez et al. [106]

Figure 2.2: Comparison between models provisions and measures using Erbs method for vertical surface facing to South.

mated values decreases when third generation models are applied. Besides, the Reindl et al. [113] and Muneer [92] models exhibit a quite consistently lower bias error and therefore appear to better preserve the mean solar irradiance recorded. In Figure 2.3 similar results are obtained with Erbs [44] and Reindl [114] decomposition models. Conversely, when the Spencer [120] relation is used, the errors seem to cancel each other out. This diverse behavior between simplified and

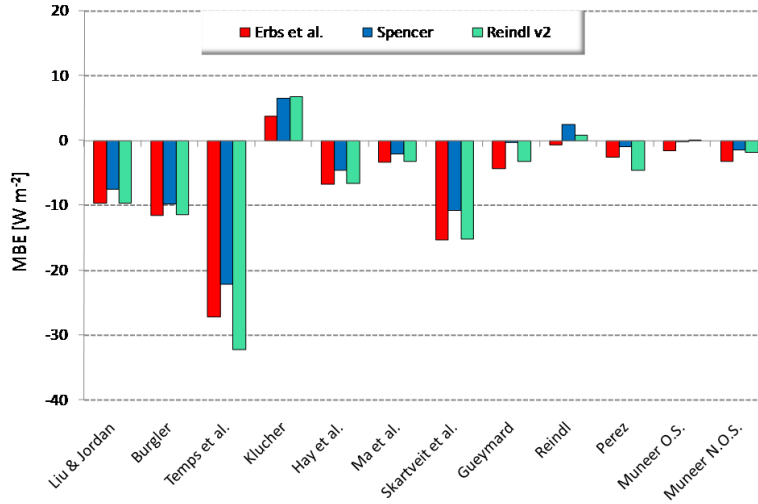


Figure 2.3: Mean Bias Error

third generation models is not so evident in the $RMSE$ values (Figure 2.4). In fact, for all projection models, except for Temps and Coulson [125], the $RMSE$ are in the range of $40 \div 50 W m^{-2}$. Moreover, there are no appreciable spread among $RMSE$ values obtained with different decomposition methods. Badescu [14] affirmed that the dimensional values of $RMSE$ and MBE do not allow model testing. For this reason, with the purpose of better understanding the magnitude of model deviations with respect to the measured solar irradiance, the relative $RMSE$ and MBE proposed by Davies and Mc Kay [33] is calculated. These indexes are a dimensionless measure of $RMSE$ and MBE and can be defined as follows.

$$MBE_{\%} = \frac{\sum_{i=1}^N M_i - E_i}{N \cdot \bar{M}} \quad (2.3)$$

$$RMSE_{\%} = \sqrt{\frac{\sum_{i=1}^N (M_i - E_i)^2}{N \cdot \bar{M}^2}} \quad (2.4)$$

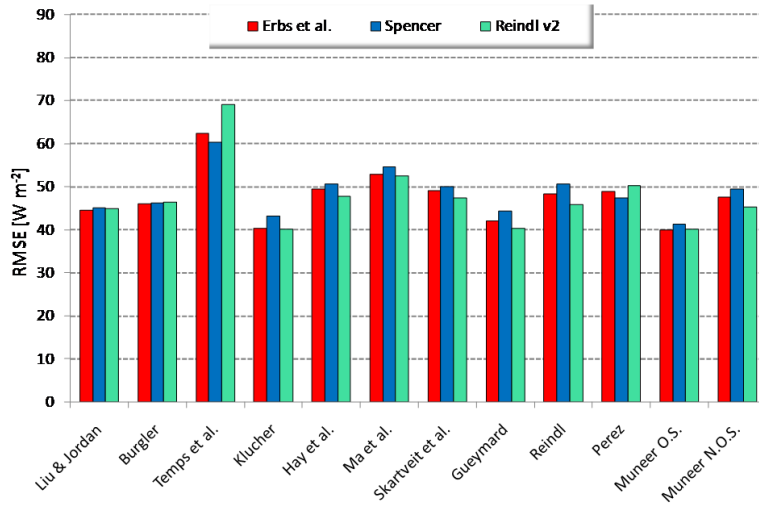


Figure 2.4: Root Mean Square Error

where \bar{M} indicates the mean values of measured solar irradiation on tilted surface.

In Table 2.6 the percentage values of MBE and $RMSE$ are reported. Except for some projection models, the $MBEs$ are always below the $\pm 5\%$ with very low values for the third generation models. The low bias percentage error suggests that the anisotropy models preserve the mean value of solar irradiation. Instead, Temps and Coulson [125] model underestimates solar irradiance on a tilted surface by a wide margin in comparison to other models.

Table 2.6 exhibits also a small sensitivity of both MBE and $RMSE$ to the change of decomposition model. In fact, in every column, the variability of the percentage indexes is limited. Due to the compensation of over and under estimations, for the bias error the influence of decomposition model increases. These results reveal that the uncertainty in solar models is principally in the transposition model. Besides, the relative high uncertainty in model provisions for vertical surfaces can be related to the high ratio of diffuse to global solar radiation. Consequently, model predictions become very sensitive to any inaccuracies in the evaluation of the effective ground albedo and to the incorrect modeling of the sky anisotropy behavior.

2.4.2 Enhanced Statistical indicators

Since the final purpose of the building energy simulation is the evaluation of energy consumptions, it is essential to correctly predict the average behavior of the building. Consequently, it is more important to correctly estimate the

Table 2.6: Results of percentage MBE and RMSE for different couples of models.

(a) Results of percentage MBE

Models	Liu et al.	Burgler et al.	Temps et al.	Klucher et al.	Hay et al.	Ma Iqbal et al.	Skartveit et al.	Gueymard	Reindl	Perez	Muneer O.S.	Muneer N.O.S.
Orgill	-4.3%	-5.1%	-12.2%	2.1%	-3.0%	-1.4%	-6.5%	-1.7%	0.1%	-1.7%	-0.6%	-1.3%
Erbs	-4.1%	-4.9%	-11.7%	1.6%	-2.9%	-1.4%	-6.6%	-1.9%	-0.3%	-1.1%	-0.7%	-1.4%
Spencer	-3.2%	-4.2%	-9.5%	2.8%	-2.0%	-0.9%	-4.6%	-0.1%	1.1%	-0.4%	-0.1%	-0.6%
Hawlander	-3.9%	-4.8%	-11.9%	3.4%	-2.5%	-1.2%	-5.3%	-0.1%	1.0%	-1.6%	0.1%	-0.6%
Muneer	-4.6%	-5.3%	-14.0%	3.5%	-3.0%	-1.4%	-6.0%	-0.8%	0.9%	-2.6%	-0.1%	-0.8%
Reindl v1	-4.2%	-5.0%	-11.8%	1.8%	-2.9%	-1.4%	-6.4%	-1.8%	-0.1%	-1.3%	-0.7%	-1.3%
Reindl v2	-4.2%	-4.9%	-13.9%	2.9%	-2.8%	-1.4%	-6.5%	-1.3%	0.4%	-2.0%	0.1%	-0.8%
Reindl v3	-7.5%	-8.2%	-15.5%	-1.5%	-6.8%	-2.3%	-11.1%	-5.9%	-3.9%	-1.1%	-3.8%	-5.1%
Chandrasekaran	-4.3%	-5.1%	-12.6%	2.2%	-2.9%	-1.5%	-6.5%	-1.5%	0.0%	-1.3%	-0.5%	-1.2%
Chendo v1	-5.5%	-6.2%	-16.3%	2.6%	-3.9%	-1.9%	-7.7%	-2.5%	-0.3%	-4.5%	-0.9%	-1.5%
Chendo v2	-6.2%	-6.8%	-16.2%	1.5%	-4.6%	-2.1%	-8.5%	-3.6%	-1.0%	-5.1%	-1.9%	-2.3%
Lam - Li	-4.3%	-5.1%	-13.6%	3.4%	-2.8%	-1.4%	-5.9%	-0.7%	0.6%	-2.1%	0.1%	-0.7%
de Miguel	-4.2%	-5.0%	-12.1%	2.0%	-2.9%	-1.4%	-6.5%	-1.6%	-0.1%	-1.3%	-0.6%	-1.3%
Boland	-4.4%	-5.2%	-12.0%	1.9%	-3.0%	-1.5%	-6.4%	-1.8%	0.1%	-1.5%	-0.8%	-1.3%
Oliveira	-3.9%	-4.8%	-11.4%	2.0%	-2.7%	-1.3%	-6.1%	-1.3%	-0.2%	-1.2%	-0.4%	-1.1%
Karatasou	-4.0%	-4.9%	-12.2%	3.3%	-2.6%	-1.2%	-5.4%	-0.2%	0.9%	-1.7%	0.0%	-0.7%
Soares	-3.6%	-4.5%	-10.8%	2.4%	-2.4%	-1.2%	-5.5%	-0.7%	0.2%	-0.9%	-0.1%	-0.9%

(b) Results of percentage RMSE

Models	Liu et al.	Burgler et al.	Temps et al.	Klucher et al.	Hay et al.	Ma Iqbal et al.	Skartveit et al.	Gueymard	Reindl	Perez	Muneer O.S.	Muneer N.O.S.
Orgill	19.1%	19.7%	27.3%	16.9%	20.8%	22.6%	20.6%	17.5%	20.3%	20.6%	16.9%	19.9%
Erbs	19.2%	19.8%	26.9%	17.4%	21.3%	22.8%	21.1%	18.1%	20.8%	21.1%	17.2%	20.5%
Spencer	19.4%	19.9%	26.0%	18.6%	21.8%	23.5%	21.5%	19.1%	21.8%	20.4%	17.8%	21.3%
Hawlander	18.7%	19.3%	27.4%	17.0%	20.7%	23.0%	20.4%	17.4%	20.3%	19.7%	16.5%	19.8%
Muneer	18.8%	19.5%	29.2%	16.3%	19.8%	22.4%	19.5%	16.2%	19.1%	20.1%	16.3%	18.6%
Reindl v1	19.0%	19.7%	26.9%	17.1%	21.0%	22.8%	20.8%	17.7%	20.5%	20.7%	16.9%	20.2%
Reindl v2	19.4%	20.0%	29.7%	17.2%	20.6%	22.6%	20.4%	17.4%	19.8%	21.6%	17.3%	19.5%
Reindl v3	30.1%	30.5%	33.6%	29.2%	31.3%	22.5%	35.1%	31.8%	30.9%	20.7%	29.1%	30.8%
Chandrasekaran	18.9%	19.5%	27.6%	16.8%	20.8%	22.6%	20.6%	17.4%	20.2%	20.5%	16.6%	19.8%
Chendo v1	19.9%	20.6%	31.3%	16.1%	19.4%	21.6%	19.2%	15.8%	17.9%	22.7%	17.2%	17.8%
Chendo v2	21.2%	21.9%	31.0%	16.5%	19.7%	21.3%	19.6%	16.5%	18.0%	24.9%	18.3%	18.1%
Lam - Li	18.7%	19.3%	29.0%	16.7%	20.2%	22.7%	20.0%	16.7%	19.5%	19.8%	16.3%	19.1%
de Miguel	19.0%	19.6%	27.1%	17.0%	21.0%	22.7%	20.8%	17.7%	20.5%	20.8%	16.8%	20.1%
Boland	19.3%	19.9%	27.2%	17.1%	20.9%	22.6%	20.6%	17.6%	20.4%	20.6%	17.0%	20.0%
Oliveira	18.9%	19.5%	26.7%	17.4%	21.3%	23.1%	21.1%	18.1%	20.8%	20.2%	16.8%	20.5%
Karatasou	18.6%	19.3%	27.6%	16.9%	20.6%	23.0%	20.3%	17.3%	20.2%	19.5%	16.4%	19.7%
Soares	18.9%	19.5%	26.5%	17.9%	21.6%	23.4%	21.3%	18.5%	21.3%	20.0%	17.1%	20.9%

average solar radiation rather than the peak solar irradiance. Furthermore the *RMSE* and *MBE* do not indicate whether model estimations are statistically significant.

Thus, Stone [123] proposed the t-statistic hypothesis test of the mean as an assessing index. Besides, he demonstrated that the use of the root mean square and mean bias errors separately can lead to an incorrect selection of the suitable method for solar estimation. The t-statistic assumes that the samples have a normal or moderately skewed distribution. It is a signal to noise indicator and t is defined as:

$$t = \frac{\sum_{i=1}^N M_i - E_i}{\sqrt{\frac{\sigma^2}{N}}} \quad (2.5)$$

Starting from the definition of *RMSE* and *MBE*, relation (2.5) can be written as:

$$t = \sqrt{\frac{(N-1) \cdot MBE^2}{RMSE^2 - MBE^2}} \quad (2.6)$$

where σ is the standard deviation between measured and estimated values.

The smaller the value of t , the better the performance of the model is. In order to determine whether model provisions are statistically significant, a critical t-value (t_{cr}) should be simply determined from standard statistical tables for the two tailed test at the specified level of significance $\left(\frac{\beta}{2}\right)$ and $N-1$ degrees of freedom. Model predictions are statistically significant at the $1-\beta$ confidence level, if the t-value is less than t_{cr} [123].

The rule of thumbs, for environmental analysis, is to set the β level at 0.05 that means for this experimental activity a t_{cr} equal to 1.96. Consequently, if the null hypothesis is correct, the confidence level of the model provisions is 95 %.

The t-statistic values obtained for different couples of decomposition-projection models are reported in Table 2.7(a). T-statistic test leads to similar conclusion with respect to the *MBE* analysis. As shown in Table 2.7(a), it is obvious that the third generation models have lower t-statistic values and consequently they perform best as the *MBE* values are lower. The relevant result of this comparison is the magnitude of t-statistic indexes. In fact, only two projection models (see Reindl et al. [113] and Muneer [92]) have t lower than t_{cr} for most of the decomposition procedure and, consequently, are statistically significant with a 95% of confidence interval. For the other third generation models (i.e. Gueymard [54] and Perez et al. [106]), the null hypothesis is confirmed only for

few decomposition models hence, these methods do not generally preserve the mean values of measured data.

However, the t-statistic analysis has a weakness. In fact, this procedure is based on the assumption of normal or moderately skewed distribution of sample data. Generally, the distribution can be approximated as normal if it is moderately skewed, unimodal, without outliers and with a large sample size.

In the solar data collected, the assumption of unimodal distribution is not verified. Indeed, due to the mountain shadow on the experimental locations, the solar irradiation on the vertical surface has a bimodal distribution, Figure 2.5(a). When the sun goes behind the mountains, the direct solar irradiation decreases and, consequently, there is a second maximum in the probability density function (PDF) at about 100 Wm^{-2} . Therefore the boundary conditions of the experimental test reduce the reliability of the t-statistic test.

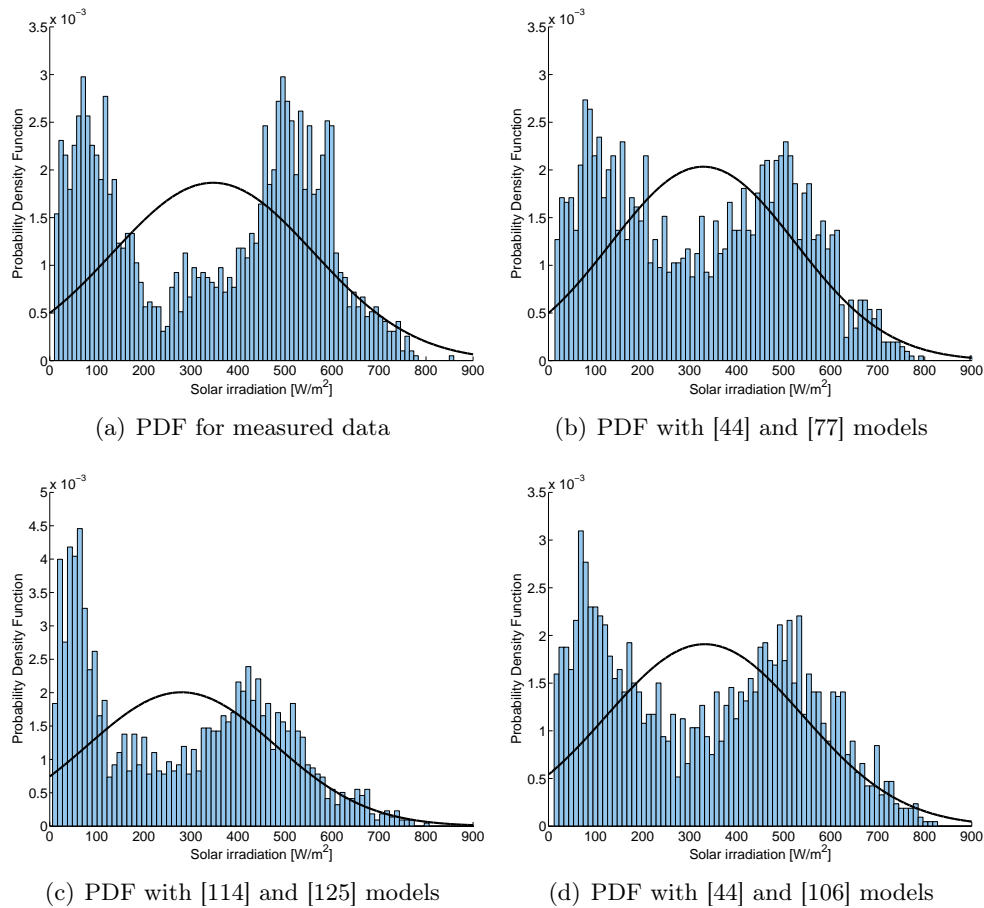


Figure 2.5: *Probability Density Function for measured and estimated data.*

Table 2.7: Result of *t*-statistic and correlation index for different couples of models.

(a) Results of *t*-statistic test.

Models	Liu et al.	Burgler	Temps et al.	Klueber	Hay et al.	Ma Iqbal et al.	Skartveit et al.	Gueymard	Reindl	Perez	Muneer O.S.	Muneer N.O.S.
Orgill	15.6	18.0	33.7	8.4	9.6	4.3	22.2	6.4	0.4	5.5	2.5	4.3
Erbs	14.8	17.3	32.5	6.3	9.1	4.2	22.1	7.0	0.8	3.6	2.6	4.5
Spencer	11.3	14.4	26.5	10.3	6.1	2.5	14.8	0.4	3.3	1.3	0.3	1.9
Hawlander	14.5	17.2	32.4	13.5	8.1	3.4	17.9	0.2	3.3	5.3	0.3	2.1
Muneer	16.8	19.1	36.6	14.8	10.3	4.3	21.8	3.3	3.0	8.7	0.3	2.8
Reindl v1	15.3	17.7	32.8	7.3	9.3	4.2	21.8	6.7	0.3	4.3	2.7	4.4
Reindl v2	14.8	17.1	35.5	11.6	9.3	4.1	22.7	5.2	1.3	6.1	0.2	2.7
Reindl v3	17.2	18.8	34.8	3.4	14.9	6.9	22.4	12.7	8.6	3.5	8.9	11.4
Chandrasekaran	15.8	18.2	34.5	8.8	9.6	4.4	22.5	5.8	0.1	4.4	1.9	4.1
Chendo v1	19.4	21.1	40.9	11.0	13.9	5.8	29.5	10.7	1.0	13.5	3.5	5.8
Chendo v2	20.6	22.1	41.2	6.2	16.0	6.7	32.4	14.9	3.9	14.0	6.9	8.7
Lam - Li	16.1	18.5	35.7	14.0	9.5	4.1	20.9	2.8	2.2	7.1	0.4	2.5
de Miguel	15.3	17.8	33.4	7.7	9.3	4.3	22.0	6.2	0.2	4.2	2.2	4.3
Boland	15.7	18.1	33.1	7.6	9.6	4.3	22.0	6.8	0.2	5.0	3.2	4.5
Oliveira	14.4	17.0	31.8	7.8	8.4	3.9	20.4	4.9	0.6	4.0	1.5	3.6
Kararason	14.9	17.6	32.9	13.4	8.4	3.6	18.4	0.8	3.0	5.9	0.2	2.3
Soares	13.1	15.9	29.9	8.9	7.4	3.4	18.0	2.5	0.7	3.2	0.5	2.7

(b) Results of correlation index

Models	Liu et al.	Burgler	Temps et al.	Klueber	Hay et al.	Ma Iqbal et al.	Skartveit et al.	Gueymard	Reindl	Perez	Muneer O.S.	Muneer N.O.S.
Orgill	98.4%	98.4%	97.4%	98.6%	97.9%	97.4%	98.1%	98.5%	97.9%	97.9%	98.6%	98.0%
Erbs	98.4%	98.3%	97.3%	98.5%	97.8%	97.4%	98.0%	98.4%	97.8%	97.8%	98.5%	97.9%
Spencer	98.2%	98.2%	97.2%	98.3%	97.6%	97.2%	97.8%	98.2%	97.6%	97.9%	98.4%	97.7%
Hawlander	98.5%	98.5%	97.4%	98.6%	97.9%	97.3%	98.0%	98.3%	97.9%	98.1%	98.7%	98.0%
Muneer	98.6%	98.6%	97.5%	98.7%	98.1%	97.5%	98.3%	98.7%	98.2%	97.9%	98.7%	98.3%
Reindl v1	98.4%	98.4%	97.3%	98.6%	97.8%	97.4%	98.0%	98.5%	97.9%	97.7%	98.6%	98.0%
Reindl v2	98.4%	98.4%	97.1%	98.6%	97.9%	97.4%	98.1%	98.3%	98.0%	97.7%	98.3%	98.1%
Reindl v3	95.9%	95.9%	96.3%	95.7%	95.3%	97.5%	94.3%	95.0%	95.2%	97.9%	95.8%	95.3%
Chandrasekaran	98.5%	98.4%	97.4%	98.6%	97.9%	97.4%	98.1%	98.5%	98.0%	97.9%	98.6%	98.0%
Chendo v1	98.6%	98.5%	97.6%	98.7%	98.3%	97.7%	98.5%	98.8%	98.4%	97.8%	98.6%	98.4%
Chendo v2	98.4%	98.6%	97.6%	98.7%	98.3%	97.4%	98.5%	98.7%	98.4%	97.3%	98.4%	98.4%
Lam - Li	98.6%	98.6%	97.4%	98.6%	98.0%	97.4%	98.2%	98.6%	98.1%	98.2%	98.7%	98.2%
de Miguel	98.4%	98.4%	97.4%	98.6%	97.8%	97.4%	98.0%	98.5%	97.9%	97.9%	98.6%	98.0%
Boland	98.4%	98.4%	97.3%	98.5%	97.9%	97.4%	98.1%	98.5%	97.9%	97.9%	98.6%	98.0%
Oliveira	98.4%	98.4%	97.3%	98.5%	97.8%	97.3%	98.0%	98.4%	97.8%	98.0%	98.6%	97.9%
Kararason	98.5%	98.5%	97.4%	98.6%	97.9%	97.3%	98.1%	98.5%	98.0%	98.1%	98.7%	98.0%
Soares	98.4%	98.3%	97.3%	98.4%	97.7%	97.3%	97.9%	98.3%	97.7%	98.0%	98.5%	97.8%

The analysis of the PDF provides further consideration about model expectations. Figure 2.5 (c) shows as Temps model [125] tends to underestimate solar irradiation. In fact, with respect to measured data, there is a concentration of *PDF* in the range $0 \div 150 \text{ Wm}^{-2}$ and lower density for higher solar irradiance. Figure 2.5(b) and Figure 2.5(d), as well as Figure 2.2, highlights how with both isotropic and anisotropic models, there is an overprediction of solar irradiance in the range of $150 \div 300 \text{ Wm}^{-2}$. This increase in *PDF* is more evident for the isotropic model [77], instead with the anisotropy procedure [106], the shape of probability density function is quite similar to measured data as shown in Figure 2.5(a).

Due to the impossibility to use the t-statistics, the Pearson's correlation index (1.1) is applied with the purpose of better analyzing the model provisions. This test indicates the spread between measures and estimated data. Index closer to one yields better model provisions. Results of correlation indexes are reported in Table 2.7(b). These data exhibit a general uniformity with small deviation between minimum and maximum values to such an extent the Temps and Coulson [125] model, that generally underestimates by a wide margin, shows a relative high average Pearson's index (0.974). Consequently, also this parameter is not a good index to assess the best model combination. Besides, it is generally impossible to assess the best model combination because of the number of variables involved and the different boundary conditions. However, for the site analyzed, using a combination of the various indexes, the best performing models are generally those of Reindl [113] and Muneer [92].

2.5 Several parameters influence on model deviations

As demonstrated in the previous section, the spread in model provisions of solar irradiation on tilted surface is high and can not be removed. Consequently, it is interesting to know how several boundary conditions influence the variability of results with respect to actual data.

2.5.1 Sky condition effects

In order to assess the effects of sky conditions on the model provisions, the *RMSE* is calculated separately for the three category of k_t :

- overcast sky, measured and estimated data with a k_t lower than 0.3;
- partial sky, intermediate conditions that are for $0.3 \leq k_t < 0.7$;

- clear sky, including all the data recorded and predicted with k_t greater than 0.8.

Figure 2.6 shows a comparison between $RMSE$ obtained for clear and overcast skies. Interestingly, the $RMSE$ changes in a different way and, consequently, the sensitivity differs from each model. For isotropic [77] and simplified models [20, 62, 117] the variation between overcast and clear sky conditions is limited, about $2 \div 3\%$. Instead, Ma and Iqbal [83] method, due to the assumption that diffuse radiation comes from sun disc, clearly demonstrates a better behavior for high values of k_t . Similarly, anisotropic models seem to better predict solar irradiation with clear sky conditions. The magnitude of the average solar irradiation can explain this behavior. In fact, when the sky is overcast the beam radiation decreases and in global irradiation there is only the diffuse part. Thus, when the percentage $RMSE$ proposed by Davies and Mc Kay [33] is calculated, the reduction of the denominator stresses the errors. Moreover, when the percentage of cloud decreases, the anisotropic behavior of the sky increases.

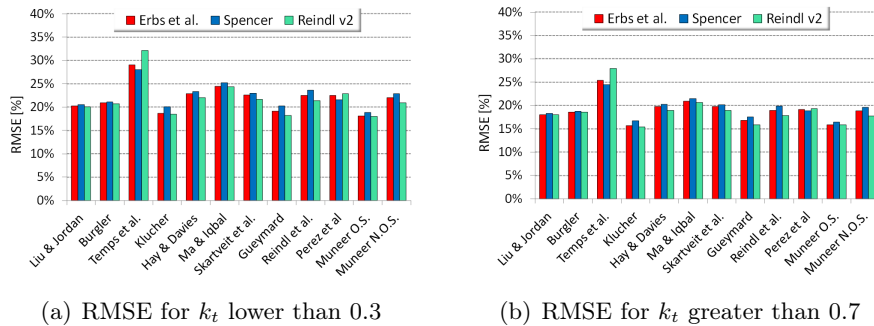


Figure 2.6: Influence of k_t class on percentage $RMSE$.

Finally, notice that for [74], [54], [92] models with clear sky conditions, the $RMSE$ is about 15%. This value is close to the equipment uncertainties, i.e. 10% (Table 2.5).

2.5.2 Season effects

The data collected in the experimental activity belong ideally to two climatic periods. Consequently, with the aim of investigate how diffuse and projection models response to different weather conditions, the dataset is divided in two parts:

- summer months, from June to August, when the solar altitude and beam radiation are high;

- autumn months, from September to November, that means low solar altitude and high ratio of diffuse to global.

The reliability of all couples of decomposition and projection methods appears to degrade when they are applied to autumn months Figure 3.9. Except for Temps model [125], that shows a considerable reduction, the other *RMSE* errors tend to align to a value of 20%.

The significantly lower performance of all models can be related to a noticeable change in boundary conditions. Since the solar altitude decreases in autumn months, the troubles due to mountain interactions grow. It is highly likely that, since the cosine error increases, the accuracy of the global solar irradiation on horizontal plane, that is the model input data, diminishes. Moreover the low solar altitude involves an increase of noise in measure due to the shading and to the parasitic reflections and emissions.

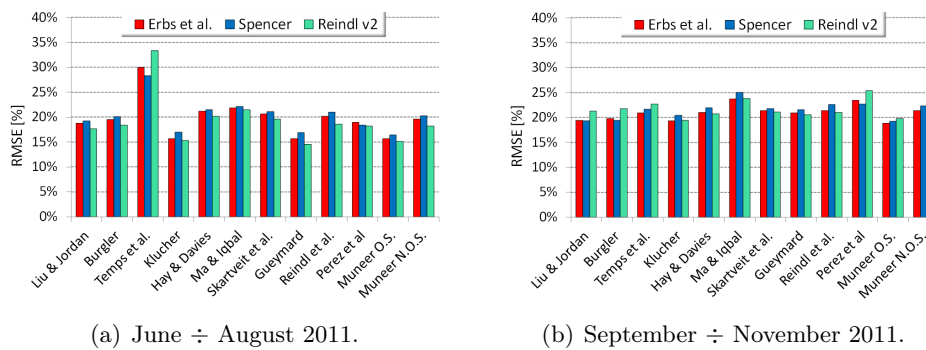


Figure 2.7: Influence of seasons on *RMSE*.

2.6 Summarizing

In this chapter, a briefly review of literature models for the postprocessing of solar radiation is presented. Besides, a comparison between several couples of decomposition and projection methods and actual data measured is carried out.

Although a single set of measurements carried out in a mountain site does no allow to draw some concluding remarks, this analysis reveals that no reliable couple of models which produces trivial errors is available. Moreover, it is difficult to define an index for assessing the most suitable method for the select locations. Hence, solar irradiation used in building simulation tools will be always affects by uncertainties. In addition, also the effects of topography and orography can produce an increasing in misprediction of solar irradiation.

Taking into account these consideration, in the following chapter, in order to assess to what extent the uncertainty in solar radiation models can lead inaccuracy to cooling load predictions, a sensitivity analysis of dynamic energy simulation is carried out.

Chapter 3

Sensitivity of cooling demand to weather data

Since the summer behavior of a building is strongly affected by the external climate conditions, a collection of weather data representative of the climate features of the site is needed.

As said in Chapter 1, in Italy there is not yet a set of hourly weather data representative of the urban context covering all the national territory consequently, monthly average data or hourly values for a typical day (MTD) are commonly used for energy calculations. In order to promote the use of dynamic simulations to calculate energy consumption, a technical committee is developing a standard that will include a typical reference year (TRY) for every Italian province [15].

Unfortunately, due to the orography, especially in northern Italy, and to the particular shape of the cities (diffuse city), a considerable part of the building stock belongs to areas with climate conditions differing from the reference city in each province. Even if some corrections to adjust data trends are proposed (e.g. to take into account the site altitude and latitude) weather data will always be affected by uncertainty. Moreover, only few weather stations in Italy have measured solar radiation and other climate variables consistently and accurately over a long period.

Furthermore, if a site has a high interannual change of climate conditions, a short period of data recording could not provide a dataset with means and amplitude of variations similar to those seen over a long periods of measurements. Likewise, a high spatial variability does not permit to extend the dataset from a location to a site some distance away.

The literature is currently very limited on the topic of the effects of weather data variability. Dubayah and Rich [42] presented an overview of the effects

of topography and plant canopies on solar radiation. One of the important aspects of that work is the presentation of the influence of shade and shadowing on the land mass surrounding hills. Another work is carried out by Gueymard and Wilcox [56]. They investigated, starting from satellite measurements, the spatial and time variability of solar radiation across the United States. Instead, Sun et al. [124] analyzed the influence of urban heat island and of the urban microclimate on energy simulation results.

For these reasons, in this chapter, the influence of several climate parameters on the energy performance and on the reliability of a quasi steady state method [130] for the prediction of cooling loads are analyzed using a sensitivity approach.

There is a subtle distinction between uncertainty and sensitivity analysis. The purpose of a sensitivity analysis is to find out the parameters to which the numerical model is sensitive, regardless to the reliable variation of input data. Conversely, the key aspect of an uncertainty analysis is the investigation of the likely variation of the input data. Consequently, a model could be sensitive to a specific input but, if the variability of this parameter is limited, it is not an important parameter for the uncertainty analysis because it does not affect the reliability of the model predictions.

This chapter deals with the sensitivity analysis of the building energy balance and, in particular, of the cooling demand to the weather data. Although a realistic variation of input data is not required for the sensitivity analysis, a likely range of changes for both dry bulb temperature and global solar irradiation has been sought in the previous chapter and uses in this analysis.

3.1 Test Cases

The choice of the building typology is a key point in the sensitivity analysis. In fact, the energy consumption is strictly connected to the shape and to the percentage of glazing area [10, 49]. Therefore, a building with a high glazing area might be more sensitive to solar irradiation while a construction with a low ratio of windows to wall will be more influenced by the temperature variations. Consequently, one building responds differently to a specific climate than another. The fact excludes the generalization of conclusions regarding the impact of a specific climate file across different building types.

Even though this analysis does not investigate the shape effects, the influence of different glazing area and orientation are taken into account. Furthermore, two different thermal masses of the envelope are considered. Cases 600 and 620 are lightweight building with a time constant of 15 h [4], instead cases 900 and 920 are massive and the time constant increases to 64 h [4].

The basic buildings (Figure 3.1) are the test cases proposed by the International Energy Agency (IEA) and reported in the standard ASHRAE 140-2007 [4]. They are a single zone building with a rectangular base (8 m and 6 m) and a height of 2.7 m without interior partitions. The glazing area is of 12 m^2 on the South façade for case 600 and 900 and of 6 m^2 both with East and West exposure for cases 620 and 920.

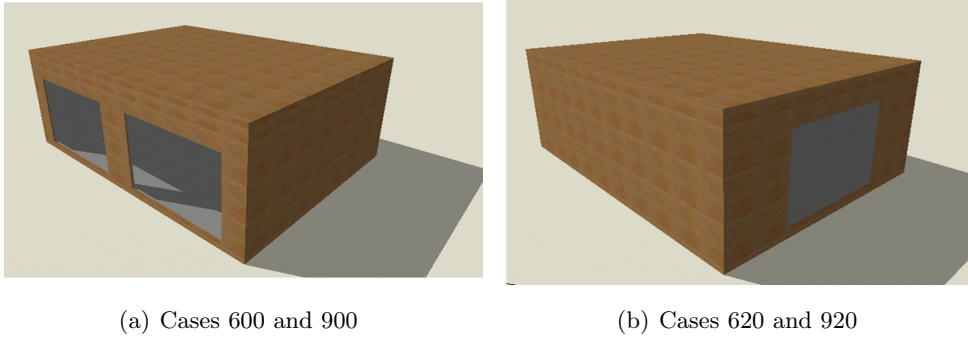


Figure 3.1: Reference building used in the analysis [4].

The construction characteristics and further details are described in Table 3.1. In addition, the internal gains due to occupancy and electrical appliances are assumed to be constant and equal to $4.17\text{ W} \cdot \text{m}^{-2}$ divided in 60% of convective part and 40% of radiative contribution. Moreover, the solar radiation incoming through glazing surfaces is distributed in the same way as the diffuse radiation using an absorbance weighted area ratios.

Table 3.1: Construction characteristics of test buildings.

	case 600/620	case 900/920
$U_{wall}\text{ W m}^{-2}\text{ K}^{-1}$	0.510	0.510
$U_{roof}\text{ W m}^{-2}\text{ K}^{-1}$	0.316	0.316
$U_{floor}\text{ W m}^{-2}\text{ K}^{-1}$	0.039	0.039
Solar transmittance	0.79	0.79
Time Constant h^{-1}	15	63
Heating setpoint [$^{\circ}\text{C}$]	20	20
Cooling setpoint [$^{\circ}\text{C}$]	26	26
Ventilation [ach]	0.5	0.5

The international standard EN ISO 13790 [3] defines two basic types of calculation procedure, i.e. a dynamic hourly energy balance and a quasi steady

state approach. In this analysis the dynamic method described in Section 3.2 is used either for the calculation of the cooling demand and for the evaluation of the loss utilization factor used in the quasi steady state approach (Section 3.3). Several dynamic simulations are carried out by means of the software TRNSYS [127] .

3.2 Dynamic simulation

The building model implemented in TRNSYS (*type 56*) [127] is a non-geometrical balance model with one air node representing the thermal capacity of the zone air volume. This calculation procedure involves an hourly based heat balance of the air node that could be represented by the following equation:

$$\dot{q}_c + \dot{q}_v + \dot{q}_i + \dot{q}_{sys} = C_i \cdot \frac{\partial \theta}{\partial \tau} \quad (3.1)$$

- where
- \dot{q}_c are the convective exchanges with wall,
 - \dot{q}_v are the ventilation heat losses,
 - \dot{q}_i are the internal convective heat gains,
 - \dot{q}_{sys} is the supplied or removed heat by the systems,
 - C_i is the internal heat capacitance of the thermal zone,
 - θ is the temperature of the internal air node of the thermal zone.

The opaque components of the envelope are modeled by means of the conduction transfer function proposed by Mitalas and Stephenson [91]. The coefficients of the time series are evaluated using a direct root finding procedure (DRF) of the governing equation in the Laplace s-domain [63, 64].

The glazing surfaces are thermally considered as an external wall without thermal capacitance, partially transparent to solar radiation but opaque to long-wave internal gains.

The long-wave radiation is modeled in a different way for internal and external sides of the envelope. For external surfaces the long-wave radiation exchange is considered explicitly using a fictive sky temperature (T_{sky}), which is an input to the *type 56* model, and a view factor to the sky (f_{sky}) for each component. Instead, the surfaces within the zone and the convective heat fluxes from the inside surfaces to the zone air are approximated using the star network [115]. This method uses an artificial temperature node (T_{star}) to consider the parallel

energy flow from a wall surface by convection to the air node and by radiation to other wall and window elements. Also the emissivity of surface differs from internal to external side of the wall. In fact, the software assumes an external emissivity equal to 0.9. Instead, since the internal zone is assimilable to a cavity subjected to multiple reflections, the internal surfaces are treated as black body radiator. An hourly time step is used for the simulations. Type 16 and type

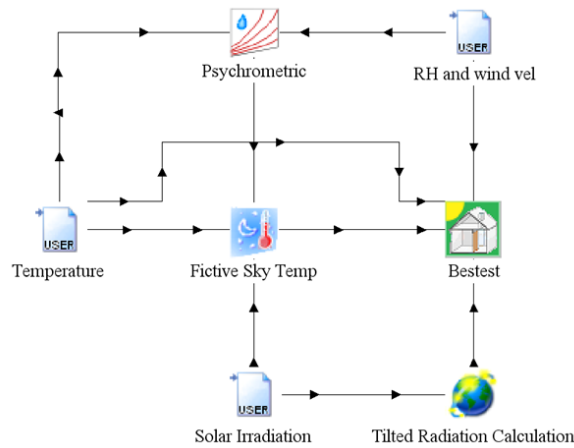


Figure 3.2: Scheme of type connection in TRNSYS [127] simulation.

56 are used with the goal of modeling respectively the solar radiation on tilted surface and the building thermal zone (Figure 3.2). In particular, the Erbs' relation [44] is used to decompose solar radiation into beam and diffuse part and Perez model [106] for the projection on a tilted surface (Section 3.4).

3.3 Quasi steady state method

In the quasi steady state method, the dynamic effects are taken into account by introducing a correlation factors that is the loss utilization factor for cooling. This parameter takes into account the fact that only a part of the transmission and ventilation heat transfer is utilized to decrease the cooling needs. In fact, generally the heat loss through the envelope and the cooling effect of the ventilation occur during night periods when they have no effect on the cooling needs caused primary by solar irradiation through the windows. Therefore, the heat balance equation becomes:

$$Q_{c,nd} = Q_{gn} - \eta_c \cdot Q_{ht} \quad (3.2)$$

where $Q_{c,nd}$ is the energy need for cooling,
 Q_{gn} is the sum of internal and solar heat gains,
 Q_{ht} are the thermal losses through the envelope and for ventilation,
 η_c is the loss utilization factor.

Consequently, the most important aspect of this method is the correct estimation of the loss utilization factor. In this work, a procedure derived from annex I of standard EN ISO 13790 [3] is adopted in order to determine the loss utilization factor starting from results of dynamic hourly simulations. The method consists in three simulations with different boundary conditions:

Simulation 0 ($sim, 0$) dynamic simulation of the building with a dual setpoint (i.e. 20°C for heating and 26°C for cooling) and deadband;

Simulation 1 ($sim, 1$) dynamic simulation without heat gains and with an unique setpoint of 26°C both for heating and cooling. Accordingly to the technical standard, the temperature-dependent heat fluxes are distinguished from the independent ones. Thus, the heat gains are decreased by the extra flow radiation towards the sky dome;

Simulation 2 ($sim, 2$) dynamic simulation with heat gains and with an unique setpoint of 26°C for both heating and cooling.

The monthly heating demand and cooling demand are computed by integration of the hourly results of the dynamic simulation over the whole month. Starting from this point, the monthly heat losses by transmission Q_{ht} are evaluated as:

$$Q_{ht} = Q_{h,nd}^{sim,1} - Q_{c,nd}^{sim,1} \quad (3.3)$$

while the monthly heat gains Q_{gn} are:

$$Q_{gn} = Q_{ht} - \left(Q_{h,nd}^{sim,2} - Q_{c,nd}^{sim,2} \right) \quad (3.4)$$

where $Q_{h,nd}$ is the energy need for heating,

From these parameters the monthly loss utilization factor for cooling η_c is derived by means of the following equation:

$$\eta_c = \frac{Q_{gn} - Q_{c,nd}^{sim,0}}{Q_{ht}} \quad (3.5)$$

3.4 Weather data preprocessing

The influence of climate features on cooling demand calculation ($EP_{e,inv}$) and on loss utilization factor for cooling is investigated by perturbing the weather data. In particular, both real trends and periodic variations of the main external weather variables, such as dry bulb temperature and solar radiation, are considered.

With the purpose of investigating to what extent the weather uncertainties affect results, several dynamic simulations with different levels of mean value and daily amplitude of each external weather variable and various combination of these are performed.

The research, as shown in [109] and [110], is carried out taking into account the light and massive buildings described in Section 3.1. Furthermore, two different cities are considered with the end of evaluating the continental and marine climate (Table 3.2).

In order to perform hourly simulations, the typical meteorological year developed in Section 1.6 for Palermo and the TRY proposed by the *Comitato Termotecnico Italiano* [30] are used.

Table 3.2: *Climate classification of Italian cities*

	ASHRAE Zone [8]	Köppen classification [75]
Milan	4A Mixed - Humid	Cfa "humid subtropical climate"
Palermo	3A Warm - Humid	Cfa "humid subtropical climate"

Starting from TRYs, for each calendar month an hourly trend of the monthly typical day (MTD) is computed. Since in the Italian TRY only the global solar irradiance is defined, the Erbs' relation [44] is used to decompose the global solar irradiance on horizontal plane in beam and diffuse part. Furthermore, the solar radiation incident on a tilted surface is calculated by means of Perez's model [106]. The choice of these models depends not on their reliability (Section 2.4), rather to the fact that they are widely used and implemented in commercial simulation codes. So the widespread use has elected the pair of Erbs-Perez models to the role of international benchmarks in building energy simulations.

Then, with the aim of setting a variability of weather data, the MTD signal is firstly decomposed in different harmonics, as shown in Figure 3.3, by means of a Fast Fourier Transform (FFT) [111].

The daily trend of dry bulb temperature DBT as a function of time τ is

then:

$$DBT(\tau) = \overline{DBT} + \sum_{n=1}^{12} A_n \cos(\omega_n \cdot \tau + \varphi_n), \quad (3.6)$$

while the solar irradiation GSI can be approximated with a Fourier series as:

$$GSI(\tau) = \overline{GSI} + \sum_{n=1}^{12} B_n \cos(\omega_n \cdot \tau + \psi_n). \quad (3.7)$$

where \overline{DBT} is the daily mean of dry bulb temperature,

\overline{GSI} is the daily mean of solar irradiation,

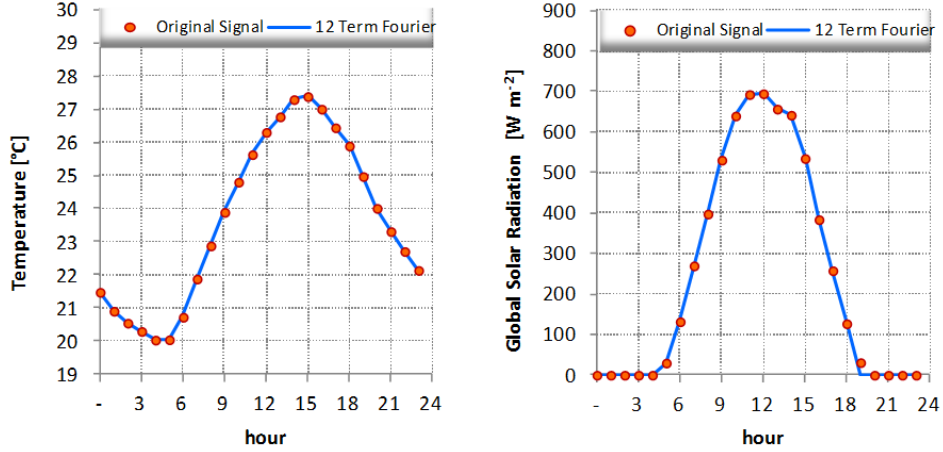
A_n, B_n are the amplitudes of the n -th harmonic,

ω_n is the angular frequency of the n -th harmonic,

φ_n is the phase lag of the n -th harmonic of dry bulb temperature,

ψ_n is the phase lag of the n -th harmonic of solar irradiation.

Secondly, taking into account the possible uncertainty in weather data, mean values and amplitudes of dry bulb temperature and global solar irradiance on horizontal plane are scaled (e.g. $\pm 5\%$ and $\pm 10\%$).



(a) July MTD temperature in Milan

(b) July MTD solar irradiation in Milan

Figure 3.3: MTD approximation by a Fourier series

The primary effect of data perturbing is the changing of the annual global radiation on an horizontal surface and of the cooling degree days (CDD_{18})

as shown in Table 3.3. Moreover, since in the Erbs' model the fraction of diffuse solar radiation depends on the ratio between global and extraterrestrial solar radiation, an amplitude variation leads to a different percentage of diffuse radiation (Figure 3.4). Hence, an error in the estimation of global solar radiation does not lead only to an uncertainty in the magnitude of the flux but it causes also a different composition of the heat flux. Moreover, since the beam and

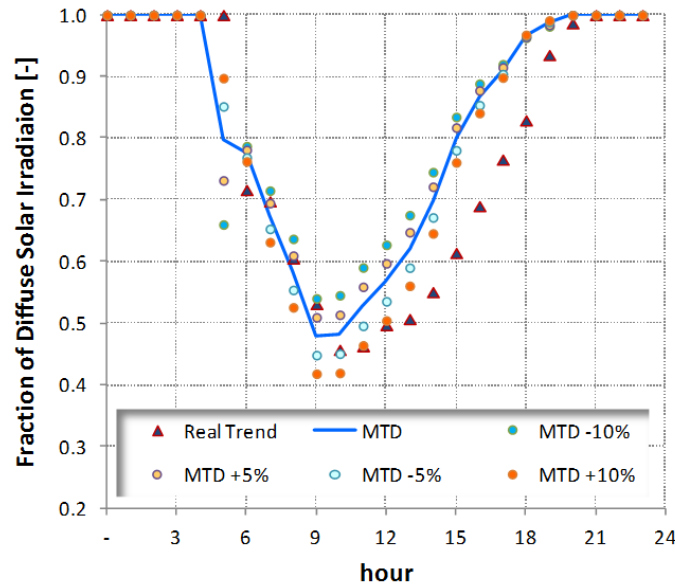


Figure 3.4: July diffuse fraction in Milan

diffuse solar radiations have different incident angles, which, in turn, affect the solar transmittance of glasses, an uncertainty in the composition of solar radiation could be quite relevant in the building heat balance.

3.5 Results

With the end of analyzing the influence of weather data on monthly cooling needs and on monthly loss utilization factors, several hourly simulations are performed.

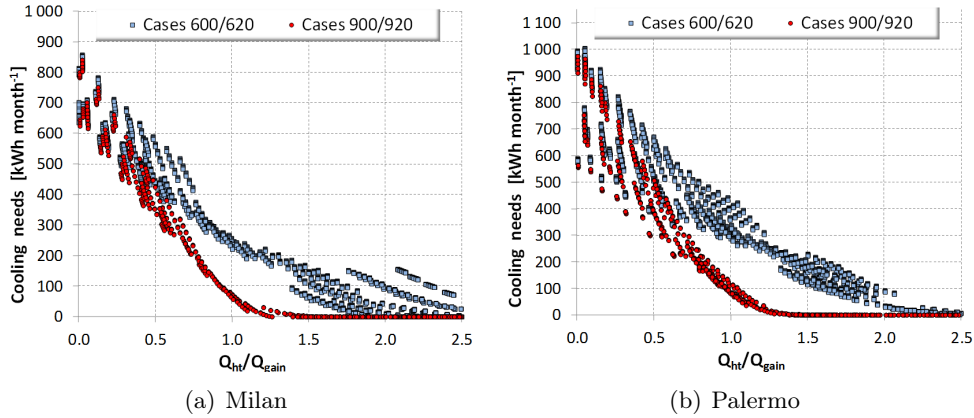
In Figure 3.5 the trend of monthly cooling demand is plotted against the ratio of heat losses to heat gains.

It should be noticed that for low values of the ratio of Q_{ht} to Q_{gain} , massive and lightweight buildings have the same cooling consumptions. This happens because in this part of the graph becomes predominant the solar irradiation through glazing area. Besides, the heat losses are kept down due to the limited

Table 3.3: *Effects of weather data perturbations*

(a) Annual solar energy on horizontal surface				
	MTD-10%	MTD-5%	MTD+5%	MTD+10%
Milan	-4.61%	-2.30%	-2.33%	-4.61%
Palermo	-4.88%	-2.30%	-2.30%	-4.88%

(b) Annual cooling degree days CDD_{18}				
	MTD-10%	MTD-5%	MTD+5%	MTD+10%
Milan	-40.4%	-21.3%	21.4%	43.4%
Palermo	-46.9%	-23.5%	26.2%	54.3%

**Figure 3.5:** *Monthly cooling demand as a function of the ratio of loss to gain*

difference between external air and internal setpoint temperature (Figure 3.6).

The greatest differences of thermal response between massive and lightweight envelope are found for losses over gains included in the range of $0.5 \div 1.5$. In fact, using the analogy to the electrical circuit, these conditions permit the charge and discharge of the capacitor. Consequently, for these configuration the massive component has the possibility to store heat and to release it during the night with a noticeable reduction of the cooling requirements.

In the Figure 3.7 the deviations of the monthly cooling need from the reference conditions (MTD weather data), caused by amplitude and mean value changes, are plotted for both the city of Milan and Palermo. In the graphs the data points are distinguished according to the BESTEST cases. In particular, light blue points refer to buildings with lightweight envelope, i.e. case 600 and case 620, instead the red points are the results for massive buildings, i.e. case

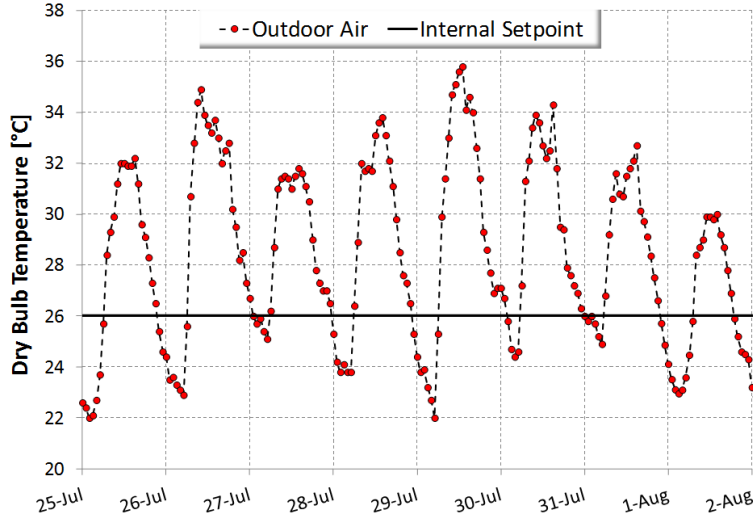


Figure 3.6: External DBT for Palermo in a typical summer period.

900 and case 920. In both contexts, most of the monthly deviations belong to the range $\pm 200 \text{ kWh}$, that means $\pm 4.15 \text{ kWh m}^{-2} \text{ month}^{-1}$, and decrease with the increment of the ratio of thermal losses vs heat gains.

The data points are aligned along parametric lines but for the massive cases the data are less tilted than the lightweight cases. This could be expected because an increment in the mean temperature value makes the ratio of Q_{ht} to Q_{gain} to decrement and the cooling needs to grow. Since the relationship between the change of the ratio of Q_{ht} to Q_{gain} and the one of the thermal needs is not linear, the thermal response depends on the envelope thermal inertia.

Instead, since the integral sum of the thermal losses does not depend on the changes in temperature amplitude, the ratio between the losses and the gains is the same of the reference cases. Consequently, the variation of the amplitudes in the external temperatures seems to have a small influence on the energy needs.

Furthermore, for changes in the amplitudes of the solar irradiation, a light decrement of the ratio between Q_{ht} and Q_{gain} is observed with an increase of the deviation in the cooling demand. The differences of energy needs caused by the irradiation amplitude are more evident when the ratio of Q_{ht} to Q_{gain} is greater (i.e., when Q_{ht} over Q_{gain} is more sensitive to the parameter changes).

The graphs in Figure 3.8 shows the deviations from the reference loss utilization factors, defined with MTD weather data, for the city of Milan, Figure 3.8 (a), and Palermo, Figure 3.8 (b). In both contexts, most of the deviations belongs to the range ± 0.10 . A group of values has larger deviations but in correspondence of the ratio of Q_{ht} to Q_{gain} close to zero and, consequently, they are considered negligible. Likewise, for Q_{ht} over Q_{gain} greater than 1.5 in

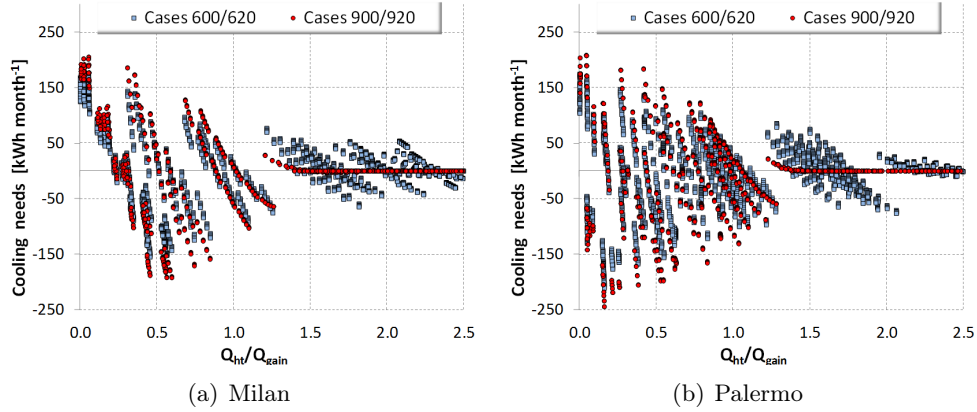


Figure 3.7: Deviation in monthly cooling demand as a function of the ratio of loss to gain

massive buildings there is an high variation in loss utilization factor due to the high level of heat losses with respect to cooling demand.

Similarly to cooling needs, also the loss utilization factor points are aligned along parametric lines which have lower slope for massive cases due to the non linearity of linking function.

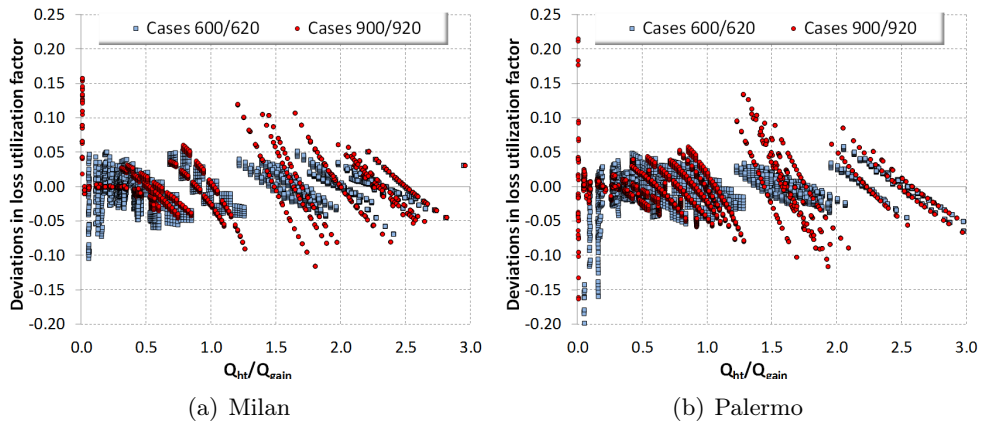


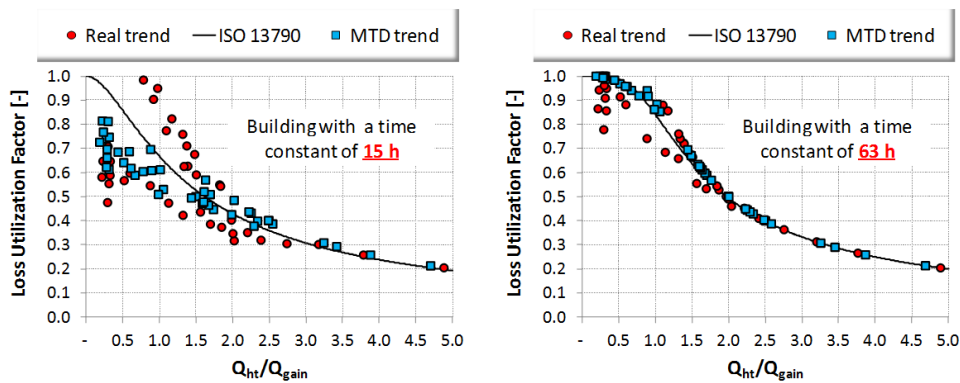
Figure 3.8: Deviation in Monthly loss utilization factor as a function of the ratio of loss to gain

Since the same percentage of uncertainty causes different effects on energy balance terms (Table 3.3), a direct comparison between weather variable influence is not possible. Consequently a sensitivity analysis is required as described in the next sections.

3.6 Real vs synthetic trend of weather data

As reported in Section 1.1 a key requirement of weather data for energy simulation is the use of true sequences. In fact, since the heat balance of a building is not linear, it is important to ensure that weather data follow each other in a similar manner to the recorded data.

Figure 3.9 shows the comparison between the loss utilization factors for cooling obtained both with real trends of weather data and using monthly typical days. Since dawn and dusk hours depend on Julian date, in the early and late parts of the month some values in the MTD profile are outside the interval between sunrise and sunset and, consequently, are set to zero. This adjustment in solar radiation produces a small deviation in the ratio of losses to gains (see Figure 3.9).



(a) Low mass buildings (case 600 and 620) (b) High mass buildings (case 900 and 920)

Figure 3.9: Loss utilization factor with both real and MTD weather data

For massive buildings, with a time constant of 63 hours, only small deviations are found between real and periodic trends, Figure 3.9 (b), in particular for low values of the ratio of Q_{ht} to Q_{gain} . Instead for light envelope (i.e. with a time constant of 15 hours) the graph clearly highlights a high spread of data when the ratio between heat losses and heat gains is lower than two. The different behavior of test cases is caused by the envelope mass. In fact, a massive component is a low-pass filter. Therefore, only low-frequency signals (i.e. the fundamental harmonic) pass and the envelope reduces the amplitude of signals with frequencies higher than the cutoff. Instead, for low mass buildings, also the high frequencies pass through the envelope and, consequently, the spread between building response and real signal increases with respect to mean periodic day.

Another interesting result is the loss utilization factors obtained for low value of the ratio of Q_{ht} to Q_{gain} . Oppositely to the EN ISO 13790 [3] relation, the limiting value of η_c is not equal to one if the ratio of losses to gains approaches zero. The curve obtained with dynamic simulations points out that, more realistically, not all the heat losses can be used to decrease the cooling demand if the thermal zone has not enough capacitance.

Finally, Figure 3.9 clearly shows that there is not a bijective link between loss utilization factor and monthly ratio of heat losses to heat gains. For the same value of losses over gains there are more than one loss utilization factor, especially for low mass building when real trends of weather data are used. These errors rise up when the true sequences of weather data are neglected. In fact, the monthly ratio of Q_{ht} to Q_{gain} does not distinguished between an equal alternation of warm days and cold nights with respect to a sequence of warm and cold weeks. Instead, the building thermal response and, consequently, the cooling demand are different.

These considerations suggest the unreliability of the loss utilization factor approach for cooling prediction and highlight the importance of the true sequences of weather data.

3.7 Procedure of sensitivity analysis

The relative influence of stochastic variations on building energy needs increases for low energy constructions. Consequently, in the last few years the interest in uncertainty and sensitivity analysis has grown up. Besides, several studies, for the definition of uncertainty and sensitivity techniques and on the applicability of these procedures to energy simulation have been carried out [28, 32, 39, 58, 89, 90, 126, 135, 137].

As reported by Macdonald [84], the uncertainty analysis can be divided in two categories:

- External methods where, for all uncertain model inputs, random samples are generated. Subsequently, the deterministic numerical model is executed for every input. Then, the probability density function (PDF) of the output variables is derived starting from the model individuals predictions.
- Internal methods that directly evaluate the PDF of output data from the PDF of inputs and from the differential equations of the mathematical model. Due to the nonlinearities of the building behavior this technique required not trivial manipulations of the governing equations.

The external procedures are also divided in two branches, i.e. local and global. In local methods the output uncertainty is evaluated with respect to changes in individual parameters, whereas global methods quantify the output variation with a simultaneous perturbation of all the input data.

In this work, a sensitivity analysis is carried out with a local external approach using two different procedures, i.e. differential sensitivity analysis and factorial method.

The Differential Sensitivity Analysis (DSA) is the backbone of local methods and it works by perturbing an input data around the mean value while all the other parameters remain fixed. For each perturbed value the numerical simulation is carried out and the model response is calculated. Due to its robustness and simplicity, the DSA is the most diffuse method for a local uncertainty evaluation. The effects of an uncertain parameter are estimated by comparing the results of these simulations against those with unperturbed inputs. Consequently, a sensitivity index of the model prediction to the uncertain parameter is defined as:

$$s = \frac{\Delta o}{\Delta i} \quad (3.8)$$

where o is the model output,

i is the input perturbed while the other parameters influencing the output are held fixed.

The main weakness of this calculation procedure is that it is based on the assumption of perfect independency among all parameters. Consequently, the combined effects can be estimated by a superposition only if the problem is linear. With the aim of overcoming to this issue, the Factorial Method (FM) is also used.

The FM is a further development of the DSA approach, that includes the interactions between parameters and permits the estimation of the higher order effects. In this procedure all the uncertain parameters are perturbed simultaneously around their mean values. Usually two different perturbation levels are considered (e.g. +10 % and -10 %). The drawback of this technique is the number of simulations required that is factorially related to the number of inputs.

3.8 Differential sensitivity analysis

The sensitivity of the three parameters previously listed is analyzed. The DSA approach required 6 simulations for each test case both in Milan and Palermo using an upper and lower value of the perturbed parameter, i.e. $\pm 10\%$. These simulations were created and performed by means of TRNSYS software [127].

3.8.1 DSA of cooling demand

For the calculation of the sensitivity index of cooling demand, the equation 3.8 is used. In this context, the dependent variable is the monthly cooling energy need $EP_{e,inv}$ and the independent variables are respectively the mean outdoor temperature T_M , the outdoor temperature amplitude T_A and the horizontal global radiation amplitude Q_A .

Table 3.4: Monthly sensitivity indexes s for the mean outdoor temperature (T_M), for the amplitude of the external temperature (T_A) and for the max global solar radiation on the horizontal plane (Q_A)

Month	Milan			Palermo		
	T_M [kWh/°C]	T_A [kWh/°C]	q_A [kWh/W]	T_M [kWh/°C]	T_A [kWh/°C]	q_A [kWh/W]
Jan	-	-	0.06	13.20	17.23	2.17
Feb	14.79	8.95	2.25	11.53	14.53	1.22
Mar	6.45	4.63	0.48	16.57	13.28	0.86
Apr	21.02	10.75	0.81	37.75	16.25	0.74
May	42.03	11.23	0.64	54.62	14.67	0.45
Jun	64.15	6.36	0.20	62.36	9.94	0.33
Jul	65.21	9.39	0.47	70.40	8.67	0.28
Aug	64.50	8.30	0.91	71.22	8.07	0.63
Sep	52.91	8.32	1.48	60.11	10.95	1.23
Oct	11.83	7.73	1.09	47.48	14.82	1.86
Nov	9.39	5.21	1.96	26.02	19.05	2.02
Dec	15.84	6.40	4.65	8.47	6.00	1.40

In Tables 3.4 the average monthly indexes are reported for Milan and Palermo. All the elaborated indexes have a positive sign (i.e., the correlation between the energy need and the parameters is positive). For the mean external temperatures, both in Milan and Palermo, the same trends are registered. The sensitivity index has a parabolic-type trend with the maximum, about $60 \div 70 \text{ kWh } ^\circ\text{C}^{-1}$, in summer months. The calculated values are quite similar with larger deviations in spring and autumn months.

For the amplitude variation of the outdoor temperature, in Milan all the indexes are slightly lower than $10 \text{ kWh } ^\circ\text{C}^{-1}$, while in Palermo they are between 10 and $20 \text{ kWh } ^\circ\text{C}^{-1}$. For both cities the sensitivity seems to present little deviations for different months. By considering the solar radiation, a parabolic-type behavior is noticed for Palermo with the minimum values in summer months. Similar values are observed for Milan but with a more irregular behavior.

Since the absolute sensitivity index depends on the magnitude of parameter perturbation, a direct comparison between weather variable influences is not possible. In order to overcome this aspect, a percentage sensitivity index is defined as:

$$s_{\%} = \frac{\Delta o / o_{un}}{\Delta i / i_{un}} \quad (3.9)$$

where o_{un} is the model output with unperturbed input,

i_{un} is the unperturbed input.

All the reference cases with an energy need lower than 10 kWh are neglected in order to avoid misleading evaluation of the percentage indexes. Table 3.5 shows the average summer values of percentage sensitivity index for the different test cases and climate conditions analyzed.

These results clearly demonstrate that the interaction between building and climate features depends on the envelope characteristics. In fact, it should be noticed that even if the $s_{\%}$ index for temperature amplitude perturbations is negligible, it has a higher value for lightweight envelope (i.e. case 600 and 620). This can be explained with the attitude of massive envelope to filter the high frequencies signal and to decrement the amplitude of oscillations.

Likewise, since the high mass components can store solar irradiation and loss heat during the night, they are more sensitive to mean temperature perturbation than light mass structures. For the latter cases the perturbation of mean temperature affects primary only the heat losses/gains through the envelope. Instead, in cases 900 and 920, the mean temperature changes the possibility of the wall to work like a condenser with daily cycles of charge/discharge.

Furthermore, the difference of building response with regard to the sensitivity to solar radiation is still more striking. Since in summer period the solar altitude is high, the cooling demand is more sensitive to solar irradiation changes in building with glazing area orientated to east and west, i.e. case 620 and 920. Moreover, an increase of solar irradiation on horizontal plane implies a decrement of the diffuse radiation and a growth of beam part that has a low incident

Table 3.5: *Percentage sensitivity index for cooling demand.*

City	Case	T_M	T_A	Q_A
Milan	600	2.18	0.08	0.48
	620	2.24	0.06	0.44
	900	3.83	0.01	0.56
	920	3.59	0.02	0.50
Palermo	600	2.33	0.08	0.15
	620	1.79	0.05	0.43
	900	3.56	0.01	0.15
	920	2.45	0.00	0.45

angle on vertical façade. Consequently, especially in Palermo where the solar altitude is higher, it is possible for cases 600 and 900 that, in some months, an increment of the peak of solar irradiation produces a decrement of cooling need. Thus, the influence of solar irradiation perturbations on cooling demand decreases due to errors compensations.

From the comparison among the different climate perturbations emerges that the primary variable is the mean external temperature. A low order of magnitude is registered for solar irradiation while the temperature amplitude is trivial for cooling consumptions. But, if the spring and autumn periods are taken into account, the influence of solar irradiation changes on cooling demand increases due to the lower solar altitude. The yearly average percentage of sensitivity indexes on cooling needs becomes:

Milan, 2.91 for the mean temperature, 0.19 for the temperature amplitude and 2.63 for the solar irradiation;

Palermo, 2.77 for the mean temperature, 0.17 for the temperature amplitude and 1.67 for the radiation.

Notice that while, for temperature mean and amplitude, the sensitivity index are quite similar for Milan and Palermo, a greater difference is registered for solar radiation index. Therefore, the sensitivity to solar radiation perturbations is strictly related to the latitude of the site that affects the solar altitude and, consequently, the incident angle of solar beams.

In Figure 3.10(a) and Figure 3.10(b) the percentage sensitivity index, respectively to mean temperature and to solar irradiation changes, is plotted against the ratio of losses to gains.

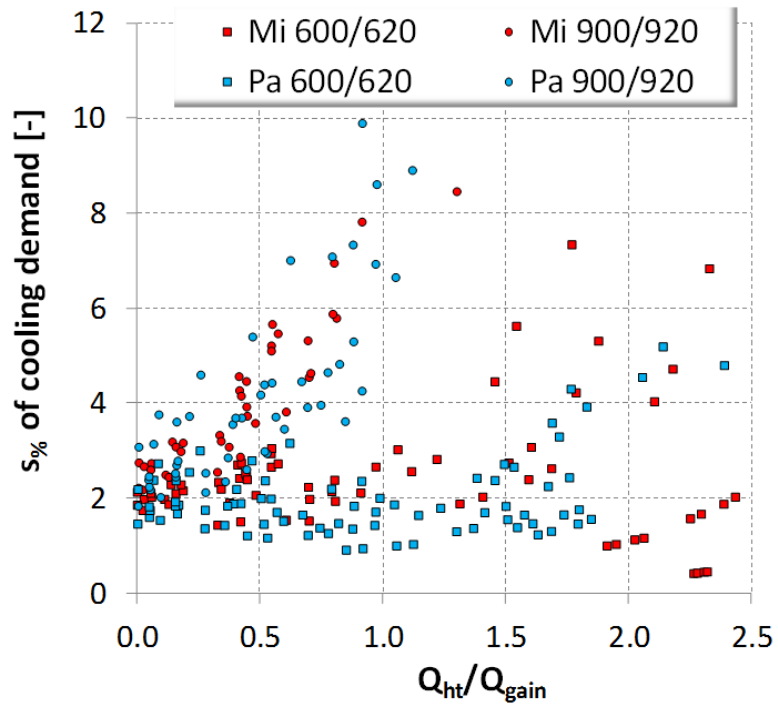
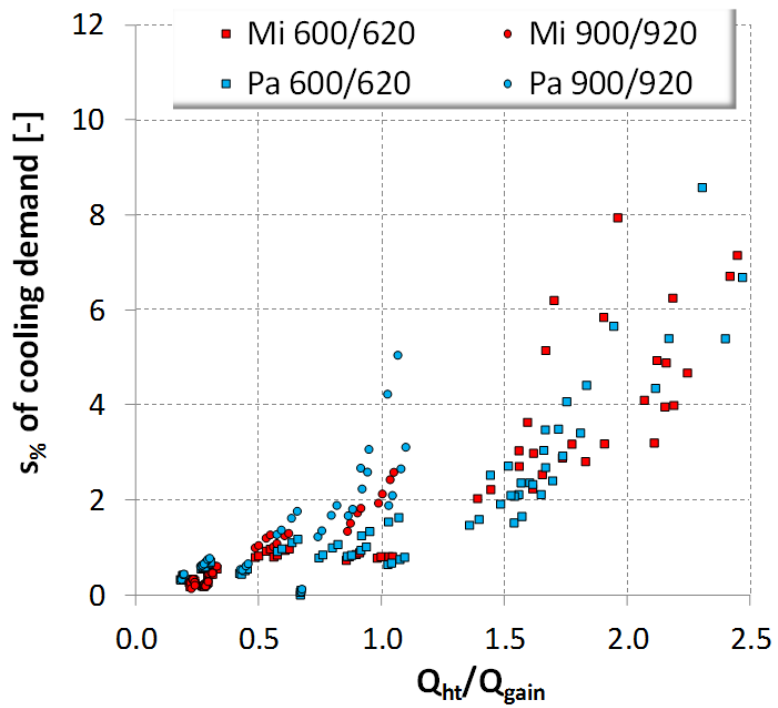
(a) $s_{\%}$ trend due to mean temperature perturbation(b) $s_{\%}$ trend due to amplitude perturbation of global horizontal solar irradiation**Figure 3.10:** Percentage sensitivity index as a function of the ratio of losses to gains.

Figure 3.10 clearly shows a huge growth of the $s\%$ either for light and massive buildings for the ratio of losses to gains that is respectively about 1.0 and 2.5. These values are the balance points of the buildings, i.e. the points in which the cooling demand becomes null (Figure 3.5). Consequently, if the need of heat extraction approaches zero the sensitivity to weather data increases.

Figure 3.10(a) clearly shows the different behavior of buildings due to the thermal mass of the envelope. In fact, for light walls (i.e. cases 600 and 620) the sensitivity index is quite constant to the value of 2 and it increases when the ratio of losses to gains approaches the balance point. Instead, for massive buildings a gradual growth is registered. This is because, for light constructions, the temperature changes affect only the heat losses/gains through the envelope. Instead, for massive components it modifies also the capability of the wall to discharge to the external environment the heat stored during the hottest hours.

Likewise, the internal thermal capacitance is also the cause of the different response to solar irradiations showed in Figure 3.10(b). Indeed, the lightweight components have larger sensitivity indexes because they have not the capacity to use the storage effects and the night heat losses to reduce the increment of cooling demand due to the growth of solar irradiation.

3.8.2 DSA of loss utilization factor

A similar analysis is carried out in order to investigate to what extent weather data influence loss utilization factor for cooling. For both cities the sensitivity indexes are calculated by means of Equation (3.9). In this context, the dependent variable is the loss utilization factor η_c and the independent variables are, respectively, the mean outdoor temperature T_M , the outdoor temperature amplitude T_A and the horizontal global radiation amplitude Q_A .

In Table 3.6 the percentage sensitivity indexes are reported for Milan and Palermo for both low and high mass envelope.

With respect to the variations of solar radiation, both in Milan and Palermo negligible changes in loss utilization factor are registered. In fact, an increase of solar radiation peak produces limited variation of daily solar energy and, consequently, of the ratio of losses to gains. The solar perturbation primarily affects the lightweight buildings, in which the envelope has not the capability to store the solar gains. Besides, an increment in solar radiation during the day will reduce the possibility of using both the night heat losses and the cooling effects of ventilation and, consequently, the sensitivity index is negative.

For the same reason the sensitivity index is always negative also for amplitude perturbation of temperature. In fact, a change in amplitude of daily

variations affects neither the mean daily temperature nor the daily heat losses. Therefore, the sensitivity index is greater in cases 600 and 620 because they have not the capability to store the extra heat gains due to the increment of external temperature during the day and to discharge them during the night.

Table 3.6: *Percentage sensitivity index for loss utilization factor.*

City	Case	T_M	T_A	Q_A
Milan	600	0.35	-0.28	-0.03
	620	0.26	-0.18	-0.11
	900	0.20	-0.01	0.01
	920	0.14	-0.01	0.01
Palermo	600	0.81	-0.48	-0.07
	620	1.01	-0.36	-0.02
	900	0.21	-0.01	0.01
	920	0.06	-0.01	0.02

Oppositely, a growth of mean temperature induces a reduction of the ratio of losses to gains and, consequently, an increment of the loss utilization factor. It should be noted that, for both Milan and Palermo, the percentage sensitivity index to mean temperature perturbation is greater for low mass building. Furthermore, since in Palermo the climate is warmer, there is a greater concentration of points in the region with low values of the ratio of losses to gains. Consequently, the sensitivity index obtained for Palermo are greater than those of Milan.

In conclusion, it should be emphasized that the results obtained for the utilization factor differ significantly from those for the cooling demand. In fact, for the dynamic simulation, the final results are primarily affected by the uncertainty of the average temperature and peak solar irradiation. Moreover the influence of changes in daily amplitude of temperature variations are negligible. Oppositely, when a quasi-steady state method is applied for the cooling demand calculation, in the evaluation of the utilization factor the correct estimation of the average value and the daily amplitude variation of the temperature becomes essential. These results confirm the considerations already set out in Section 3.6 on the reliability of loss utilization factor obtained with synthetic days.

3.9 Factorial Method

The implementation of the factorial method is essentially the same as for the differential method (Section 3.8). The main difference is that multiple parameters are perturbed simultaneously in the same simulation process. Consequently the possible synergistic effects of variable perturbations can be observed. In this analysis all variables are tested at two values, that correspond to a perturbation of $\pm 5\%$. In Table 3.7 the required states of each variable are reported for each run.

Table 3.7: *Factorial design scheme for three variables analysis [84]*

RUN	First order			Second order			
	T_M	T_A	Q_A	$T_M - T_A$	$T_M - Q_A$	$T_A - Q_A$	$T_M - T_A - Q_A$
1	-	-	-	+	+	+	-
2	+	-	-	-	-	+	+
3	-	+	-	-	+	-	+
4	+	+	-	+	-	-	-
5	-	-	+	+	-	-	+
6	+	-	+	-	+	-	-
7	-	+	+	-	-	+	-
8	+	+	+	+	+	+	+

The first order effects of each variable perturbations can be determined by combining the simulation results as reported in the following equations:

$$\begin{aligned}
 FT_M &= \frac{(Z_2 + Z_4 + Z_6 + Z_8) - (Z_1 + Z_3 + Z_5 + Z_7)}{4} \\
 FT_A &= \frac{(Z_3 + Z_4 + Z_7 + Z_8) - (Z_1 + Z_2 + Z_5 + Z_6)}{4} \\
 FQ_A &= \frac{(Z_5 + Z_6 + Z_7 + Z_8) - (Z_1 + Z_2 + Z_3 + Z_4)}{4}
 \end{aligned} \tag{3.10}$$

where Z_i is the model response of the i -th simulation run, (see appendix B);

FT_M is the 1st order effect to mean temperature changes;

FT_A is the 1st order effect to temperature amplitude changes;

FQ_A is the 1st order effect to amplitude changes of solar radiation;

Similarly, the second order effects are given using the signs reported in Table 3.7. These signs are found by multiplying the sign of the individual variable state

[84]. The second order effects can be determined as:

$$\begin{aligned}
 T_M - T_A &= \frac{(Z_1 + Z_4 + Z_5 + Z_8) - (Z_2 + Z_3 + Z_6 + Z_7)}{4} \\
 T_M - Q_A &= \frac{(Z_1 + Z_3 + Z_6 + Z_8) - (Z_2 + Z_4 + Z_5 + Z_7)}{4} \\
 T_A - Q_A &= \frac{(Z_1 + Z_2 + Z_7 + Z_8) - (Z_3 + Z_4 + Z_5 + Z_6)}{4} \\
 T_M - T_A - Q_A &= \frac{(Z_2 + Z_3 + Z_5 + Z_8) - (Z_1 + Z_4 + Z_6 + Z_7)}{4}
 \end{aligned} \tag{3.11}$$

where $T_M - T_A$ is the 2nd order effect due to T_M and T_A changes;
 $T_M - Q_A$ is the 2nd order effect due to T_M and Q_A changes;
 $T_A - Q_A$ is the 2nd order effect due to T_A and Q_A changes;
 $T_M - T_A - Q_A$ is the 2nd order effect due to T_M , T_A , Q_A changes.

Thus, with this procedure the three first order effects and the four interactions parameters between data perturbations can be determined. In the following sections results obtained for cooling demand and loss utilization factor will be presented.

3.9.1 FM of cooling demand

The results displayed in Table 3.8 confirm what already found in section 3.8.1. The cooling consumption is primarily affected by uncertainty in mean temperature for both Milan and Palermo. The influence of solar irradiation changes is an order of magnitude lower. It should not be forgotten, however, what emerged from the data shown in the Table 3.3. In fact, the constant variation of $\pm 5\%$ induces different effects on energy balance terms, with a high adjustments for heat losses/gains through the envelope with respect to the solar heat gains. Besides, the data reported in Table 3.8 again show for Palermo in June and July a negative index for building with glazing area facing to South, i.e. case 600 and 900. This is due to the increase in the direct solar radiation evaluated by the Erbs et al. [44] model and, consequently, a higher portion of solar irradiation reach the glazing surface with a low angle of incidence.

Furthermore, the factorial method results underline how changes of daily temperature amplitude produce limited variation of cooling demand with respect to the mean temperature effects. In particular, notice that the sensitivity to temperature amplitude changes decreases with the growth of envelope heat

Table 3.8: Results of factorial analysis for cooling demand in kWh.

(a) Milan

		Z_M	FT_M	FT_A	FQ_A	$T_M - T_A$	$T_M - Q_A$	$T_A - Q_A$	$T_M - T_A - Q_A$
case 600	JUN	512.01	127.08	4.13	10.58	-0.63	0.03	-0.03	0.02
	JUL	551.61	124.58	4.97	14.08	-0.38	-0.07	0.03	-0.03
	AUG	524.18	121.05	3.65	28.70	-0.05	0.10	0.00	0.00
	SEP	540.55	83.15	4.90	47.65	-0.55	0.30	0.05	0.00
case 620	JUN	651.71	140.08	2.87	3.92	-0.28	-1.12	0.18	0.13
	JUL	686.60	139.45	3.55	23.00	-0.10	-0.35	0.05	0.00
	AUG	541.35	135.25	2.50	24.55	0.05	0.00	-0.05	0.00
	SEP	417.73	90.10	3.80	37.90	-0.45	0.45	-0.05	0.00
case 900	JUN	460.31	172.98	0.38	10.23	-0.38	0.17	-0.03	0.03
	JUL	490.61	175.83	0.38	13.03	-0.43	0.23	-0.03	-0.03
	AUG	468.53	173.70	0.35	27.90	-0.30	0.45	0.00	0.05
	SEP	404.16	132.78	1.28	45.53	-0.38	1.07	-0.02	0.03
case 920	JUN	613.01	174.23	0.13	0.37	-0.07	-0.03	-0.02	-0.03
	JUL	639.99	177.83	0.17	20.43	-0.18	0.18	0.03	-0.02
	AUG	501.09	174.48	0.22	23.93	-0.18	0.22	-0.03	-0.02
	SEP	306.14	131.13	1.28	35.88	-0.18	0.83	-0.02	0.03

(b) Palermo

		Z_M	FT_M	FT_A	FQ_A	$T_M - T_A$	$T_M - Q_A$	$T_A - Q_A$	$T_M - T_A - Q_A$
case 600	JUN	456.91	117.73	5.72	-3.88	-0.38	-0.07	0.02	0.03
	JUL	669.96	170.13	4.17	-7.62	-1.72	-0.13	0.02	0.03
	AUG	772.34	175.83	2.72	11.77	-2.03	-0.17	0.03	-0.03
	SEP	621.46	110.93	5.53	37.68	-0.08	0.28	-0.03	-0.03
case 620	JUN	820.13	135.75	4.45	31.10	-0.45	0.10	0.00	0.00
	JUL	1054.40	175.70	3.75	29.30	-1.25	0.20	-0.25	-0.25
	AUG	1025.10	179.80	2.60	38.80	-1.60	0.20	0.00	0.00
	SEP	587.25	118.80	4.80	38.00	0.00	0.30	0.00	0.00
case 900	JUN	388.58	168.35	0.55	-4.70	-0.55	0.00	0.00	0.00
	JUL	646.58	205.85	0.10	-8.25	0.10	0.25	0.00	0.00
	AUG	755.25	206.40	0.00	11.10	0.00	0.20	0.00	0.00
	SEP	545.36	167.78	0.33	36.77	-0.32	0.52	-0.03	0.03
case 920	JUN	769.01	174.33	0.18	30.58	-0.13	0.18	0.03	0.02
	JUL	1034.88	205.25	0.00	28.65	0.00	0.35	0.00	0.00
	AUG	1011.95	206.10	0.00	38.00	0.00	0.00	0.00	0.00
	SEP	523.11	166.68	0.37	37.33	-0.37	0.57	-0.03	0.03

capacitance. In fact, the mass has the property to dampen the uncertainty propagation. Moreover, as one might expect, the perturbation of temperature amplitude has a greater influence on lighter than massive buildings.

This method allows some considerations on the combined effects due to simultaneous uncertainties of weather variables. Table 3.8 clearly shows that the second order effects, as well as higher order, are trivial compared with the first order results. The only contribution, that has an order of magnitude comparable to the first order effects, is the interaction between daily mean and amplitude of temperature variations. Generally, the link between mean temperature and amplitude perturbations has a negative sign, which means that there is not a synergic effects.

3.9.2 FM of loss utilization factor

Factorial analysis has also been performed in order to evaluate the sensitivity of the utilization factor. In Table 3.9 the results are reported for the different months and test cases for both Milan and Palermo.

In according to DSA, the most significant parameter appears to be the average value of the external dry bulb temperature. The magnitude of loss utilization changes, due to perturbation of daily mean temperature, decreases for cases 900 and 920 i.e. the massive buildings. In addition, notice that the major variations are found in Palermo with the highest values during July and August. This is because the average daily temperature in Palermo is very close to the internal setpoint for cooling. Therefore, a perturbation of mean temperature produces a significant change in the usability of night heat losses through the envelope.

As already shown by the results in Table 3.6, contrary to what is found for the cooling demand, the loss utilization factor is more sensitive to uncertainties in daily temperature amplitude than to the variations of solar irradiation peaks. Besides, it is interesting to note that the values of FT_A and FT_M are of the same order of magnitude, especially for lightweight buildings.

Finally, factorial analysis allows to draw some considerations about the synergic effects of uncertainties that affect the various climate parameters. The data reported in the Table 3.6 show as second order effects are generally negligible. The only significant interactions are between the perturbation of mean temperature and the changes of daily amplitude of temperature variations and solar irradiation. However, the second-order effects decrease when the thermal capacitance of the envelope increases. Consequently the thermal mass of the envelope acts as a filter to the propagation of errors in weather data uncertainties.

Table 3.9: Results of factorial analysis of loss utilization factor for cooling.

(a) Milan

		Z_M	FT_M	FT_A	FQ_A	$T_M - T_A$	$T_M - Q_A$	$T_A - Q_A$	$T_M - T_A - Q_A$
case 600	JUN	0.73	-0.09 %	-2.83 %	-0.26 %	-1.03 %	-0.11 %	-0.04 %	-0.04 %
	JUL	0.68	-1.14 %	-3.07 %	-0.54 %	-1.18 %	-0.14 %	0.01 %	-0.01 %
	AUG	0.74	4.86 %	-1.97 %	-0.18 %	-0.77 %	-0.08 %	0.01 %	-0.02 %
	SEP	0.64	3.10 %	-1.19 %	0.06 %	-0.09 %	-0.03 %	-0.01 %	0.01 %
case 620	JUN	0.81	0.33 %	-2.02 %	-2.55 %	-0.86 %	-0.57 %	-0.20 %	-0.16 %
	JUL	0.76	-2.01 %	-2.28 %	-1.37 %	-0.99 %	-0.37 %	-0.02 %	0.00 %
	AUG	0.81	3.47 %	-1.37 %	-0.20 %	-0.57 %	-0.03 %	0.02 %	0.02 %
	SEP	0.68	3.01 %	-0.91 %	-0.11 %	-0.06 %	-0.10 %	0.03 %	0.00 %
case 900	JUN	1.00	1.05 %	-0.12 %	-0.02 %	0.14 %	-0.05 %	0.00 %	0.00 %
	JUL	0.99	1.00 %	-0.11 %	0.02 %	0.16 %	-0.06 %	0.03 %	0.02 %
	AUG	0.99	0.93 %	-0.03 %	0.08 %	0.15 %	-0.12 %	-0.01 %	-0.03 %
	SEP	0.97	3.00 %	-0.28 %	0.52 %	0.03 %	-0.14 %	0.02 %	0.00 %
case 920	JUN	1.00	0.16 %	0.02 %	-0.09 %	0.05 %	0.00 %	-0.01 %	0.02 %
	JUL	1.00	0.18 %	-0.08 %	0.00 %	0.04 %	-0.05 %	-0.03 %	-0.02 %
	AUG	1.00	0.56 %	-0.01 %	0.05 %	0.09 %	-0.05 %	0.00 %	0.00 %
	SEP	0.96	2.99 %	-0.29 %	0.40 %	-0.03 %	-0.11 %	0.01 %	0.00 %

(b) Palermo

		Z_M	FT_M	FT_A	FQ_A	$T_M - T_A$	$T_M - Q_A$	$T_A - Q_A$	$T_M - T_A - Q_A$
case 600	JUN	0.57	-9.31 %	-4.08 %	-0.76 %	-1.83 %	-0.26 %	0.00 %	0.00 %
	JUL	0.62	79.48 %	-5.02 %	-1.25 %	6.64 %	1.41 %	0.06 %	-0.03 %
	AUG	0.66	67.57 %	-4.95 %	-0.07 %	5.45 %	-0.18 %	-0.05 %	0.05 %
	SEP	0.61	-2.74 %	-3.18 %	-0.39 %	-1.28 %	-0.38 %	0.02 %	0.03 %
case 620	JUN	0.70	-7.05 %	-3.21 %	-0.79 %	-1.29 %	-0.56 %	0.08 %	-0.08 %
	JUL	0.69	65.02 %	-4.13 %	0.07 %	5.85 %	0.26 %	-0.16 %	-0.16 %
	AUG	0.72	56.60 %	-4.27 %	-0.65 %	4.96 %	0.65 %	0.00 %	0.00 %
	SEP	0.65	-3.45 %	-2.75 %	-0.14 %	-1.14 %	-0.10 %	0.00 %	0.00 %
case 900	JUN	0.98	2.18 %	-0.17 %	-0.12 %	0.18 %	0.01 %	0.01 %	-0.01 %
	JUL	1.00	0.47 %	0.08 %	-0.19 %	0.12 %	0.19 %	0.00 %	0.00 %
	AUG	1.00	-1.11 %	-0.02 %	0.20 %	0.08 %	-0.01 %	0.00 %	0.00 %
	SEP	0.99	1.54 %	-0.11 %	0.03 %	0.12 %	-0.28 %	0.00 %	0.00 %
case 920	JUN	1.00	0.22 %	-0.17 %	-0.49 %	-0.05 %	-0.34 %	-0.03 %	-0.03 %
	JUL	1.00	-0.95 %	-0.26 %	-0.12 %	-0.01 %	0.45 %	0.17 %	0.17 %
	AUG	1.00	-1.30 %	0.62 %	0.54 %	-0.56 %	-0.54 %	-0.54 %	0.54 %
	SEP	0.99	1.85 %	-0.17 %	0.20 %	0.09 %	-0.11 %	0.02 %	-0.02 %

3.10 Conclusions

In this chapter, a sensitivity analysis of numerical models for the prediction of cooling consumptions is carried out. In particular, in order to increase the representativeness of the sample analyzed, massive and lightweight buildings with different orientations of the glazing area are used. Besides, the weather data of two different cities are used with the purpose of taking into account both warm and mixed climates [8]. Furthermore, with the purpose of modeling the data uncertainty, the weather variables are perturbed in both the daily average value and the amplitude of the daily oscillations.

The results of dynamic simulations reveal the importance of using real sequence of weather data. In particular, analyzing the curves of the loss utilization factor, taken back by the results of dynamic simulations, a large gap between real trend and mean typical day (MTD) is recorded, especially for lightweight buildings. In fact, the envelope with high capacitance work like a low pass filter and, consequently, only the fundamental and a few higher harmonics actually affect the heat balance of the thermal zone. Another important result of this analysis concerns the comparison between the loss utilization factor obtained from dynamic simulation and that proposed by the EN ISO 13790 [3]. Contrarily to the standard, a bijective link between loss utilization factor and the ratio of losses to gains has not been found. In fact, the ratio of losses to gains takes into account only the frequencies of the external conditions but not the information about the sequences.

Secondly, the sensitivity analysis identifies the climate parameters that mainly affect the building energy balance in summer period. The results of Differential Sensitivity Approach (DSA) clearly show that the interactions between climate and cooling demand depend on the envelope features. However, the parameter with the greatest sensitivity index is the daily average of outside dry bulb temperature. An order of magnitude lower are the sensitivity index to solar irradiation changes. But if spring and autumn are also taken into account the influence of solar irradiation becomes comparable to that of mean dry bulb temperature. In fact, the strong dependence of the solar sensitivity index on the incident angle of solar beams is pointed out by this work.

Besides, the utilization factor has a different sensitivity to weather data. In fact, while the sensitivity index to solar radiation perturbations is low, the indices for changes in mean temperature and daily amplitude of variations have the same order of magnitude.

In conclusion, the Factorial Method demonstrates the negligibility of the second and higher order effects. Consequently, the assumption of perfect inde-

pendence between the uncertainties of climate variables is realistic for energy simulations.

Part II

Analysis of building envelope issues

Chapter 4

Monte Carlo method for the uncertainty analysis of the heat transfer

Dynamic energy simulation has the potential to provide relevant information about the building summer behavior and to indicate the possible conservation measures for the reduction of energy consumptions. One of the problems in the application of enhance simulation methods, that sometimes can undermine the reliability of their results, is the difficulty to gather reliable input data.

Among the terms of the energy balance of buildings, one of the greatest contributions is without doubt the heat transfer through the envelope. This is mainly affected by the uncertainty of the thermophysical properties such as conductivity, specific heat and specific mass.

In order to perform an uncertainty analysis, in this chapter firstly the Monte Carlo method is presented. This procedure is applied for the recursive solution of the partial differential equation of the heat conduction. Secondly, a brief review of the numerical methods suitable for the solution of unsteady conduction through the envelope is reported. This survey allows the identification of the widely used method that, due to the complexity of numerical operations involved, could be very sensitive to uncertainties in input data. Finally, some considerations are presented about the uncertainty of thermophysical properties of the envelope materials, that constitute the inputs of the Monte Carlo method. Following on from this point, the test cases and the assumptions made are fully described.

4.1 Overview

The simulation is a representation of key characteristics or behaviors of a selected physical system. Consequently, simulations can show the possible real effects of alternative conditions and courses of action. Moreover, simulations are used when the real system cannot be tested because it may not be accessible, or it may be dangerous or expensive to test. Key issues in simulations include acquisition of valid source information and the use of simplifying approximations and assumptions. Subsequently, it becomes relevant the verification and validation of the simulation outcomes.

In the last few years, increasing attention has been paid to the uncertainty and sensitivity analyzes on building energy simulations. In fact, the influence on the outputs of variations in simulation inputs has numerous consequences. For instance, uncertainty and sensitivity analyzes are used to identify the parameters which must be chosen with care so that the accuracy of simulation predictions is not compromised. Moreover, the identification of the primary features of a building, to which the energy consumption is sensitive, can lead engineers and architects to improve the building design. Finally, the uncertainty analysis provides information about the maximum accuracy which can be expected in model predictions and the likelihood that energy use will not exceed the mandatory provisions.

In one of the earliest work, Lomas and Eppel [78] compared three different techniques for sensitivity analysis. Following on from this work, Macdonald [84] integrated some uncertainty procedures in the software Esp-r and de Wit and Augenbroe [39] studied, with a Monte Carlo approach, the uncertainty of either thermal comfort and natural ventilation. A similar work is carried out also by Hyun et al. [68] where the influence of changes in ventilation rate on the indoor air quality is estimated with Monte Carlo method.

More recently, Corrado and Mechri [31] performed a sensitivity analysis of the quasi steady state approach proposed by EN ISO 13790:2008 [3] for the calculation of the energy performance for heating. Instead, Hopfe et al. [65, 66] analyzed the influence of uncertainty in the early stage of design process.

In this chapter, the influence of thermophysical properties on the heat flux through the envelope is investigated. In fact, when an energy modeler is going to implement a building energy simulation, one of the major difficulties encountered is the retrieval of reliable thermophysical properties. This issues is further emphasized when the model refers to existing buildings.

In early design phase and when adequate data are not available, the reference thermophysical properties [2] are often used in lieu of declared and certified

values. These properties are safe values and they refer to the worst case, which normally stand for the 90 % fractile.

Besides the thermal characteristics, especially for porous media, are related to the water content and, to a lesser extent, to temperature and age [2].

In addition to this, the uncertainties due to simplifying assumptions, commonly made in thermal analysis, should not be forgotten. For instance, the material apparent conductivities, as well as the other thermophysical properties, are the macroscopic results of various basic mechanisms such as the solid and gas conduction, the gas convection and the long wave radiation.

Furthermore, for non homogenous material the physical properties are averaged values that depend on the percentage composition of individual components.

The question then becomes to what extent the uncertainties of thermophysical properties affect the reliability of the heat transfer through envelope and, consequently, of the energy simulation predictions? In order to answer to this question, the Monte Carlo method is herein presented (Section 4.3). This procedure is applied to the heat transfer process. The uncertainty in the thermophysical properties, that are the inputs in the simulations, are indeed studied (Section 4.6).

4.2 Probability Density Function for input/output data

Before describing the Monte Carlo method and the model equations, some definitions and references to the probability theory are essential and herein presented, as well as the description of the most popular distribution curves.

Random variable $g(x)$, it is a function defined on a sample space x that is the space of all possible outcomes of an experiment;

Distribution function $F(x')$, it is the probability that a measured value of x is less than or equal to x' , then:

$$F(-\infty) = 0, \quad (4.1)$$

$$F(+\infty) = 1. \quad (4.2)$$

The distribution function F is a non-decreasing function of x .

Density function $PDF(x)$, it is defined in a continuous variable sample as

$$PDF(x) = \frac{dF}{dx}. \quad (4.3)$$

In particular, $PDF(x')dx'$ is the probability that x lies between x' and $x' + dx'$. The integral over all x' of $PDF(x')$ is equal to one;

Expectation value E of g , where $g(x)$ is a random variable. It is defined as

$$E\{g\} = \bar{g} = \int_{x=-\infty}^{x=+\infty} g dF = \int_{x=-\infty}^{x=+\infty} g PDF dx \quad (4.4)$$

for x continuous variable;

Probability moments . They are expectation values of various powers of random variable. Let $g = x$ then the mean value or first moment is defined as:

$$E\{x\} = \bar{x} = \int_{x=-\infty}^{x=+\infty} x PDF dx. \quad (4.5)$$

Let $g = (x - \mu)^2$, the second central moment (or variance) is

$$Var\{x\} = \overline{(x - E\{x\})^2} = \int_{x=-\infty}^{x=+\infty} (x - E\{x\})^2 PDF dx. \quad (4.6)$$

Notice that $\sqrt{Var\{x\}}$ is called the standard deviation.

4.2.1 Normal or Gaussian distribution

The normal or Gaussian distribution is the most used distribution in probability theory. It is the appropriate distribution to model random errors in measured physical data. This distribution is defined by the following density function:

$$PDF(x) = \frac{1}{\sqrt{2\pi\sigma^2}} \cdot e^{-\frac{(x - \mu)^2}{2\sigma^2}} \quad (4.7)$$

Typically, in building simulation, measured lengths or temperatures are example of normal distributed data. As the distribution is unbounded there is a possibility that data have a non-physical value. For example, a measured thickness or thermal conductivity can not be negative.

4.2.2 Lognormal distribution

It is a variation of the Gaussian distribution. In fact, a lognormal distribution is a continuous probability distribution of a random variable whose logarithm is normally distributed. Consequently, it can be derived assuming that $\ln(x)$ is

distributed according to a normal distribution:

$$PDF(x) = \frac{1}{x\sqrt{2\pi\sigma^2}} \cdot e^{-\frac{(\ln(x) - \mu)^2}{2\sigma^2}} \quad (4.8)$$

A variable might be modeled as lognormal if it can be thought of as the multiplicative product of many independent random variables each of which is positive. For example, area which is the results of two length product might be assumed to be lognormally distributed as well as the resolution of an instrument which has a number of error sources or the thermal capacitance that is the product of specific mass and specific heat.

The expectation value and the variance of the distribution are not simply μ and σ but:

$$E\{x\} = e^{[\mu+(1/2)\sigma^2]}, \quad (4.9)$$

$$Var\{x\} = e^{(2\mu+\sigma^2)} (e^{\sigma^2} - 1). \quad (4.10)$$

4.2.3 Weibull distribution

The Weibull distribution is one of the most widely used lifetime distributions in reliability engineering. It was originally proposed to quantify fatigue data, but it is also used in analysis of systems involving a weakest link. In 1939 Weibull obtained this distribution from the study of the fracture of materials under repetitive stress. It is a versatile distribution that can take on the characteristics of other types of distributions, based on the value of the shape parameter β . The two parameter Weibull density function is

$$PDF(x) = \frac{\beta}{\alpha} \left(\frac{x}{\alpha}\right)^{\beta-1} e^{-\left(\frac{x}{\alpha}\right)^\beta} \quad (4.11)$$

where α is a scale or size parameter, β shape or slope parameter.

The size parameter formalizes what already observed experimentally by Leonardo da Vinci who stated: *"for the same gauge, long strings are less resistant than shorter ones"*. By changing the value of the shape parameter, the Weibull distribution can model a wide variety of data while the scale parameter determines the range of the distribution.

4.3 Monte Carlo Method

The Monte Carlo method provides approximate solutions to a variety of mathematical problems by performing statistical sampling experiments on a computer.

The name refers to a famous casino in Monaco because the use of randomness and the repetitive nature of the process are analogous to the activities conducted at a casino. The Monte Carlo method is very flexible and so often used to carry out stochastic analysis, where other methods fail. Furthermore, the continuous growing of computer power makes it a method which is continuously appreciated.

The idea behind the Monte Carlo approach is that if a set of data with the same statistic of the population can randomly be found, these data can be used as deterministic input in the heat transfer model (Section 4.4) and, subsequently, the distribution of the model expectation could be generated (Figure 4.1).

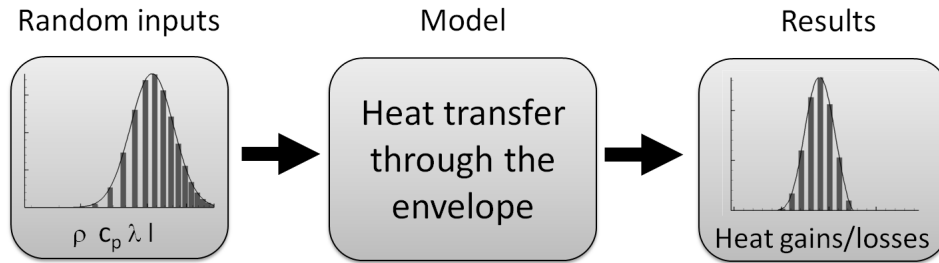


Figure 4.1: *Scheme of the Monte Carlo procedure adopted.*

A Monte Carlo method entails full random selection, out of all possible values of the inputs in a correct statistical combination. If the selection of data is improved, the amount of simulations can be reduced (Section 4.3.1). However, with enhanced sampling methods the unbiasedness of results can not be taken for granted and it should be verified with additional computational costs.

The Monte Carlo method is based upon the Central Limit Theorem. The method can be summarized as following:

1. the probability distribution function of the random variables involved has to be known (Section 4.2).
2. a large number of realizations of the random inputs are generated numerically (Section 4.3.1).
3. for each random input set, the problem is considered deterministic and so numerically solved (Section 4.4).

4.3.1 Generating Sample Data

In order to reduce the number of simulation in Monte Carlo analysis and to ensure an adequate coverage of the sample, a standard statistical procedure is to use sampling techniques. In literature there are three main sampling techniques [85]:

- Simple random sampling: it is the most basic method. It works by generating a random number in agreement with the probability distribution and scaling this to the target value. The results is an unbiased estimate of the population variance;
- Stratified sampling: it is an improvement of the latter case. The sample space is partitioned in a finite number of intervals with an equal probability. Subsequently one random input is then selected from each stratum.
- Latin Hypercube sampling: it is an evolution of the previous method. Each randomly generated value (e.g. λ , ρ , c_p and l) is taken from a different stratum. However, the estimated variance has been shown to be biased.

Macdonald [85] shows that the three sampling techniques produce results with the same significance level but with less variance in the mean prediction for Stratified and Latin Hypercube methods. However, no fewer simulation runs are required for the enhanced sampling method. Besides, he demonstrates that at least 100 simulations are required for Monte-Carlo approach and, if simple random sampling is used, the estimation of mean and variance will not vary significantly up to 50000 simulation runs.

4.4 Dynamical model of heat transfer through envelope

As mentioned in previous sections, one of the most important heat transfer processes in a building is the heat conduction through the envelope. Even if many methods have been proposed in literature to solve the problem of unsteady heat conduction in building elements, all of them are to some degree a simplification of the actual process and are based on strong assumptions. The two main hypothesis commonly assumed are:

- one-dimensional heat conduction, notice that edge effects are neglected and the temperature distribution is assumed to be uniform throughout a cross section of the wall. Usually the two dimensional effects due to

geometry or to material coupling (i.e. thermal bridges) are taken into account with the linear thermal transmittance;

- homogeneous material with constant thermal properties while in reality most building materials are non-homogeneous and they exhibit some variations in their thermal properties as a result of temperature changes. However, these effects are generally neglected on the actual heat transfer calculation.

These assumptions let to write the following governing equation for heat conduction in building elements [21]:

$$\frac{\partial \theta}{\partial \tau} = \frac{\lambda}{\rho c_p} \frac{\partial^2 \theta}{\partial x^2} \quad (4.12)$$

that is generally coupled with the Fourier equation

$$\dot{q}(x, \tau) = -\lambda \frac{\partial \theta(x, \tau)}{\partial x} \quad (4.13)$$

where θ is the temperature,

λ is the thermal conductivity of the layer,

ρ is the specific mass of the layer,

c_p is the specific heat of the layer,

\dot{q} is the transmitted heat flux.

For this system of partial differential equations, analytical solutions exist for the single homogenous layer. The complexity of the solution increases for multilayer wall and when the boundary conditions become not trivial. Consequently, in most cases, numerical solutions are searched. There are, however, numerous methods available for modeling heat conduction in a building and many strategies to determine the model parameters (Figure 4.2).

Among the possible ways to model this process are:

- Finite Differences (FD);
- Finite Elements Method (FEM);
- Conduction Transfer Function (CTF);
- Response Factor (RF);
- Admittance Method (AM).

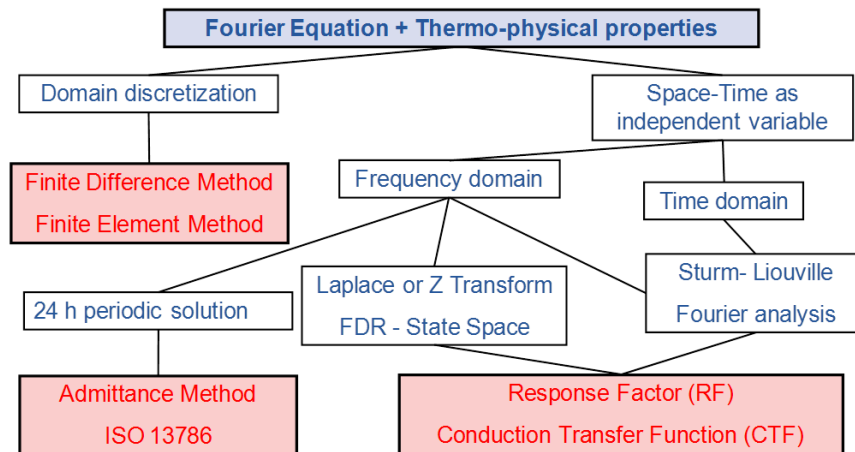


Figure 4.2: Solution strategies for unsteady heat transfer through envelope.

While each of these methods has advantages over the others in various applications, traditionally, building thermal simulation softwares have used CTF method for transient heat conduction.

Finite element techniques are typically slower and better suited for complex geometries. Since it is a time consuming method it is not suitable for annual simulation of high rise residential building, as well as, straight transform methods or analytical solutions have limited applicability to more complex building elements.

Finite difference solutions offer a great advantage because of their simplicity and ease of understanding. The key obstacles in using a FD approach is finding a general application technique for every building element definition, implementing a solution strategy which guarantees stability, and time and storage considerations.

Despite some initial complexities in the methods required to calculate coefficients, time series methods (i.e. CTF and RF) are faster and have a low computational cost. In fact, the CTF and RF coefficients are calculated for each building element type at the beginning of the simulation process and they have not to be recalculated at each step. Besides, the resulting conduction equation is simply a linear summation. Consequently, whereas a FD solution has many nodes where the variables must be evaluated at small time steps, the time series approach only requires to compute temperature and heat flux at specific points that are internal and external surfaces of each envelope components.

4.4.1 Conduction Transfer Functions

The CTF approach [91, 121] for the solution of the partial differential equation (4.12) takes advantage of the time linearity of the heat equation by means of the superposition principles. The method results in a simple linear equation that expresses the current heat flux in terms of the current temperature and temperature and heat flux histories as shown in the following equations

$$\dot{q}_o(\tau) = - \sum_{j=0}^{N_y} Y_j \cdot T_{i,\tau-j\delta} + \sum_{j=0}^{N_x} X_j \cdot T_{o,\tau-j\delta} + \sum_{j=1}^{N_\phi} \phi_j \cdot \dot{q}_{i,\tau-j\delta} \quad (4.14)$$

$$\dot{q}_i(\tau) = - \sum_{j=0}^{N_z} Z_j \cdot T_{i,\tau-j\delta} + \sum_{j=0}^{N_x} Y_j \cdot T_{o,\tau-j\delta} + \sum_{j=1}^{N_\phi} \phi_j \cdot \dot{q}_{i,\tau-j\delta} \quad (4.15)$$

where \dot{q}_o is the heat flux on the external side of the component,
 \dot{q}_i is the heat flux on the internal side of the component,
 X_j, Y_j, Z_j are respectively the exterior, the cross and the internal CTF j-th coefficient,
 τ is the time,
 δ is the time step of energy simulation,
 T_i, T_o are the temperature of the internal and outside surfaces.

Despite the simplicity of the equations (4.14) and (4.15), the complexity of the method lies in the evaluation of the CTF coefficients. Several calculation techniques have been proposed. For instance, while in [34, 129, 136] a transform approach in time domain is used and Fatemi [47] employs a neural network approach, a frequency domain regression is applied in [23, 24, 25, 26, 35, 131, 132, 133]. The latter substitutes a simple ratio of two polynomial in Laplace space to the Laplace transform of the transfer function, with a relevant increase in the root finding efficiency. However, the two most widely diffused are the direct root finding approach [63, 64] and the state space method [70, 115]. The DRF approach introduced by Hittle [63] transforms the governing equations (4.12) and (4.13) into the form:

$$\begin{bmatrix} \dot{q}_i(s) \\ \dot{q}_o(s) \end{bmatrix} = \begin{bmatrix} \frac{D(s)}{B(s)} & \frac{-1}{B(s)} \\ \frac{1}{B(s)} & \frac{-A(s)}{B(s)} \end{bmatrix} \begin{bmatrix} T_i(s) \\ T_o(s) \end{bmatrix} \quad (4.16)$$

where $T_i(s), T_o(s)$ are the temperature in Laplace domain,
 $\dot{q}_i(s), \dot{q}_o(s)$ are the heat fluxes in Laplace domain,
 s is the coordinate of the Laplace domain,
 $A(s), B(s), D(s)$ are overall transmission matrices.

Equation (4.16) relates the flux at either surface of the element to the temperature histories at both surfaces.

For a multilayer component the transmission matrix is computed using the electrical analogy. In fact, the whole transfer matrix is computed by means of a matrix multiplication of single layer matrices in which the single elements are calculated as

$$\begin{aligned} A_i(s) &= \cosh\left(l_i \cdot \sqrt{\frac{s \cdot \rho_i c_{p,i}}{\lambda_i}}\right) \\ B_i(s) &= \frac{1}{\lambda_i \cdot \sqrt{\frac{s \cdot \rho_i c_{p,i}}{\lambda_i}}} \sinh\left(l_i \cdot \sqrt{\frac{s \cdot \rho_i c_{p,i}}{\lambda_i}}\right) \\ D_i(s) &= \cosh\left(l_i \cdot \sqrt{\frac{s \cdot \rho_i c_{p,i}}{\lambda_i}}\right) \end{aligned} \quad (4.17)$$

where l_i is the thickness of the i-th layer,
 λ_i is the conductivity of the i-th layer,
 ρ_i is the specific mass of the i-th layer,
 $c_{p,i}$ is the specific heat of the i-th layer,

Hittle and Bishop [64] describe a simplified method for finding the roots of the Laplace domain equations and in particular they draw attention to circumstances where two consecutive roots are very close together and might remain undetected by an insufficiently small time step.

When the temperature histories are formulated as triangular pulses made up of two simple ramp functions, the roots of this equation can be found and results

are the response factors coefficients (RF). The response factors are infinite coefficient series that use only temperature terms. The RF equations, that can be obtained using $N_\phi = 0$ in equations (4.14) and (4.15), can be simplified by the introduction of flux history terms to form conduction transfer functions (CTF). Moreover, the CTF approach let N_x , N_y and N_z terms, that for response factor equations are theoretically infinite, to be less or equal to 6 in order to obtain a stable solution with the addition of less than 5 flux terms [13].

The number of CTF terms will increase to satisfy the convergence criteria for heavy mass constructions, although a greater number of terms does not always mean better accuracy in the solution [16, 17, 50].

Source of CTF errors

Since it is a numerical solution, some errors can arise in CTF approach. The errors come both from the approximation of the method and from the root finding procedure. The error sources in Laplace transform approach are categorized as follows [112, 116]:

- Root finding tolerance: in order to calculate CTF terms, it is necessary to find the root of $B(s) = 0$ [63]. Since the expression for $B(s)$ becomes not trivial for multilayer components, the root finding procedure relies on numerical methods. The procedures iteratively continues until the root is found within a root finding tolerance or the maximum number of iterations is reached;
- Number of CTF terms: CTFs are derived from RFs and it is necessary to determine the number of CTF terms so that the equivalence is ensured;
- Solution time step: the temperature variation is sampled at discrete time steps and the actual temperature variation is approximated with linear temperature profiles. Therefore, this error becomes evident when the time step is too large to adequately approximate the actual temperature variation.
- Number of flux history terms: it can alter the value of the current heat flux. The number of terms needed varies: for light weight materials, the thermal response is fast and a few history terms are enough to accurately calculate the current heat flux while for heavy weight materials, more terms are needed.

Qian et al. [112] show an increasing in CTF error for massive component. They uses the Fourier number (Fo) as indicator of the thermal capacitance of

the component. In fact, since the time step δ is constant in the CTF calculations, changes in the Fo only represent changes in material properties: the higher the thermal capacity of the component, the greater the reciprocal of Fo . However, for multilayer components, not only material properties but also the layer sequence, described by means of the thermal structure factor (S_{ie}), influences CTF terms (Figure 4.3). Notice that for massive building components,

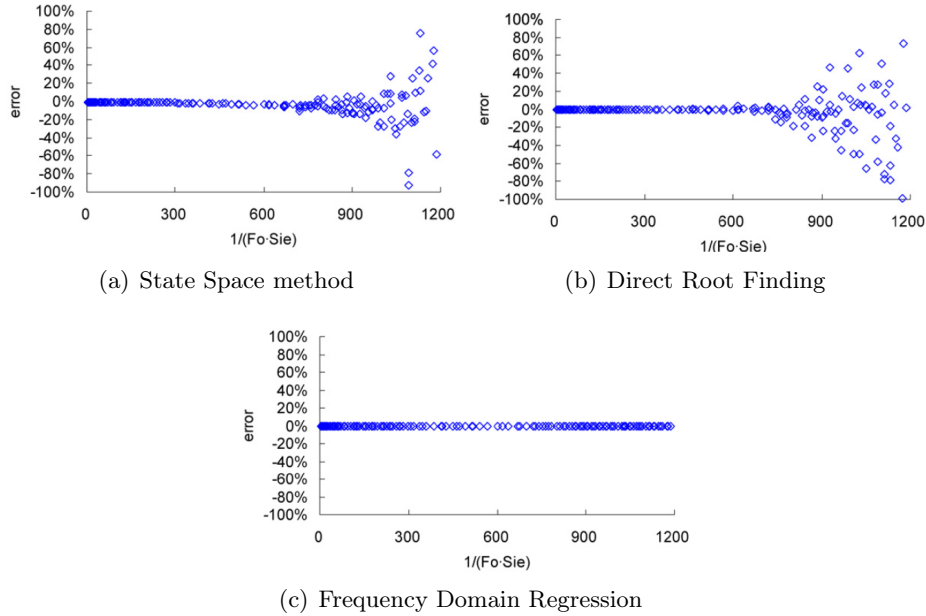


Figure 4.3: CTF errors with different calculation procedure Qian et al. [112]

the DRF approach is subject to more errors than other methods, especially for issues related to tolerance in roots finding. Nevertheless, this method is widely used in dynamic simulation codes [127]. Therefore, the DRF method is chosen for the sensitivity analysis of CTF calculation to the variability of material thermophysical properties. Then, in order to perform the uncertainty analysis, an embedded code that matches the simple random sampling with Monte Carlo simulation and the calculation of CTF, by DRF approach, has been implemented in Fortran.

4.5 Error classification in thermophysical properties

The purpose of this analysis is the investigation of the reliability of unsteady conduction prediction when uncertain input data are adopted. Since thermophysical properties of construction material are derived from measurement, they are always affected by uncertainty. The errors in measurement can be divided

in two categories [96]:

- Systematic errors: they cause all the readings on average to be biased away from the true value. Systematic errors are the results of the whole measurement chain and they are constant or change in a regular manner for the same experimental process. Typical causes are the uncalibrated equipment or imperfect definitions of the measured entities and the non representative sampling;
- Random errors: they are not caused by the measuring process, consequently a sequence of readings will be scattered unpredictable.

Extending these definitions to dynamic simulation, the systematic errors arise when incorrect input data or wrong numerical model are adopted. For instance, in early stage of design a different insulation material properties can be erroneously used. Or, for an hygroscopic material, the thermophysical properties of dry sample can be used in lieu of the wetted values.

Instead, random errors occurs when suitable data are adopted but there is still a variability in the input [84] or when there is an uncertainty in the measures. For instance, the right thermal conductivity of insulation is chosen but there is a change in the characteristics of the same sample production. While systematic errors can be redacted through the correct use of available characteristics, random errors are unpredictable and unmodelable.

Furthermore the two error categories differ also for the distribution type. In fact, while systematic error are generally described with an even distribution, the normal distribution (Section 4.2) is commonly adopted for the random errors [84].

Another classification is made on the method by which uncertainty is evaluated. The simplest way of assessing uncertainty is to make many measurements and to use these results to estimate the range of possible values. The uncertainties evaluated with this strategy are called Type A. An alternative procedure is to bring other information to bear on the problem such as physical theory, information from handbooks, or similar situations. These uncertainties are called Type B uncertainties [96].

Although it is frequently to associate the Type A and Type B uncertainties respectively with random and systematic errors, this is not true. In fact, Type A and Type B characterize methods for assessing uncertainty, while random and systematic refer to types of error. When random and systematic errors contribute to uncertainty both may be assessed by either Type A or Type B methods.

Since, due to the controllability of the analysis, it is not convenient to combine different source of uncertainties [65] and systematic errors can be limited. This research deals only with the random errors. Consequently a Gaussian distribution of the input data is adopted (Section 4.2.1).

In order to better describe the distribution of the thermophysical properties in the following section some definitions are presented.

4.6 Uncertainty in thermophysical properties

As described in Section 4.5 every measurement is subjected to a degree of uncertainty. Although the purpose of this thesis is not the evaluation of the reliability of thermophysical property measurements, a brief analysis is useful for a correct representation in the uncertainty model. In fact the following analysis, based on literature review and on manufacturer product sheets, allows the detection of the variability in the input data and the definition of the Gaussian distribution parameters, i.e. mean and variance (Section 4.2.1).

4.6.1 Thermal conductivity

The measurement of thermal conductivity are usually performed with a guarded hot box apparatus. In this equipment both surface temperature and heat flux are measured and recorded. An Heat Flux Meter (HFM) is basically composed of a thin plate made of a material with known thermal conductivity and a thermopile able to measure the temperature gradient across the plate itself. In the last few years, several studies have been carried out to better understand HFM performances and their complex measurement chain. In fact, even though many HFMs are calibrated in correspondence of large heat fluxes values (i.e., greater than 100 W m^{-2}), the measured thermal flux in residential applications is typically much lower. On the other hand, only few national measurement institutes are able to provide HFM traceability to lower heat fluxes commonly found in building applications [11].

Macdonald [84] estimates in 30% the uncertainty in thermal conductivity within samples of the same material and constant density. Another estimation of conductivity uncertainties is provided by the standard ISO 9869 [9]. This standard quantifies the error in the measurements chain as follow:

- 5% due to the imperfect calibration of temperature and heat flux sensors;
- 5% caused by the imperfect thermal contact of HFM;

- 3% related to the alteration of the temperature and heat flux fields caused by the presence of HFM;
- 10% due to the non-stationary of the boundary conditions.

The overall uncertainty that can be expected is between the 14% and 28% [9]. These values do not take into account the variability of conductivity related to moisture content and to age and temperature effects [2].

4.6.2 Specific Mass

The specific mass is normally measured weighting a dry sample of material that has been oven dried at 105 °C. In hygroscopic materials the specific mass is strongly affected by the water content. In fact, hygroscopic materials are generally low weighting elements so the effect of moisture is significant. Macdonald [84] quantifies the uncertainty of construction material due to the variation in water content in 13% and 11% respectively for non hygroscopic and organic hygroscopic material. In literature there are currently few data regarding specific mass.

Moreover, the percentage uncertainty in specific mass differs between industrially produced materials, which generally have a product standard, and products assembled on site. For instance, the standard UNI EN 771-1:2011 [7] establishes two classes of variability for clay blocks (i.e. D1 and D2), that correspond to $\pm 10\%$ and $\pm 20\%$. No data are available for hand prepared materials such as cast concrete, for which the specific mass is strictly connected to the proportions of the main ingredients.

In addition to this, in some cases the property of a local area on the specimen is measured instead of an integral property over the sample. In these cases, the measured values are scattered not only due to random errors affecting of the measurements, but also because of non uniformity of the material. This variability becomes very important for guaranteed thermophysical properties used in energy saving measures and in order to comply with mandatory provisions.

4.6.3 Specific Heat

The simple way to measure the specific heat is to supply a known heat quantity \dot{q} to a material specimen and then measure the temperature rise $\Delta\vartheta$. The specific heat c_p is so computed as:

$$c_p = \frac{\dot{q}}{m\Delta\vartheta} \quad (4.18)$$

where m is the mass of the specimen.

Another procedure for the specific heat measurement is described in annex D of the standard EN 15498:2008 [5]. This test method serves to determine the specific heat capacity of building materials, of which the density and the thermal conductivity are known. The test device is a thermally isolated container filled with silicone oil and equipped with a heating device for heating the fluid. The specimen is immersed in the heated oil bath and the core temperature of specimen is measured. Besides, the core temperature has to be computed by means of the well known relations that use the Biot and the Fourier adimensional numbers. Then, the measured and the calculated core temperature are compared and the assumed specific heat should be varied until an adequate match is reached.

The relative uncertainty of specific heat measures is affected by a high number of error sources. In fact, in addition to the output variability introduced by HFM (Section 4.6.1), there are the uncertainty of temperature measures and the error due to the unsteady conduction through the sample. The latter is closely related to the thermal conductivity: the smaller the thermal conductivity, the higher the error in the evaluation of the heat capacity. Consequently there is a cross correlation between uncertainties in conductivity and specific heat that is neglected in this analysis.

Macdonald [84] quantified the uncertainty in specific heat measures, citing the British Standard 1987, as 12.25%.

4.6.4 Thickness

Uncertainty in thickness depends on the layer and material typology. In fact, for industrial manufactures there are a series of product standard that limit the dimensional tolerance. For instance, for EPS insulation the relative tolerance in thickness has to be lower than 1%. Similarly for clay blocks the standard UNI EN 771-1:2011 [7] provide a thickness variation range of $\pm 7\%$. The uncertainties increase for in situ cast material and when the object of thermal analysis is an existing building. For the last case, for example, there is a considerable variability in the envelope thickness. Furthermore, when these historical buildings are renovated, often the non-perfect verticality of the walls leads to a local variation of the thickness (Figure 4.4).

This type of uncertainty has not been widely studied in literature because it depends on local building practices and on the age of construction. So the range of variability should be studied on a case by case basis.



Figure 4.4: *Thickness variability of insulation layer in a building retrofit*

4.7 Test Cases

This section provides a detailed description of the characteristics of test cases used for the uncertainty analysis of cooling demand depending on uncertainties in thermophysical parameters. Firstly, the stratigraphies of typical Italian walls are selected for which the uncertainty and sensitivity analysis methods will be performed. Secondly, the basic climatic features of two different cities, used in Monte Carlo approach, are defined.

4.7.1 Wall typologies

The choice of the envelope typology is a key point in the uncertainty analysis. Besides, since the unsteady heat conduction through the envelope is strictly connected to the thermal inertia of the component, also the arrangement of layers has an important role in the envelope dynamic behavior.

Since the purpose of this thesis is the verification of the applicability of dynamic simulation method to the Italian context, the most common types of building envelope in the Italian territory are investigated and adopted. In Italy the historic buildings represent an appreciable amount of the whole building stock. From the data reported in the 14th Italian census 2001 the percentage are:

- before 1919: about 20% of the building stock;
- from 1919 to 1971: about 44% of the building stock;

- from 1971 to 1991: about 29% of the building stock;
- after 1991: about 7% of the building stock.

These data show that about 20% of the Italian housing stock is build before 20th century. In this period the construction type is various and includes brick and stone walls, Figure 4.5 (d). The latter are of particular interest to the uncertainty analysis. In fact, due to the high thickness and mass, the calculation of CTF coefficients of stone walls may be subjected to errors (Section 4.4.1). Moreover, the heterogeneity of the material induces a high variability of the thermophysical properties.

The period of construction not only affects the construction techniques and conservation status of the building envelope but rather modifies the mandatory provisions to meet. In fact in Italy there are three regulatory phases that coincide with the issuing of:

- Law n°373/1976 [101],
- Law n°10/1991 [102],
- Decree n°192/2005 modified and integrated by decree 311/2006 [103].

For instance, in the 1970s the interest in issues related to thermal insulation of building increased due to the 1973 oil crisis and the subsequent enacting of law n°373/1976 [101]. As a result, the building envelope had to guarantee not only the static function but also a reduction of thermal heat losses. An example of wall typology that matched these requirements is a lightweight aggregate clay block, more commonly known by the acronym LECA block, Figure 4.5 (c). As well as, the more restrictive requirements of law n°10/1991 [102] and of decree n°192/2005 induced the division between the static and the insulating function of the envelope. Consequently, for more recent low rise residential buildings it becomes more widespread the multilayer technique, Figure 4.5 (a) and (b).

In the Monte Carlo simulations four test cases are adopted (Figure 4.5) in order to cover the majority of Italian wall typologies. The test cases differ for the stratigraphy and both materials and layer sequences as reported in Table 4.1. In the following discussions, for simplicity, the test cases are renamed as:

- **Mi case**, the Multilayer wall with internal insulation, Figure 4.5 (a),
- **Me case**, the Multilayer wall with external insulation, Figure 4.5 (b),
- **Le case**, the distributed insulation wall with expanded clay blocks, Figure 4.5 (c),

- **Sw case**, the Stone non-insulated wall, Figure 4.5 (d).

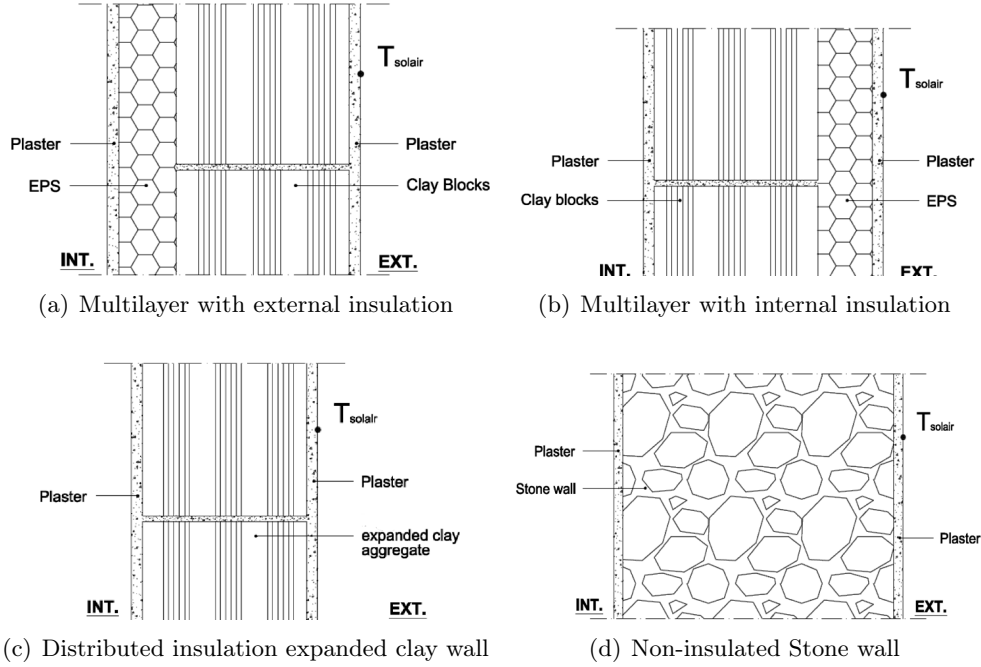


Figure 4.5: Wall typologies used in Monte Carlo analysis.

Table 4.1: Stratigraphy and layer thickness of the four test cases (Figure 4.5)

Me case		Mi case	
Layer	l [m]	Layer	l [m]
External Plaster	0.01	External Plaster	0.02
EPS	0.1	Clay blocks	0.3
Clay blocks	0.3	EPS	0.1
Internal Plaster	0.02	Internal Plaster	0.01
Le case		Li case	
Layer	l [m]	Layer	l [m]
Internal Plaster	0.01	External Plaster	0.02
Expanded clay block	0.35	Stone wall	0.7
External Plaster	0.02	Internal Plaster	0.01

4.7.2 Cities and climate

In order to ensure a greater representativeness of the Monte Carlo simulation results, two different climates are analyzed. More specifically the cities already

described in Chapter 1 (i.e. Trento and Palermo) are used with the purpose of modeling both warm and mixed climate [8]. The coordinates and the main characteristics of the sites used in the Monte Carlo simulations are shown in Table 4.2.

Table 4.2: *Climate features of the cities used in Monte Carlo simulations.*

City	Latitude	Elevation	HDD ₂₀	CDD ₂₀
Trento	46°.0231N	185 m	2798	197
Palermo	38°.1311N	50 m	994	704

4.7.3 Thermophysical properties distributions

As already mentioned in section 4.5, with the aim of ensuring a better controllability of the analysis the systematic and random error are not combined in Monte Carlo simulations. Consequently, since the systematic errors can be limited, this analysis focuses on the random errors. This kind of uncertainties can be modeled by a Gaussian distribution curve (Section 4.2.1). Normal distribution can be uniquely identified by two parameters that are mean μ and variance σ^2 .

For this study, mean and variance are defined for each material based on the information presented in section 4.6. Furthermore, the values assumed are compared with manufacturer data sheets and with data reported in literature [31, 40, 65, 66, 84]. Typical material uncertainties are summarized in Table 4.3.

Notice that there is a strong correlation between the properties of a material due to sources of uncertainty. For example, moisture content would impact upon the conductivity, density and specific heat capacity simultaneously. As well as the specific mass for insulation material is strictly connected to conductivity as shown in Domínguez-Muñoz et al. [40]. However, in this study the cross correlations are not taken into account and each thermophysical property is treated as an independent variable.

The graphs in Figure 4.6 show the pdf of each bin of random data generated and the Gaussian curves that best fit the trend. The procedure for calculating the parameters (i.e. μ and σ) of the distribution and the squared 2-norm of residuals is described in Section 5.1.

Table 4.3: PDF parameters of thermophysical property distributions used in Monte Carlo simulations(a) Thermal conductivity $Wm^{-2}K^{-1}$

	μ	σ	$f_{0.05}$	$f_{0.95}$	$\frac{f_{0.95} - f_{0.05}}{\mu}$
Internal Plaster	0.7	0.1	0.54	0.85	44.3 %
EPS	0.036	0.002	0.032	0.039	19.4 %
Clay blocks	0.26	0.04	0.19	0.32	50.0 %
External Plaster	0.9	0.1	0.74	1.05	34.4 %
Expanded clay	0.4	0.04	0.33	0.46	32.5 %
Stone	2.2	0.2	1.875	2.5	28.4 %

(b) Specific mass $kg m^{-3}$

	μ	σ	$f_{0.05}$	$f_{0.95}$	$\frac{f_{0.95} - f_{0.05}}{\mu}$
Internal Plaster	1400	100	1240	1550	22.1 %
EPS	20	1.4	17.5	22	22.5 %
Clay blocks	600	40	530	660	21.7 %
External Plaster	1800	150	1560	2030	26.1 %
Expanded clay	1350	100	1190	1500	23.0 %
Stone	2000	200	1670	2316	32.3 %

(c) Specific heat $Jkg^{-1}K^{-1}$

	μ	σ	$f_{0.05}$	$f_{0.95}$	$\frac{f_{0.95} - f_{0.05}}{\mu}$
Internal Plaster	1010	100	850	1160	30.7 %
EPS	1500	200	1180	1810	42.0 %
Clay blocks	840	100	670	990	38.1 %
External Plaster	910	100	750	1060	34.1 %
Expanded clay	1000	150	750	1230	48.0 %
Stone	1000	150	750	1230	48.0 %

(d) Thickness m

	μ	σ	$f_{0.05}$	$f_{0.95}$	$\frac{f_{0.95} - f_{0.05}}{\mu}$
Internal Plaster	0.01	0.003	0.005	0.014	90.0 %
EPS	0.1	0.008	0.087	0.112	25.0 %
Clay blocks	0.3	0.007	0.28	0.31	10.0 %
External Plaster	0.02	0.006	0.01	0.029	95.0 %
Expanded clay	0.35	0.01	0.33	0.36	8.6 %
Stone	0.7	0.05	0.62	0.77	21.4 %

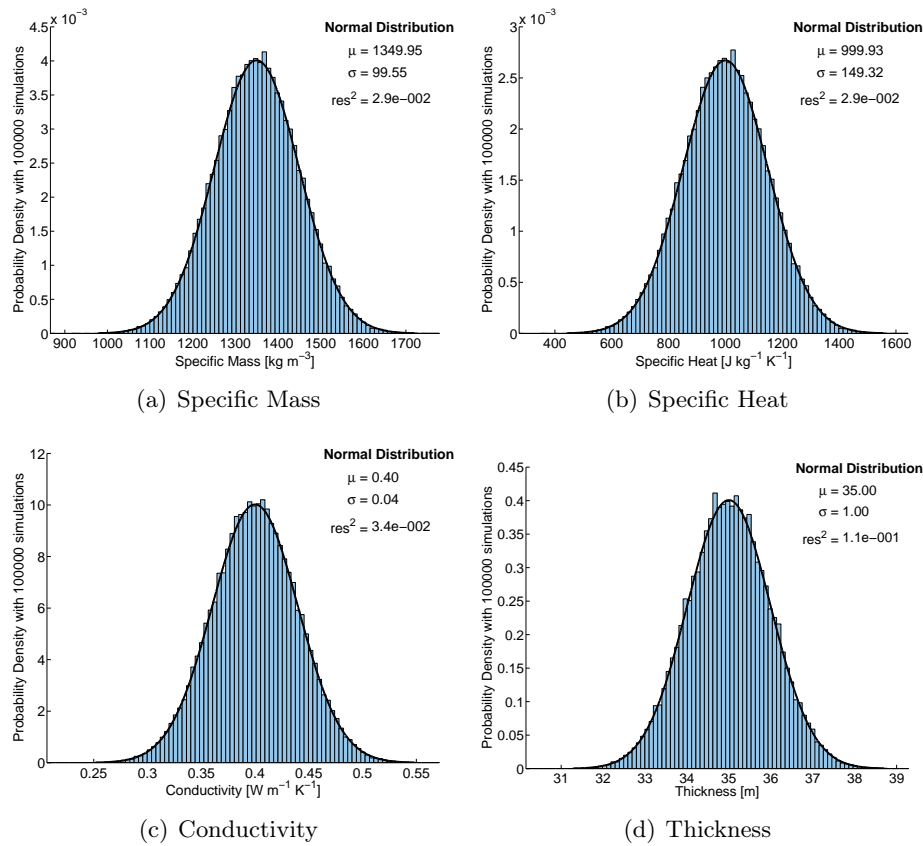


Figure 4.6: Distribution curves of input data for expanded clay wall (Le).

At this point it is significant to check the value of the residual two-norm that indicates the proper functioning of the Simple Random Sampling code (Section 4.3.1).

Finally, with the aim of ensuring the representativeness of the sampling and in order to guarantee the convergence of the problem, 100000 random input are taken for each input value of dynamic simulation (Section 4.3.1).

4.8 Summarizing

In this chapter the theoretical bases of Monte Carlo method have been detailed. Moreover the assumptions and the other relevant elements used for the choices made are fully described, with particular attention to the evaluation of the uncertainty ranges of the thermophysical properties.

Since for massive building components, the DRF approach is subject to more errors than other methods, especially for issues related to tolerance in roots finding, this method is chosen for the sensitivity analysis of CTF calculation to

the variability of material thermophysical properties.

Finally, in the last part of the chapter, a detailed description of the test cases characteristics used for the uncertainty analysis is presented.

In the following chapter the results of the Monte Carlo simulations with some consideration about the reliability and robustness of the DRF method will be presented.

Chapter 5

Results of Monte Carlo simulations

In the previous chapter the reasons of the Monte Carlo analysis and the variability of the thermophysical properties are reported. Besides, after some theoretical concepts, the test case selection is presented and motivated.

This chapter deals with the results of the uncertainty analysis. Firstly, the postprocessing of simulations results is presented. Starting from the response factors, the heat transfer through the building component is evaluated by imposing a sol-air and setpoint temperature respectively on the external surface and internal surface. Following on from this point, the PDF (Probability Density Function) curves that best fit the distribution of model outputs among Gaussian, Lognormal and Weibull distribution are investigated and computed by means of a MATLAB code that minimizes the squared 2-norm of residual with actual data.

Secondly, the probability density functions of heat gains are presented and compared. This comparison is firstly done on the shape of both monthly and annual PDFs. This analysis highlights the periods in which the non linearities of the model response are more evident. Subsequently, the relationships between each thermophysical properties and the annual energy transmitted through the envelope is derived for each test cases both in Trento and Palermo. Besides a direct comparison among the effects on heat gains of different thermophysical properties is done by means of an adimensional analysis.

Finally, the influence of climate features, and in particular of sol-air temperature, on the monthly heat gains is investigated.

5.1 Postprocessing of output data

As described in Section 4.3, Monte Carlo analysis allows to assess the distribution of the response factors (RF) obtained with the DRF approach (Section 4.4.1). The advantage of this procedure is linked to the hypothesis that the RF coefficients are independent by temperature and by time. Consequently, they can be calculated only once at the beginning of the simulation. However, the RF terms, from the theoretical point of view, are an infinite number. Although the series is usually truncated at the 24th term, a direct comparison between the distributions of the RF coefficients is not convenient.

For this reason, the RF terms, obtained from the DRF method with perturbed input, are employed for the calculation of monthly and annual distributions of heat gains and heat losses through the envelope, as shown in Figure 5.1. RF procedure operates only on temperatures in fact, the current surface heat flux is a function only of temperatures and does not rely on previous heat fluxes, as shown in Equation (5.1).

$$\dot{q}_i(\tau) = \sum_{j=0}^{23} RF_j \cdot (T_{solair,\tau-j\delta} - T_{i,\tau-j\delta}) \quad (5.1)$$

- where \dot{q}_i is the heat flux on the internal side of the component,
 RF_j is the j-th surface to surface response factor terms,
 τ is the time,
 δ is the time step of energy simulation,
 T_i is the temperature of the internal surfaces with a fixed zone setpoint of 20 °C for heat losses and 26 °C for heat gains,
 T_{solair} is the sol-air temperature.

The sol-air temperatures is a simplification that allows to greatly reduce the computational cost of the dynamic simulations and it is used for example in the Radiant Time Series approach [116]. The sol-air temperature is defined as the outside air temperature which, in the absence of solar radiation, would give the same temperature distribution and the same rate of energy transfer through the envelope as that due to the actual air temperature and incident radiation. The

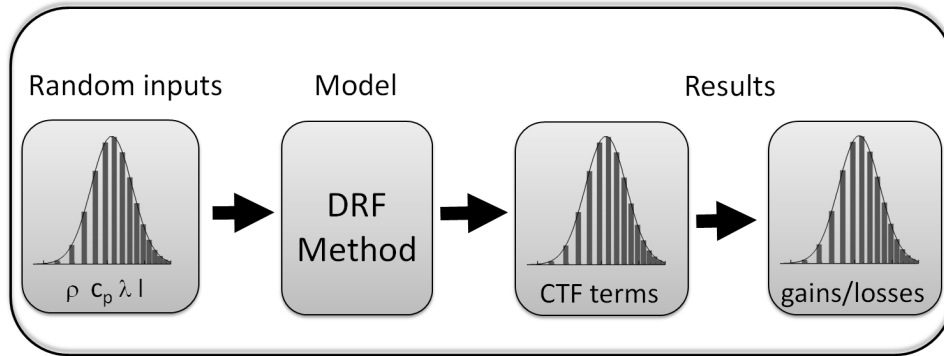


Figure 5.1: Scheme of the uncertainty analysis of heat transfer through envelope.

sol-air temperature is calculated from the following equation:

$$T_{solair} = DBT + \frac{\alpha_w \cdot GSI_\beta}{h_0} - \frac{\varepsilon \cdot \Delta R}{h_0} \quad (5.2)$$

where GSI_β is the solar radiation incident on β tilted surface,

α_w is the wall coefficient of absorption for solar radiation,

h_0 is external surface heat transfer coefficient,

ε is the wall emissivity coefficient for thermal radiation

ΔR is the difference between the long-wave radiation incident on the surface from the sky and surroundings and the radiation emitted by a black body at atmospheric air temperature.

According to ASHRAE Handbooks [13] for horizontal surfaces that receive long-wave radiation only from the sky, an appropriate value of ΔR is about 63 W m^{-2} , so that if α_w and h_0 are respectively equal to 1 and to $17 \text{ W m}^{-2} \text{ K}^{-1}$, the long-wave correction term is about 4°C . Oppositely, since vertical surfaces receive long-wave radiation from the ground and surrounding buildings as well as from the sky, accurate ΔR values are difficult to determine. When solar radiation intensity is high, surfaces of terrestrial objects usually have a higher temperature than the outdoor air. Thus, their long-wave radiation compensates to some extent for the sky's low emittance. Therefore, it is common practice to assume ΔR equal to zero for vertical surfaces.

Notice that for this analysis α_w and ε , in equation (5.2) are considered to be constant parameters. This assumption is justified for α_w only because,

whilst absorption is predominantly a surface phenomenon, emittance depends upon the temperature of the body. However, for the range of building surface temperatures, errors introduced by this simplification are acceptable. Furthermore, a small error in the evaluation of sol-air temperature does not alter the interpretation of postprocessing results.

The last step of the postprocessing procedures involves an analysis of the output data distribution on both a monthly and annual basis. To do this, a postprocessing code is implemented by means of Matlab [87]. This code allows to assess the monthly and annual heat through the envelope starting from the results of equation (5.1). Moreover these heat terms are also separated in inward "Heat Gains" and outward "Heat Losses" contributions and assigned to one of the 90 bins in which the output variability range is divided. Finally the code fits one of three probability distributions (i.e. Normal, Lognormal and Weibull) to the to the output data distributions. The distribution that best fits the data is selected automatically assuming as measure of fit goodness the sum of squares of point by point differences between output and cumulative distribution functions: the lower the squared 2-norm of residual. the better the fit. The code estimates the parameters of the curve that best approximates the actual output distribution, and in particular μ and σ for normal and lognormal distribution or α and β for the Weibull distribution (Section 4.2).

5.2 Monthly distribution curves for heat gains of South facing walls

The main issue in the uncertainty analysis is the interpretation of results. In fact, the Monte Carlo technique provides not a synthetic value but an articulate and multidimensional output that is the probability density functions of model provisions.

In this section, the shapes of the output PDFs are analyzed. A first significant results is that the use of Gaussian random fields as inputs does not imply a Gaussian structure of the heat gain distributions, most likely because of the non-linearity of the equation (4.12). Even for small stochastic perturbations, such distributions will not generally be symmetric. The distortion of the PDF shape may be represented as a propagation of probability distributions through the model, as well as the uncertainty is propagated through the DRF method. In particular, as already said, this alteration of the shape is caused by the non-linearity in the model and is also due to the presence of many uncertain inputs with different variances. For both cities, August is identified as the most representative summer month and, consequently, the results of this month are

Table 5.1: *Best fit distributions for August heat gains and February heat losses due to perturbation of input data*

(a) August Heat Gains in Trento

Uncertain Parameter	Le	Mi	Mi	Me	Sw
		Insulation	Clay block	Clay block	
ρ	Lognormal	Weibull	Lognormal	Weibull	Lognormal
c_p	Lognormal	Weibull	Lognormal	Lognormal	Lognormal
λ	Normal	Normal	Weibull	Weibull	Normal
l	Normal	Normal	Normal	Normal	Lognormal

(b) August Heat Gains in Palermo

Uncertain Parameter	Le	Mi	Mi	Me	Sw
		Insulation	Clay block	Clay block	
ρ	Weibull	Normal	Normal	Weibull	Weibull
c_p	Normal	Weibull	Weibull	Weibull	Lognormal
λ	Normal	Normal	Weibull	Weibull	Normal
l	Normal	Normal	Normal	Normal	Normal

(c) February Heat Losses in Trento

Uncertain Parameter	Le	Mi	Mi	Me	Sw
		Insulation	Clay block	Clay block	
ρ	Weibull	Normal	Lognormal	Normal	Lognormal
c_p	Normal	Weibull	Lognormal	Weibull	Lognormal
λ	Normal	Normal	Weibull	Weibull	Normal
l	Normal	Normal	Normal	Normal	Normal

(d) February Heat Losses in Palermo

Uncertain Parameter	Le	Mi	Mi	Me	Sw
		Insulation	Clay block	Clay block	
ρ	Lognormal	Weibull	Lognormal	Lognormal	Lognormal
c_p	Lognormal	Weibull	Lognormal	Lognormal	Lognormal
λ	Normal	Normal	Weibull	Weibull	Normal
l	Normal	Normal	Normal	Normal	Normal

presented in this section. Further distributions, as well as the PDF for heat losses in winter periods are reported in the tables in appendix C-D.

As shown in Table 5.1, the shape of the heat gain PDFs depends mainly on

the perturbed parameter. However, variations are also observed associated with the characteristics of the wall (i.e. massive vs. lightweight component) and with the weather conditions.

In the following sections, the PDF obtained for the test cases (i.e multi layer structure either with internal M_i and external insulation M_e , a non insulated stone wall S_w and a expanded clay wall L_e) are presented and compared each other. In particular, the PDF obtained are reported both in case of a single parameter perturbation, assuming the other as deterministic values, and in case of a simultaneous variation of all properties of a layer.

5.2.1 Perturbation of Specific Mass and Specific Heat

The distribution of the heat gains due to a perturbation of either specific mass and specific heat are very similar in terms of both typology and distribution parameters. In this section, only the PDFs obtained by perturbing specific mass are reported. Further distribution information are reported in appendix C-D.

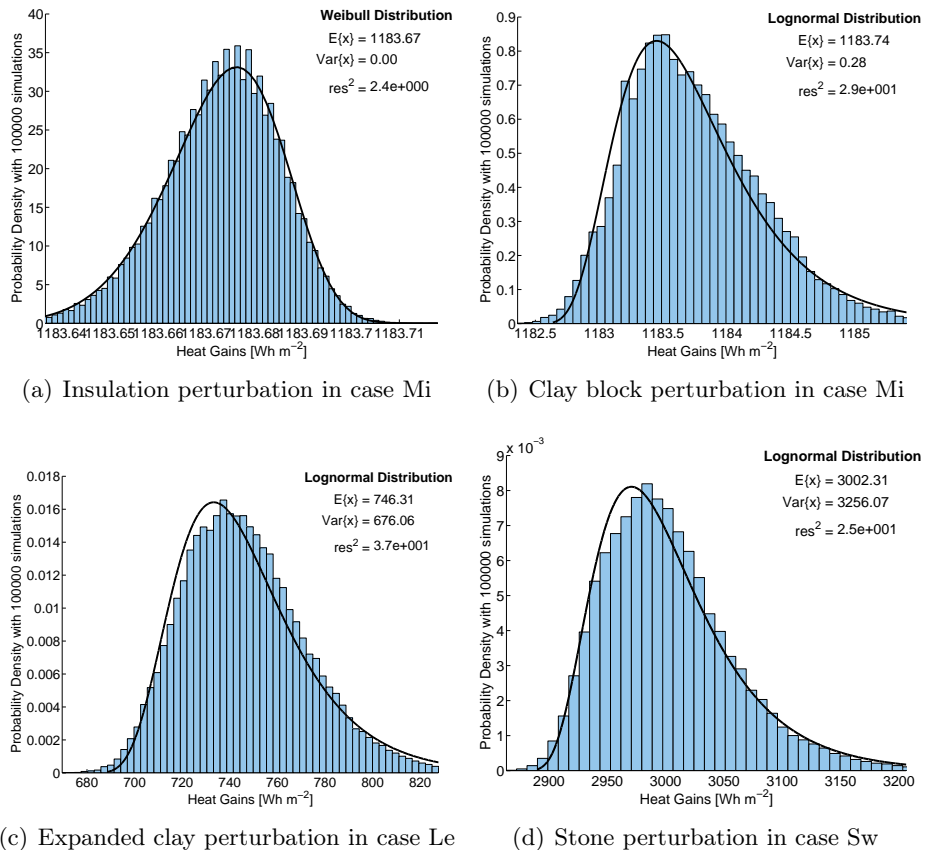


Figure 5.2: Trento distribution curves of August heat gains due to ρ perturbation.

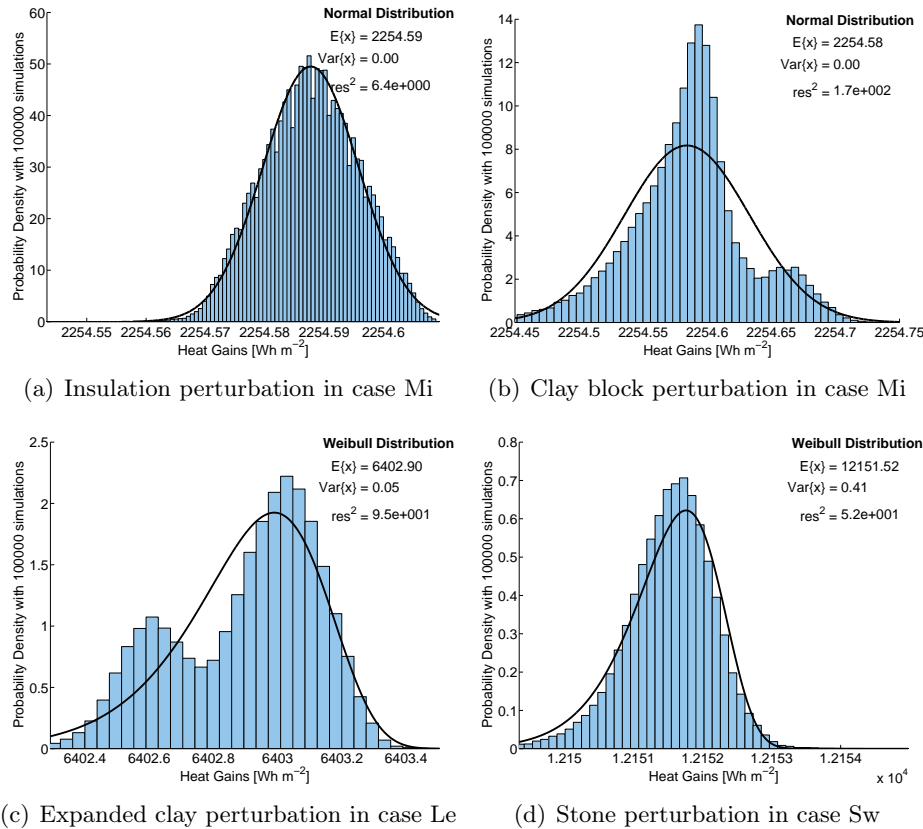


Figure 5.3: Palermo distribution curves of August heat gains due to ρ perturbation.

As shown in Figure 5.2 and Figure 5.3, the most common typology of PDF is a lognormal distribution. Only in some cases the minimum of the residual square is guaranteed by a Weibull. However, in any case, the distribution is asymmetrical. This result shows that the nonlinearities of the DRF method are primarily related to the wall capacitance. Notice that in Figure 5.3 (c) a bimodal distributions seems to arise for Le case. However, due to the limited range of heat gain variations and to the number of bins used this behavior can be reasonably attributed to numerical noise.

Figure 5.2 clearly shows that the influence of specific mass increases for non insulated components. This is justified because in these wall typologies damping and phase lag are the main mechanisms of resistance to the inward heat fluxes. Moreover, these results seem to confirm that in well insulated walls the mechanism of conductive thermal resistance prevails with respect to the storage effect. This fact becomes even more evident if the open interval of PDF curves, divided by the mean value of each distributions, is analyzed. In fact, data reported in Table 5.2 for Trento highlight a greater sensibility of Le and

Sw cases to specific mass perturbation. While for Me the spread of heat gains is limited by perturbing the specific mass of either the clay block or the insulation, for Le and Sw cases an appreciable variation is registered. In particular, it is interesting to note how for Le the opening interval is similar to the variation of specific mass reported in Table 4.3 (b).

Table 5.2: Value of $(f_{99\%} - f_{1\%})/E\{x\}$ due to uncertain ρ and c_p

(a) Specific mass perturbation

City	Le	Sw	Me	Me	Mi	Mi
			Insulation	Clay block	Insulation	Clay block
Trento	16.27 %	9.06 %	0.01 %	0.21 %	0.01 %	0.20 %
Palermo	0.01 %	0.02 %	0.00 %	0.02 %	0.00 %	0.01 %

(b) Specific heat perturbation

City	Le	Sw	Me	Me	Mi	Mi
			Insulation	Clay block	Insulation	Clay block
Trento	36.79 %	16.06 %	0.01 %	0.43 %	0.01 %	0.41 %
Palermo	0.05 %	0.03 %	0.00 %	0.02 %	0.00 %	0.02 %

The most interesting result concerns with the dependence of the output uncertainties on the climate features. In fact, analyzing the results, there is a greater variability of opening interval between Trento and Palermo (Table 5.2), where the opening interval is defined as:

$$OI := \frac{f_{99\%} - f_{1\%}}{E\{x\}} \quad (5.3)$$

where $f_{1\%}$ is the fractile 1% of heat gain distribution,
 $f_{99\%}$ is the fractile 99% of heat gain distribution,
 $E\{x\}$ is the mean value of heat gain distribution.

This seems to affirm that the influence of the envelope heat capacitance is higher in climates of Northern Italy rather than in Southern Italy. This is even more evident if the comparison deals with the heat gain distributions of the test case Me due to the specific mass perturbation either of clay block or insulating layer. Due to the materials thermophysical properties, in this wall typology the function of thermal resistance (insulation) is decoupled from that of damping and attenuation (clay block). Consequently, it is reasonable to expect a greater variation of the heat gains when the perturbed property is either the specific

mass or the specific heat of the clay blocks. While this different behavior appears in Trento albeit with slight differences, Figure 5.2 (a) and Figure 5.2 (b), in Palermo the specific mass perturbation of both materials induces comparable negligible changes. The low dependence of heat gains on heat capacitance in Palermo can be explained taking into account the daily trend of dry bulb temperature. In fact, the high night temperatures reduce the possibility of the wall to work like a capacitor with daily cycles of charge/discharge (Figure 3.6).

5.2.2 Perturbation of Conductivity

The uncertainty in material conductivity induces different trends of PDFs compared to specific mass and specific heat. In fact, since thermal conductivity primarily affects the steady solution part of the governing equation, the distortions in PDF curves are limited. Consequently, the most frequent distribution is the Gaussian and only when the conductivity of clay block is perturbed a little asymmetry in PDF is noted and modeled by means of a Weibull PDF (Figure 5.4 and Figure 5.5). This nonlinear behavior is particularly visible for clay block conductivity lower than $0.2 \text{ W m}^{-1} \text{ K}^{-1}$, Figure 5.9 (c).

Analyzing the opening intervals, reported in Table 5.3, for the test cases Me and Mi the same uncertainty is registered. Since conductivity is primarily related to the steady part of solution, the magnitude of open interval is not affected either by the layer sequences or climate conditions. This is not what happens for the massive cases (i.e. Le and Sw) where a dependence of climate conditions is noted. Probably this result is related to the secondary effect of λ perturbation that is more evident in massive component. In fact a variation of λ causes also a change of thermal diffusivity, because an increase of λ makes the ratio of λ to $\rho \cdot c_p$ increase. Therefore, since the diffusivity is strictly connected with the non linear term of the solution, a greater magnitude implies an increase of non linear terms. Obviously, since in Me and Mi cases the heat transfer is mainly controlled by conduction resistance, the effects of diffusivity variations due to λ perturbation become negligible and, consequently, for these cases the climate variation of uncertainty are trivial.

Table 5.3: Value of $(f_{99\%} - f_{1\%})/E\{x\}$ due to uncertain λ

City	Le	Sw	Me	Me	Mi	Mi
			Insulation	Clay block	Insulation	Clay block
Trento	62.41 %	41.77 %	18.05 %	22.45 %	18.05 %	22.43 %
Palermo	43.73 %	36.31 %	18.02 %	22.09 %	18.02 %	22.09 %

Furthermore the data in the Table 5.3 show similar opening intervals caused

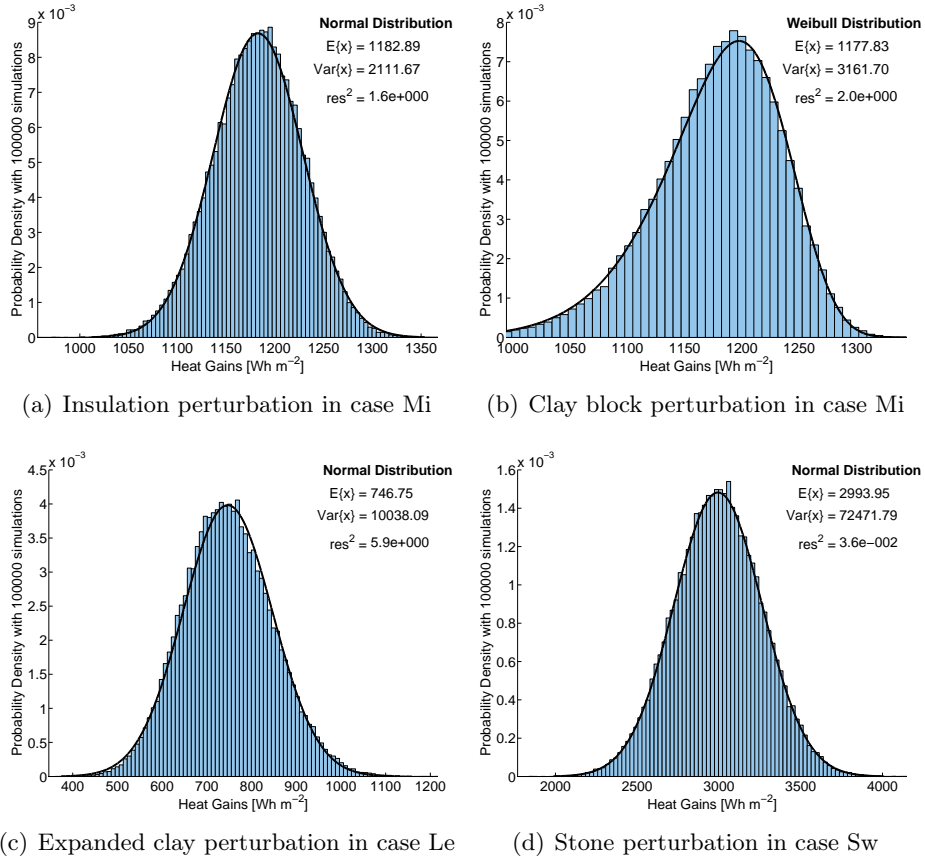


Figure 5.4: Trento distribution curves of August heat gains due to λ perturbation.

by λ perturbation of either clay block or by insulation layer. However it should be noticed that the uncertainties in input data are different, Table 4.3 (a). In fact, in clay blocks thermal conductivity is an apparent property used to model more complex heat transfer mechanisms such as convection in cavity and the mortar thermal bridges. Besides, in hygroscopic material λ is strongly affected by water content, consequently the thermal conductivity is more uncertain than in insulation material. Therefore, despite the model being more sensible to insulation conductivity, for multilayer walls the uncertainties of two materials are of the same magnitude.

5.2.3 Perturbation of Thickness

Likewise for thermal conductivity, a clear preponderance of the Gaussian distribution of heat gains is registered for thickness perturbations. Only for Sw in Trento the distribution is asymmetric and well described by a lognormal PDF (Figure 5.6 and Figure 5.7). This is because the thickness has a dual effect. A

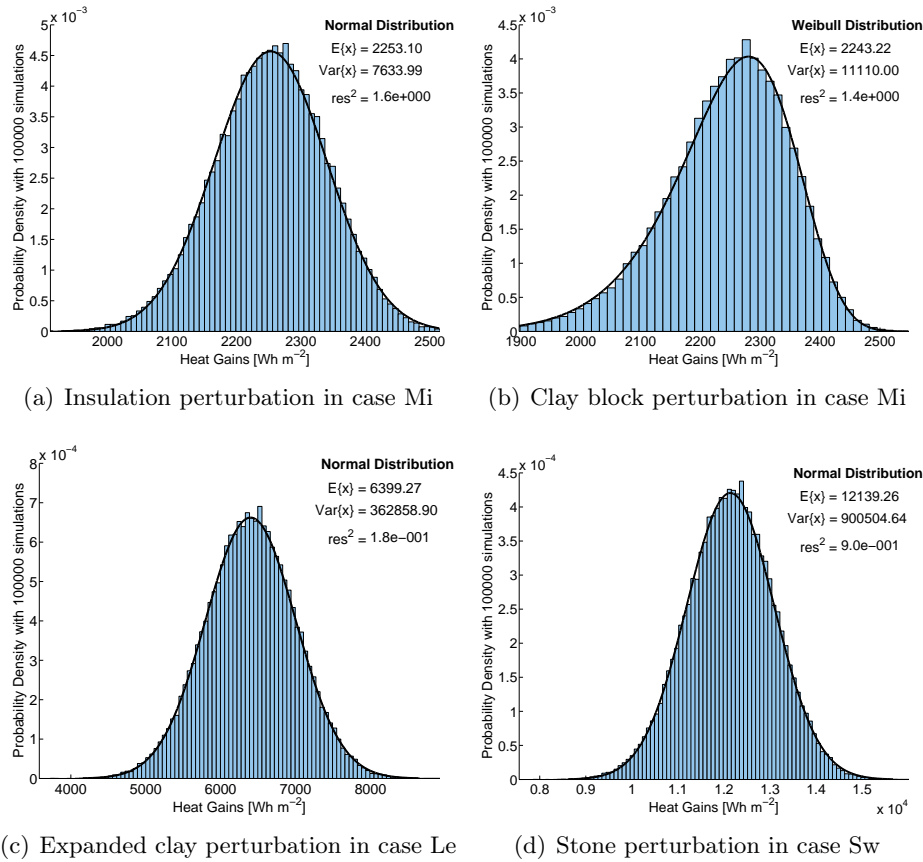


Figure 5.5: Palermo distribution curves of August heat gains due to λ perturbation.

perturbation of thickness implies an adjustment of both the conductive resistance and the heat capacitance of the wall. However the latter contribute seems to be predominant only for high mass component, like a stone wall Sw, and in climates with high differences between day-time and night-time temperatures. In fact, in Palermo, where the night temperature is often higher than internal setpoint the role of thermal mass is negligible and, consequently, the distribution returns Gaussian.

The different effect of uncertainties on thermal response between insulated and non-insulated components is also highlighted by the data in Table 5.4. In fact, while for Me and Mi cases the opening interval changes between Trento and Palermo are trivial, for Le and Sw an appreciable variation is registered.

The most important result deals with the analysis of opening intervals with respect to those of input data distributions. For the perturbation of either specific mass, specific heat and conductivity the effect of DRF method is a contraction of the heat gain variability with respect to input fractiles distances. Instead,

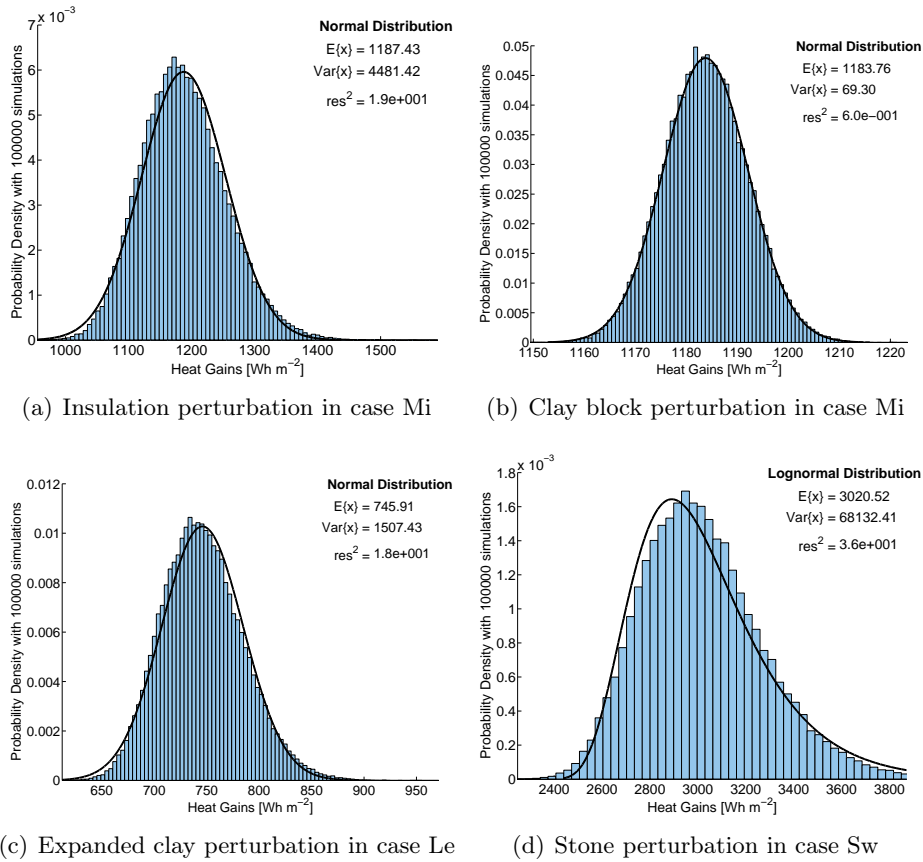


Figure 5.6: Trento distribution curves of August heat gains due to l perturbation.

Table 5.4: Value of $(f_{99\%} - f_{1\%})/E\{x\}$ due to uncertain l

City	Le	Sw	Me	Me	Mi	Mi
			Insulation	Clay block	Insulation	Clay block
Trento	16.27 %	41.17 %	26.41 %	3.28 %	26.41 %	3.27 %
Palermo	12.53 %	29.09 %	26.36 %	3.13 %	26.36 %	3.13 %

when the uncertain parameter is thickness DRF method tends to maintain or amplify the input uncertainty.

For example, after analyzing the opening interval of heat gains (Table 5.4) with respect to the input variability reported in Table (4.3), it is evident that DRF method maintains the same uncertainty of input for insulation layer. The most surprising result, however, concerns the amplification found for massive walls i.e. Le and Sw. A similar behavior is registered for both Le and Sw, for which the input uncertainty is redoubled in Trento and increased by a factor 1.5 in Palermo. Therefore, it seems that thickness is the parameter to which the

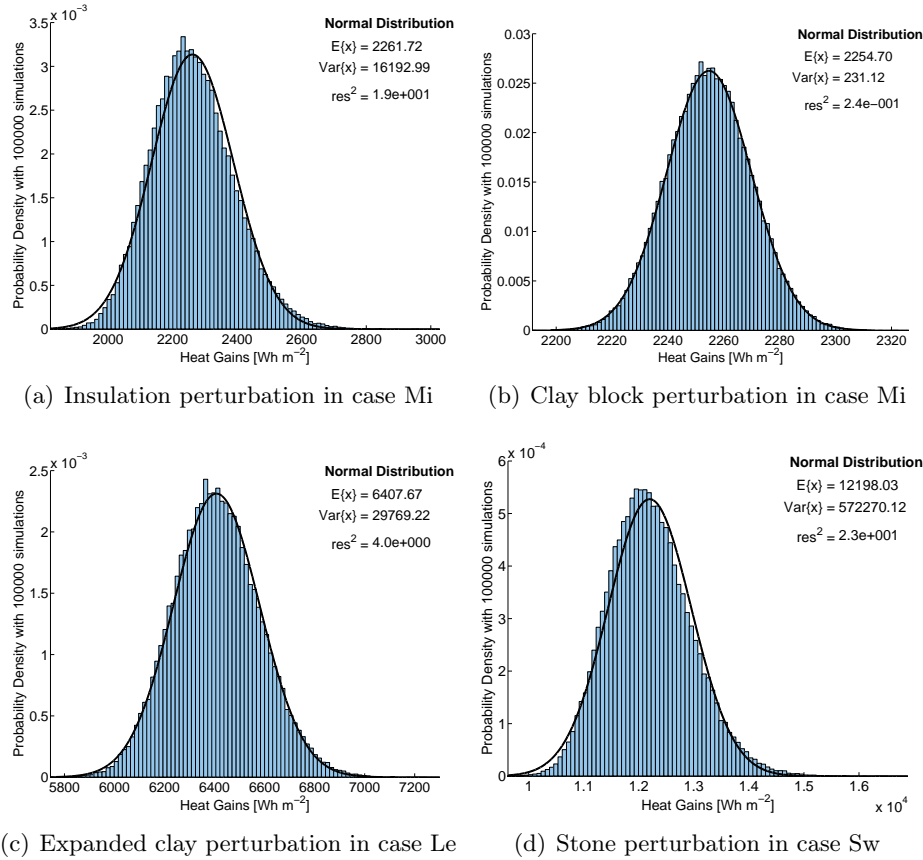


Figure 5.7: Palermo distribution curves of August heat gains due to l perturbation.

DRF is more sensitive and, especially in existing buildings, it is also the more uncertain parameter or the one with the greatest variability.

5.2.4 Perturbation of all the thermophysical properties

In the previous sections the dispersion of the heat gains is caused by a perturbation of a single thermophysical properties while the other data are treated as deterministic values. This research allows to understand the influence of any properties on energy transmitted through the envelope. But two questions remain still open: to what extent the single parameter uncertainties are added or canceled out? How varies the PDF shape of heat gains due to a simultaneous suboptimal DRF method? So the next natural step is the investigation of model provisions when all the input data of a single layer are changed according to probability distribution curves.

Notice that the PDFs obtained for multi-parameter perturbations (Figure 5.8) depends strongly on the test case analyzed. For instance, while for case Me,

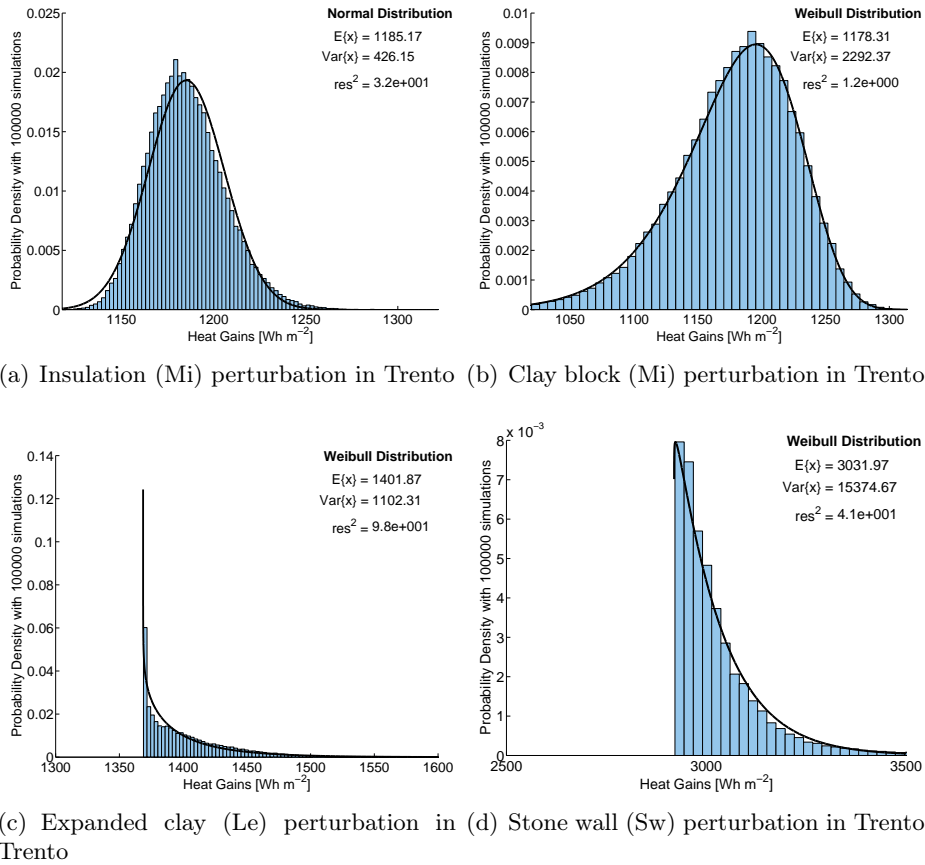


Figure 5.8: PDF curves of August heat gains due to a simultaneous variation of layer properties

Figure 5.8 (a) and Figure 5.8 (b), the PDF shape is the same of that obtained for uncertain λ (Table 5.1), Le and Sw components, Figure 5.8 (c) and Figure 5.8 (d), show a different trend. This first comparison seems to highlight that for the Me the dominant uncertainty source is the variability of thermal conductivity.

Table 5.5: Value of $(f_{99\%} - f_{1\%})/E\{x\}$ due to all uncertain parameters

City	Le	Sw	Me	Me
			Insulation	Clay block
Trento	11.03 %	20.12 %	8.16 %	19.23 %
Palermo	31.51 %	6.67 %	8.14 %	19.00 %

The different behavior is confirmed from the analysis of opening intervals (Table 5.5). In fact, while for Me the uncertainties do not depend on climate feature, for Sw and Le a strong correlation is noted. For instance a greater

opening interval is registered in Trento, where the thermal capacitance has a key role in the heat flux transition, but not in Palermo. Consequently, for this case the uncertainties of the different properties seem to add up. Oppositely, for the Le case, that to some extent is sensible to thermal capacity (Section 5.2.1), there is a noticeable decrement of the opening interval passing from Trento to Palermo. Therefore, for Le case the uncertainties of different thermal properties seem to cancel out each other. However, for every test case the opening index is lower than the sum of opening intervals obtained with single parameter perturbations.

These results seem to confirm the impossibility of an a priori assessment of the risk related to property uncertainty, especially for non-insulated walls.

5.3 Annual heat gains

The same analysis performed in the previous sections was also carried out on the distribution of the annual heat gains and heat losses. The purpose of this survey is to assess the reliability of the results on a long period of simulations such as the whole year. In fact these data result useful for the analysis of uncertainty in the evaluation of building energy consumption.

From the comparison between the monthly PDF shapes, reported in Table 5.1, with the annual PDF (Table 5.6), a greater correspondence between the distribution typologies obtained for Trento and Palermo arises, especially when the perturbed parameter is either ρ or c_p . This derives from the fact that, on an annual basis the influence of the thermal capacitance increases also in Palermo due to the periods in which the night temperature is lower than the internal setpoint. This behavior emerges more clearly from a comparison between the Table 5.1 (b) and the Table 5.6 (b). Notice that the monthly PDFs for ρ and c_p , which usually are Gaussian or Weibull distributions, become lognormal on an annual basis.

Finally, an interesting result on the opening intervals emerges. The data in Table 5.7 show that, for the Me and Mi cases, they are mainly affected by conductivity uncertainties of both the clay block and the insulation layer. Oppositely, the perturbations of the thickness and especially of specific mass and specific heat produce negligible deviations in annual energy entering through the envelope.

Table 5.6: *Best fit distributions for annual heat gains and heat losses due to perturbation of input data on wall facing South*

(a) Heat Gains in Trento

Uncertain Parameter	Le	Mi	Mi	Sw
	Insulation		Clay block	
ρ	Lognormal	Normal	Lognormal	Lognormal
c_p	Lognormal	Normal	Lognormal	Lognormal
λ	Normal	Normal	Normal	Normal
l	Normal	Normal	Normal	Lognormal

(b) Heat Gains in Palermo

Uncertain Parameter	Le	Mi	Mi	Sw
	Insulation		Clay block	
ρ	Lognormal	Normal	Lognormal	Lognormal
c_p	Lognormal	Weibull	Lognormal	Lognormal
λ	Normal	Normal	Weibull	Normal
l	Normal	Normal	Normal	Normal

(c) Heat Losses in Trento

Uncertain Parameter	Le	Mi	Mi	Sw
	Insulation		Clay block	
ρ	Lognormal	Weibull	Lognormal	Lognormal
c_p	Lognormal	Weibull	Lognormal	Lognormal
λ	Normal	Normal	Weibull	Normal
l	Normal	Normal	Normal	Normal

(d) Heat Losses in Palermo

Uncertain Parameter	Le	Mi	Mi	Sw
	Insulation		Clay block	
ρ	Lognormal	Normal	Lognormal	Lognormal
c_p	Lognormal	Weibull	Lognormal	Lognormal
λ	Normal	Normal	Weibull	Normal
l	Normal	Normal	Normal	Normal

Table 5.7: *Opening interval for annual heat gains distributions*

(a) Trento

Uncertain Parameter	Le	Sw	Mi	Mi
			Insulation	Clay block
ρ	11.4 %	6.9 %	~ 0	2.3 %
c_p	26.8 %	12.5 %	4.4 %	4.5 %
λ	56.8 %	40.4 %	26.0 %	26.2 %
l	11.4 %	38.5 %	4.5 %	4.6 %

(b) Palermo

Uncertain Parameter	Le	Sw	Mi	Mi
			Insulation	Clay block
ρ	1.4 %	2.1 %	~ 0	0.9 %
c_p	3.4 %	3.7 %	1.8 %	1.9 %
λ	45.3 %	37.5 %	23.7 %	23.8 %
l	13.5 %	31.9 %	3.7 %	3.7 %

Likewise the Le and Sw cases appear to be strongly affected by conductivity uncertainty but errors related to the heat capacitance acquire more weight, especially for the climate of Trento. It should finally be pointed out the high value of the opening interval caused by the stone thickness perturbation in the Sw case. This may not only be associated with the variation of the thermal capacity but also to some numerical errors of the method DRF (Section 4.4.1).

5.4 Relation between input and annual heat gains

As already highlighted by the analysis of the PDF shapes, the link between the various thermophysical parameters and the solution of the partial differential equation (4.12), combined with equation (4.13), is not linear. Moreover, the effect of conductivity on the component thermal response is often overlooked. Frequently, the capability of reducing and delaying the heat flow through the envelope is mistakenly attributed solely to the heat capacitance. Instead the characteristic parameter which describes this behavior is the thermal diffusivity defined as:

$$\kappa = \frac{\lambda}{\rho \cdot c_p} \quad (5.4)$$

The thermal diffusivity is the measure of how quickly the heat moves within the body. In substance the higher the thermal diffusivity, the heat moves faster through the envelope. This dependence is well known in the literature, as shown by the analytical solutions obtained with simple boundary conditions for a single layer component:

Step in Temperature (T_s) Carslaw and Jaeger [21]

$$\dot{q}(x, \tau) = \frac{\sqrt{\lambda\rho c_p}}{\sqrt{\pi\tau}} \cdot T_s \cdot e^{-x^2/(4\tau\kappa)}$$

Step in heat input (\dot{q}_s) Carslaw and Jaeger [21]

$$\dot{q}(x, \tau) = \dot{q}_s \cdot \operatorname{erfc}\left(\frac{x^2}{4\tau\kappa}\right)$$

Ramp of Temperature ($\zeta\tau$) Davies [36]

$$\dot{q}(x, \tau) = \frac{2\sqrt{\lambda\rho c_p}}{\sqrt{\tau}} \cdot \left(\pi^{-1/2} e^{-x^2/(4\tau\kappa)} - \sqrt{\frac{x^2}{4\tau\kappa}} \operatorname{erfc}\left(\frac{x^2}{4\tau\kappa}\right) \right) \cdot \zeta\tau$$

These solutions show a dependency of the flow by the square root of the product of $\lambda \cdot \rho \cdot c_p$ and by a nonlinear function of the thermal diffusivity. Then they confirm and explain the nonlinearities highlighted by the distortion of the PDF shapes founded in Section 5.2.

A further investigation on reliability of the DRF predictions with uncertain input data can be carried out by analyzing the link between perturbed inputs and model outputs. Starting from the annual heat gains obtained with Monte Carlo simulations, the links between the thermophysical properties of the various test cases and the incoming flow through the envelope are analyzed.

Figure 5.9 shows the results and the polynomial curve fitting obtained for the Mi case when the clay block parameters are changed. In particular, each figure shows the annual flow entering through the wall when a single thermophysical property is varied, i.e. the others properties are considered as deterministic values.

The Mi case is a well insulated wall with low thermal capacitance. Consequently, as shown in Figure 5.9 (a) and Figure 5.9 (b), changes in ρ and c_p produce limited variations of the annual heat gains. However, it is highlighted a non-linear relation between heat gains and these parameters. In particular, it can be seen for low values of either specific mass and specific heat a greater increase of energy transmitted through the wall. Furthermore, a consequence

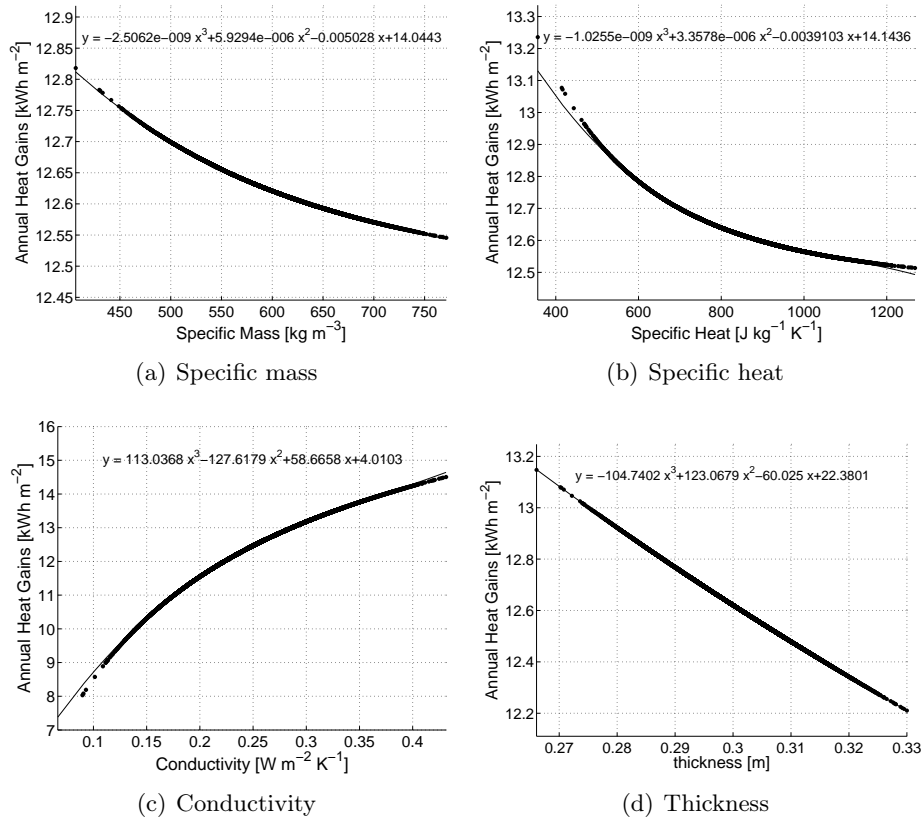


Figure 5.9: Relations between clay block parameters (M_i) and annual heat gains in Palermo

of the limited wall capacitance is that the thickness perturbations affect almost exclusively the thermal resistance of the wall and then the stationary part of the solution. For this reason, in this test case, the link between thickness and heat gain is linear.

Figure 5.9 (c) shows the trend of the annual heat gains when the thermal conductivity is perturbed. As previously mentioned, λ is present both in the heat resistance and in thermal diffusivity. Consequently, a variation of λ changes both the stationary and the transient part of the wall thermal response. This result shows that, for a well-insulated wall with low thermal capacitance, changes in the thermal conductivity can produce large variations of thermal diffusivity and, therefore, of the wall transient response. It is therefore clear how, for these types of components, the main parameter governing heat transfer in both winter and summer periods is the thermal conductivity.

Instead the behavior of a massive and poorly insulated wall, such as the test Sw case, is different. In fact, as can be seen from Figure 5.10 (c), there is a

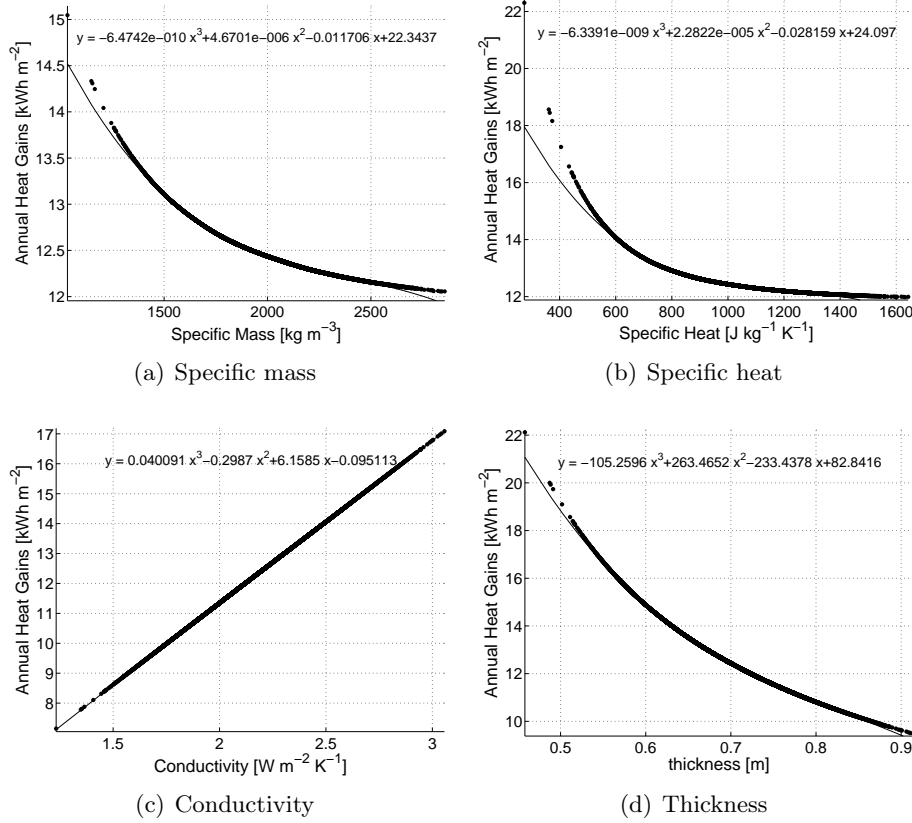


Figure 5.10: Relations between stone parameters (Sw) and annual heat gains in Trento

linear relationship between the thermal conductivity and the annual heat gains.

Since stone has high values of all together λ , ρ and c_p , the thermal diffusivity depends mostly on specific mass and specific heat. Consequently, a λ perturbation affects primary the thermal resistance and this explains the linear trend. Furthermore, from Figure 5.10 (a) strongly non-linear behavior of both ρ and c_p arises and, unlike the Mi case, the non-linearity is shown also to the thickness variation.

With the purpose of comparing each other the effects of thermophysical properties uncertainties and the heat gains obtained in Trento and in Palermo, the adimensional deviations of heat losses and heat gains from the expected values are computed. These values are calculated by dividing the deviation between perturbed and mean values by the expected value of each variable. By way of example, Figure 5.11 shows the trends of the dimensionless heat gains for the Mi and Le cases, when the thermophysical properties of respectively insulation layer and expanded clay block are perturbed.

Notice that for the Mi case there are not differences between the curves obtained for Trento, Figure 5.11 (a), and Palermo, Figure 5.11 (b). Besides, the same trends are registered also for adimensional heat losses, Figure 5.12 (a) and Figure 5.12 (b). Therefore, as already seen in previous sections, for wall whose behavior is primarily related to resistive materials, the uncertainties are independent of the climate features. Consequently, the reliability of model predictions, for given stratigraphy and material uncertainties, becomes a property of the wall.

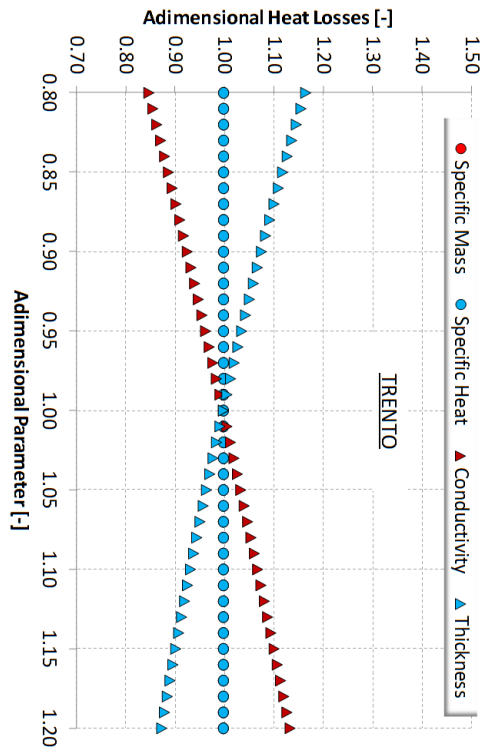
Moreover, another important aspect deals with the shape of the curves. In fact, since the trend is linear and symmetrical around the expected value, or weakly skewed (e.g. in clay block), the output uncertainty for different perturbed input can be estimated by interpolation. However this only applies in case of single uncertain parameter because, as shown in Section 5.2.4, for simultaneous uncertain parameters the output distributions is non symmetrical.

Oppositely for massive components, such as Sw and Le test cases (Figure 5.11 and Figure 5.12), a sensitivity of output uncertainties on climate features is registered. For example, analyzing the trends of non-dimensional heat gains (Figure 5.11), a different behavior in Trento with respect to Palermo is observed. Furthermore, while in Palermo the heat gain trends, Figure 5.11 (d), are similar to the heat losses curves, Figure 5.12 (d), for Trento a noticeable spread is registered. Besides, notice that the adimensional curves are not symmetrical, with larger uncertainties if the dimensionless parameter is underestimated.

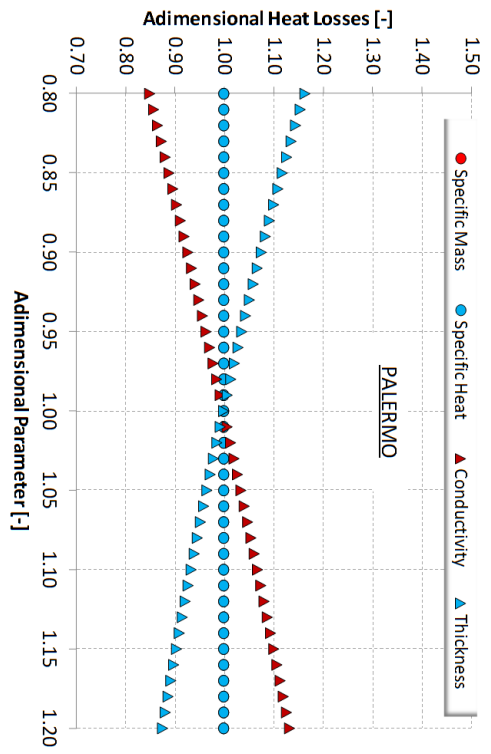
The results for massive components show the existence of a synergic effect between uncertainty in thermophysical properties and climate. Then the reliability of the model results can not be calculated with an a priori analysis. In order to investigate the interaction between materials uncertainty and climate features in the next section the monthly results will be presented as a function of sol-air temperature.

5.5 Influence of external conditions

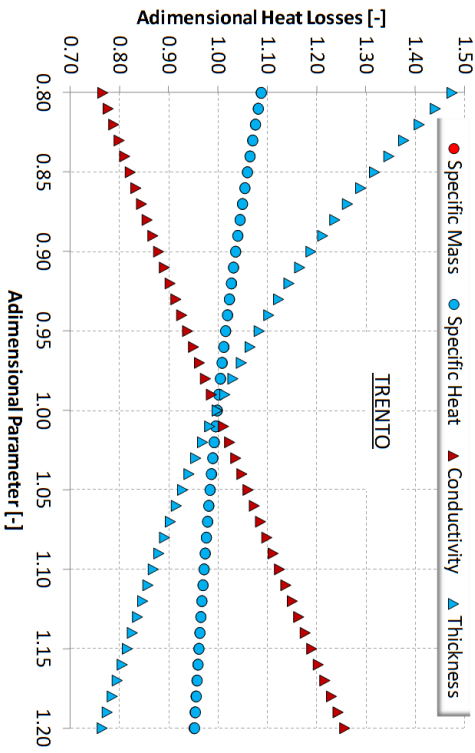
The following analysis is intended to evaluate the influence of climate on the predictions of the DRF method. The outcomes presented in the previous sections showed a dependence of the result reliability on the capability of the wall to work as a capacitor, with daily cycles of charging and discharging. Therefore the uncertainties are herein plotted as a function of the number of hours with sol-air temperature greater than heating setpoint or lower than cooling setpoint temperature, that are respectively $20\text{ }^{\circ}\text{C}$ and $26\text{ }^{\circ}\text{C}$. These parameters are an indicator of dynamism of the problem. In fact, the higher the percentage of



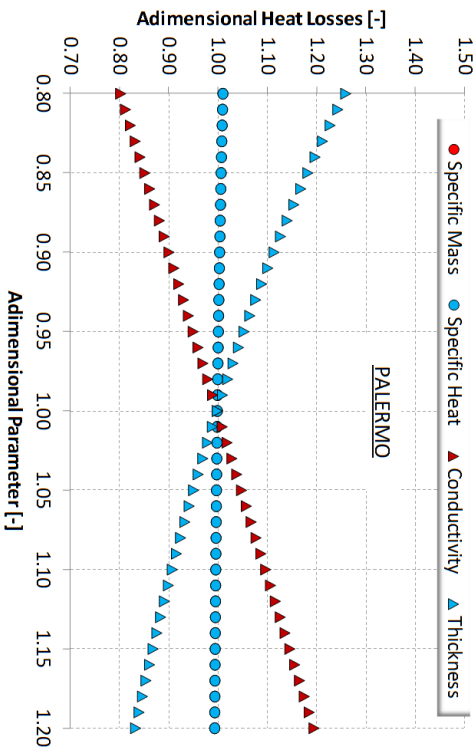
(a) Insulation (Me) in Trento



(b) Insulation (Me) in Palermo

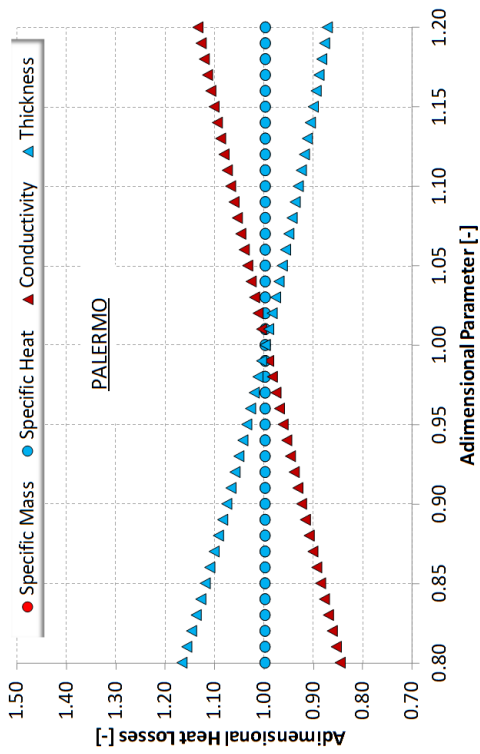


(c) Expanded clay (Le) in Trento

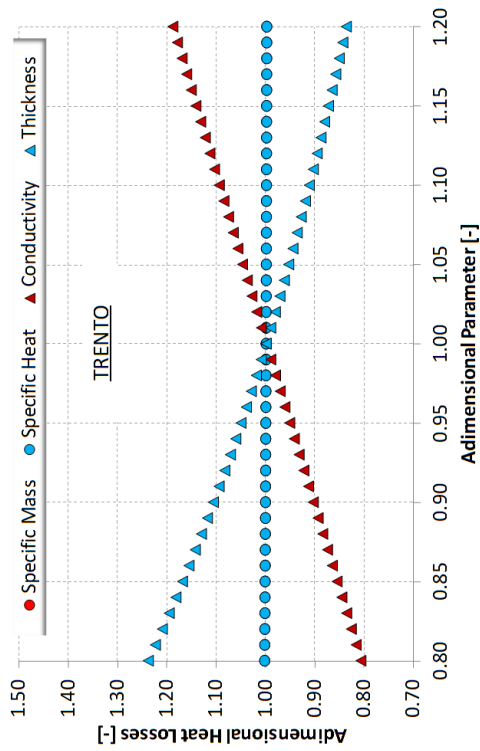


(d) Expanded clay (Le) in Palermo

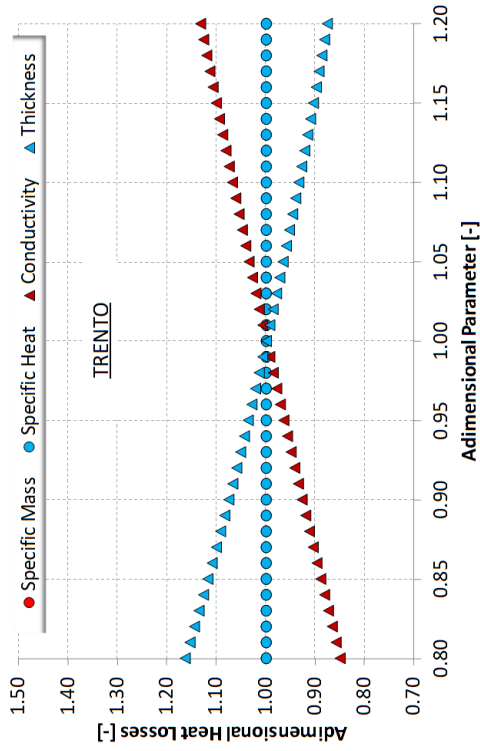
Figure 5.11: Adimensional deviation of annual heat gains as a function of adimensional perturbation of inputs.



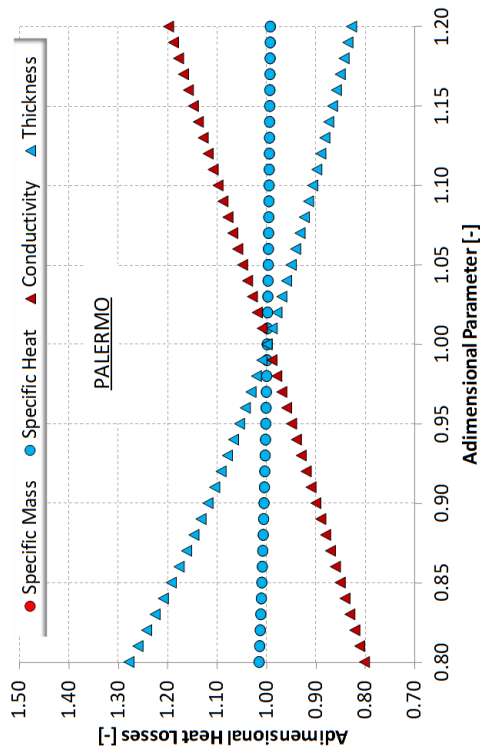
(a) Insulation (Me) in Trento



(b) Insulation (Me) in Palermo



(c) Expanded clay (Le) in Trento



(d) Expanded clay (Le) in Palermo

Figure 5.12: Adimensional deviation of annual heat losses as a function of adimensional perturbation of inputs.

monthly hours with sol-air temperature lower than the cooling setpoint, the greater is the number of inversions of the heat flux through the wall.

Table 5.8: *Percentage of monthly hours with a sol-air temperature:*

(a) lower than 26°C

City	Mar	Apr	May	Jun	Jul	Aug	Sep	Oct	Nov
Palermo	17.2 %	27.6 %	45.7 %	56.3 %	63.8 %	63.4 %	41.5 %	28.2 %	23.5 %
Trento	20.8 %	17.5 %	9.9 %	32.5 %	42.6 %	41.4 %	29.6 %	14.8 %	7.9 %

(b) greater than 20°C

City	Jan	Feb	Mar	Apr	May	Sep	Oct	Nov	Dec
Palermo	82.9 %	78.7 %	73.9 %	58.2 %	37.5 %	16.3 %	47.8 %	67.6 %	79.0 %
Trento	90.5 %	90.0 %	72.6 %	70.8 %	76.3 %	54.9 %	78.9 %	87.9 %	91.3 %

As can be seen from the data reported in Table 5.8, due to the lower night temperature in the summer months, Trento shows a higher percentage of hours with sol-air temperature lower than 26°C , as well as the higher diurnal temperature increases the non-stationarity of the Palermo heat losses in spring and autumn months.

Notice that there is an agreement between the heat losses trends shown in Figure 5.13 when both stone and clay block thermophysical properties are perturbed respectively in Sw and Mi cases. Both cases show the trends of fractiles 1 % and 99 % related to either λ or l perturbations that are constant when no more than 30 % of hours present a sol-air temperature greater than heating setpoint. In this zone the heat transfer solution is closely related to the stationary one which does not depend on the thermal diffusivity but only on thermal resistance. Besides, in the same region the uncertainties related to the ρ and c_p perturbation are close to zero. The effects of diffusivity variations occur for percentage of sol-air temperature greater than 30 %, with a lower increase in thermal conductivity and thickness with respect to the specific mass and specific heat.

This uniformity of behavior is not found in the monthly heat gains reported in the graphs in Figure 5.14. For example, while the Sw case shows an increase of the heat gains uncertainty due to ρ and c_p variations, the Mi case remains essentially independent of variable related to thermal capacitance. The limited dependence of Mi case on the climate features is also highlighted by the Figure 5.14 (d). In fact, the graph shows constant values of fractiles both for conductivity and thickness, in all the cases except for the Sw wall, Figure 5.14 (c).

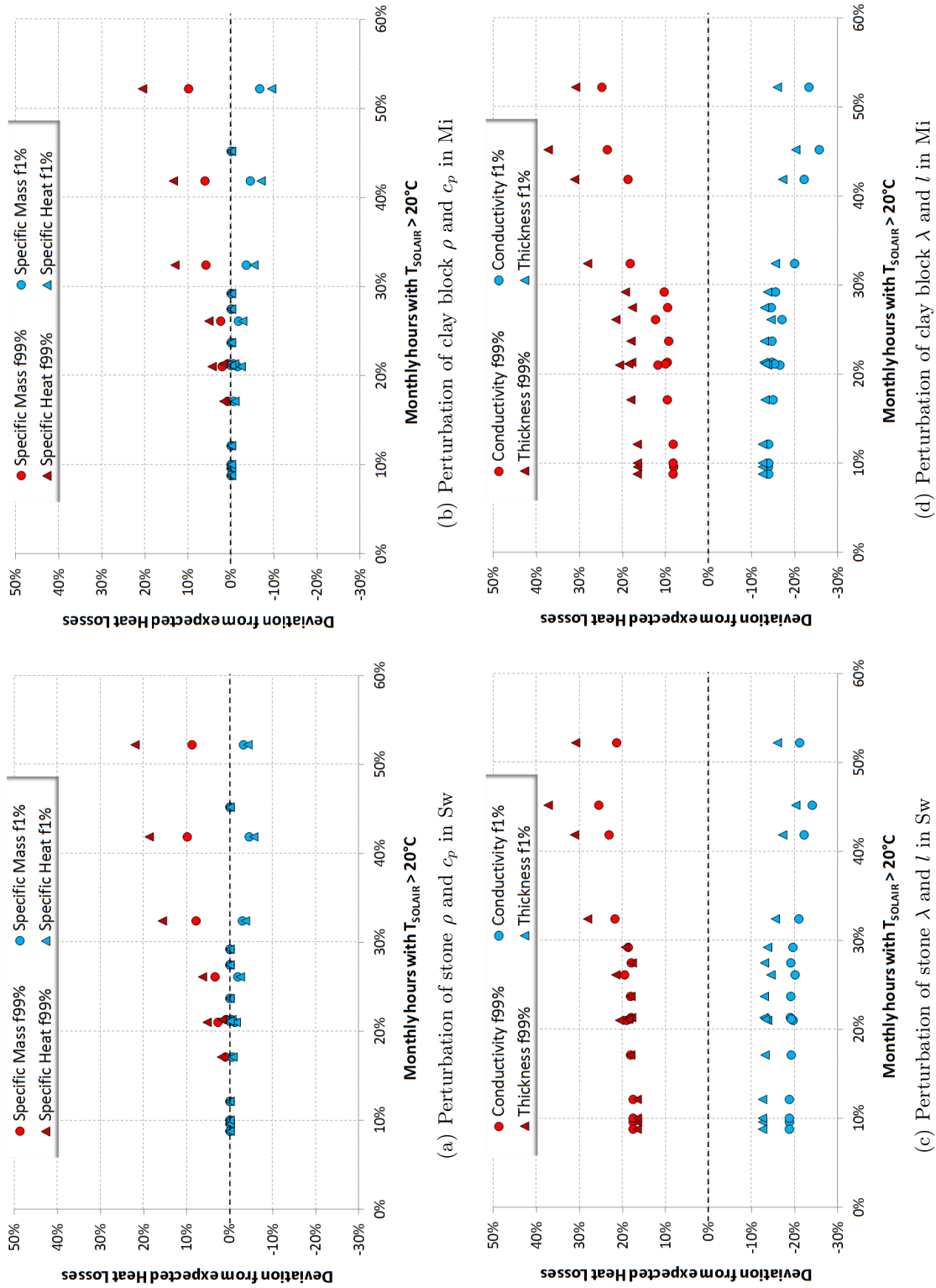
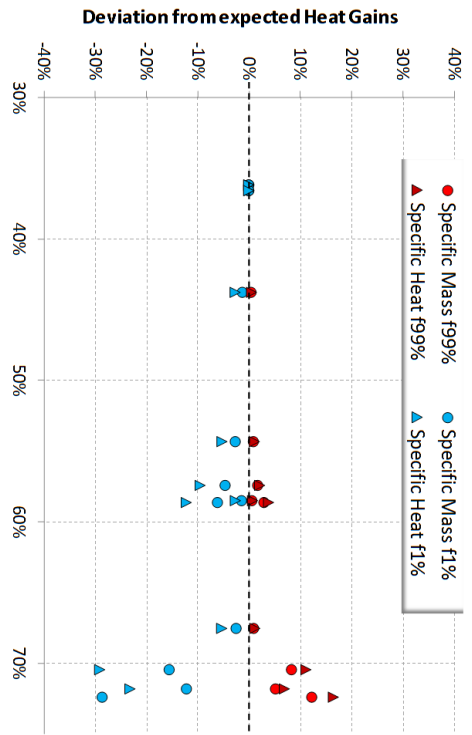
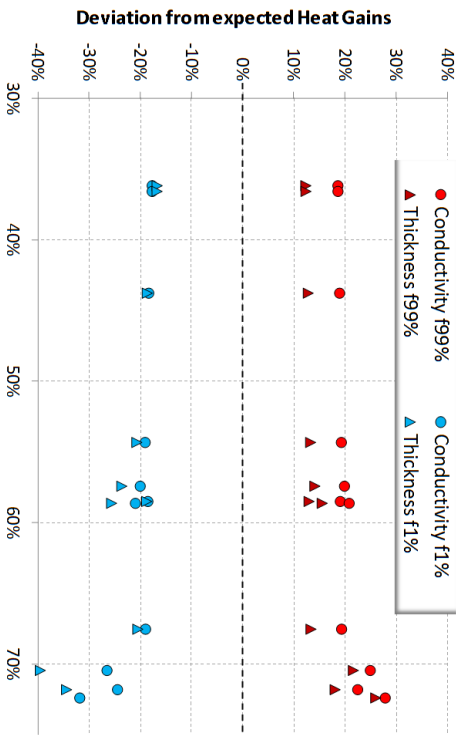


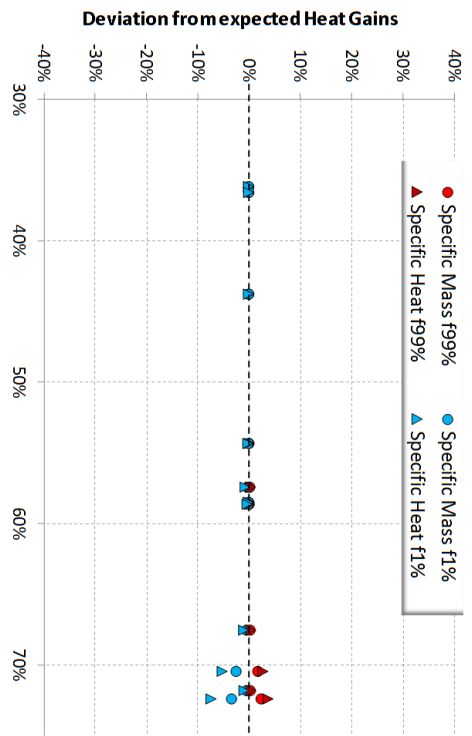
Figure 5.13: Influence of external weather conditions on deviation in monthly heat losses.



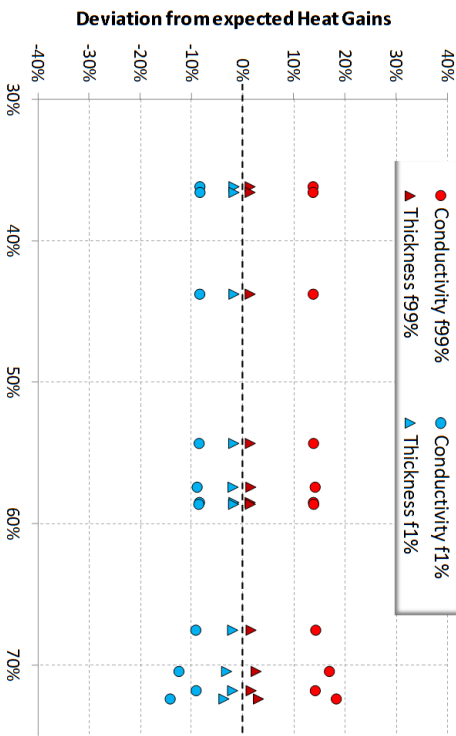
(a) Perturbation of stone ρ and c_p in Sw



(c) Perturbation of stone λ and l in Sw



(b) Perturbation of clay block ρ and c_p in Mi



(d) Perturbation of clay block λ and l in Mi

Figure 5.14: Influence of external weather conditions on deviation in monthly heat gains.

In conclusion, this survey confirms and clarifies what already pointed out in advance by the results reported in Section 5.2 and Section 5.3. For well-insulated walls, the interactions between climate and the uncertainties of material properties are negligible, since it is overshadowed by the role of the wall heat capacitance. Instead, the climate has an important role in the calculation of the CTF or the RF terms for massive and non insulated walls. Indeed, if the amplitude of the oscillations of the outside air temperature around the setpoint temperature is pronounced, the uncertainties on heat gains will be amplified. However, these results point out the role of the external heat capacitance and should not be confused with the internal areic heat capacitance. In fact, the latter is closely related to the capability of the envelope in reducing cooling demand by storage the solar gains that enter through the glazing area and it is released at night.

5.6 Conclusions

In this chapter, due to uncertain thermophysical properties, the reliability of DRF method is analyzed. In particular, in order to increase the representativeness of the results, four typical Italian walls are analyzed. Besides, the weather data of two different cities are used with the purpose of taking into account both warm and mixed climates [8].

Firstly, the results of Monte Carlo simulations reveal that the outcomes of post-processing procedure of DRF output are not always normally distributed. Consequently, the PDF shapes is distorted through the DRF model as well as the uncertainty is propagated. These alterations are primarily caused by the non-linearity of the problem. In fact, as shown in this chapter, the key parameter governing the unsteady response of the wall is the thermal diffusivity.

Secondly, the results highlight the different behavior of the insulated walls with respect to non-insulated. In fact, while the latter shows a dependency of all parameters λ , ρ , c_p and l together, the reliability of model predictions for well insulated constructions hinges upon the accuracy of only λ and l . Furthermore, while for non-insulated components an interaction between thermophysical properties and climates features is noted, the uncertainties of model predictions for well insulated walls are independent on weather characteristics. Consequently, for these components the reliability of DRF outcomes is a property of the wall.

Finally, although these results deal with the sensitivity of an approximated numerical method to the input parameters, some considerations can be drawn on the relevance of thermophysical properties. Indeed, the low sensitivity of

both Me and Mi cases to ρ and c_p perturbations shows that the role of external heat capacitance is negligible if the wall has a low stationary transmittance. Instead, as shown in Section 3.5, internal heat capacitance has a key role in reducing the cooling load through the storage and the release during the night of the solar heat gains.

Therefore, if the retrofitting of an existing building is done by installing an adequate insulating layer on the internal surface of the envelope, for the existing masonry the uncertainties of thermophysical properties are greatly reduced and the accuracy of outcomes can be guaranteed. Oppositely, if the insulation layer is installed on the external surface, it will be important to estimate the correct values of the ρ , c_p and l for existing wall, because they affect the internal thermal capacitance and consequently the building cooling demand.

Conclusions and future developments

In this research, a detailed analysis of the most widely used models for dynamics energy simulation is reported. Firstly, two test reference years (TRYs) for Italian cities are developed. The innovative point of this work with respect to the literature dataset regards the representativeness of these data and their suitability for the evaluation of energy building demand. In fact, in previous works the cross correlation of weather data were often neglected. Moreover, some misconceptions in reference year constructions are highlighted.

Following on from this point, a brief review of literature models for the postprocessing of solar radiation is presented. Besides, a comparison between several couples of decomposition and projection methods and actual data is carried out. Although a single set of measurements carried out in a mountain site does not allow to draw concluding remarks, this analysis reveals that no reliable couple of models which produces negligible errors is available. Hence, solar irradiation used in building simulation tools will be always affected by uncertainties. In addition, also the effects of topography and orography can produce an increasing in misprediction of solar irradiation.

Taking into account these considerations, a sensitivity analysis of numerical models for the prediction of cooling consumptions is carried out. More specifically, in order to increase the representativeness of the analyzed sample, massive and lightweight buildings with different orientations of the glazing area are used.

The outcomes of this analysis reveal the importance of using real sequences of weather data. In particular, analyzing the curves of the loss utilization factor taken back from the results of dynamic simulations, a large gap between real trend and mean typical day (MTD) is recorded, especially for lightweight buildings. This dependence is even greater for the quasi-stationary methods. In fact, contrarily to the standard EN ISO 13790 [3], a bijective link between loss utilization factor and the ratio of losses to gains is not found in this work. In fact, the ratio of losses to gains takes into account only the frequencies of the

external conditions but not the information about the sequences.

Secondly, the sensitivity analysis identifies the climate parameters that mainly affect the building energy balance in summer period. The results of Differential Sensitivity Approach (DSA) clearly show that the interactions between climate and cooling demand depend on the envelope features. However, the parameter with the greatest sensitivity index is the daily average of outside dry bulb temperature. Besides, the sensitivity index to solar irradiation changes is an order of magnitude lower than the daily average of outside dry bulb temperature but, if spring and autumn months are also taken into account, the influence of solar irradiation becomes comparable to that of mean dry bulb temperature. Therefore, the dependence of the solar sensitivity index on the incident angle of solar beams is pointed out.

In conclusion of the first part of the thesis, the Factorial Method demonstrates the negligibility of the second and higher order effects. Consequently, the assumption of perfect independence between the uncertainties of climate variables is realistic for energy simulations.

In the second part, the effects of the uncertainties of the thermophysical properties on the heat transfer through the envelope is studied by means of Monte Carlo approach. More specifically, the outcomes of DRF (Direct Root Finding) method for four typical Italian walls are analyzed. Besides, the weather data of two different cities are used with the purpose of taking into account both warm and mixed climates.

Firstly, the results of Monte Carlo simulations reveal that the outcomes of post-processing procedure of DRF output are not always normally distributed. Consequently, the PDF shape is distorted through the DRF model as well as the uncertainty is propagated. These alterations are primary caused by the non-linearity of the problem.

Secondly, the results highlight the different behavior of the insulated walls with respect to non-insulated. In fact, while the latter shows a dependency of all together λ , ρ , c_p and l , the reliability of model predictions for well insulated constructions hinges upon the accuracy of only λ and l . Furthermore, while for poorly insulated components an interaction between thermophysical properties and climates features is noted, the uncertainties of model predictions for well insulated walls are independent on weather characteristics. Consequently, for these components, the reliability of DRF outcomes is a property of the wall.

Finally, although these results deal with the sensitivity of an approximated numerical method to the input parameters, some considerations can be drawn on the relevance of thermophysical properties. Indeed, the low sensitivity of both Me and Mi cases to ρ and c_p perturbations shows that the role of external

heat capacitance is negligible if the wall has a low stationary transmittance. Instead, internal heat capacitance has a key role in reducing the cooling load through the storage and the release during the night of the solar heat gains.

Therefore, if the retrofitting of an existing building is done by installing an adequate insulating layer on the internal surface of the envelope, for the existing masonry the uncertainties of thermophysical properties are greatly reduced and the accuracy of outcomes can be guaranteed. Oppositely, if the insulation layer is installed on the external surface, it will be important to estimate the correct values of the ρ , c_p and l for existing wall, because they affect the internal thermal capacitance and, consequently, the building cooling demand.

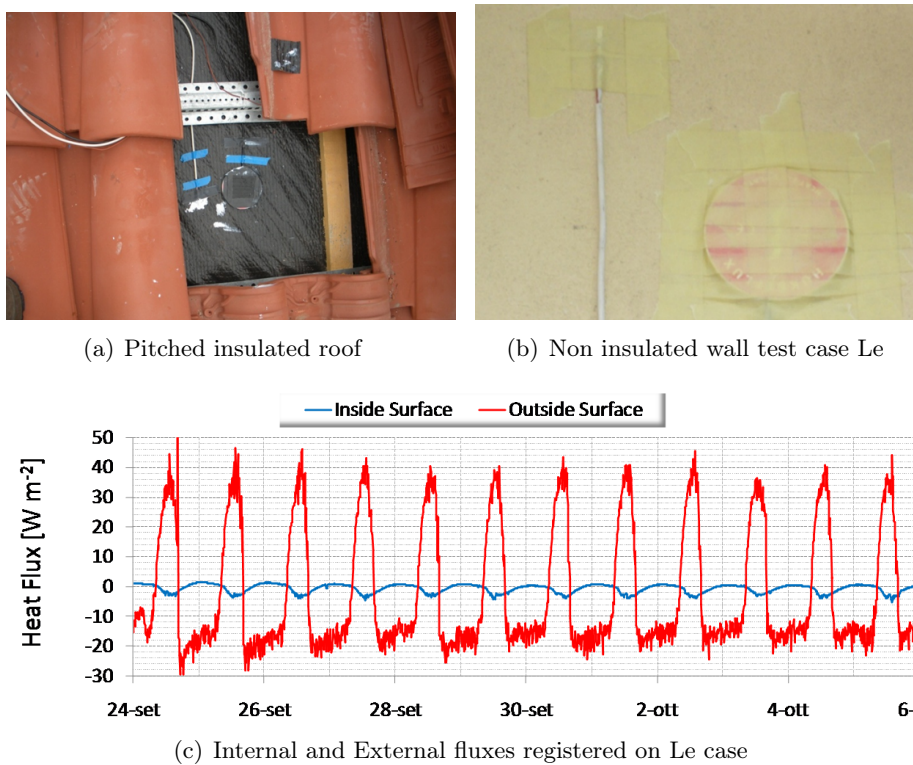


Figure 6.1: *Experimental activities on full scale building components*

Since it is difficult to accurately evaluate thermophysical properties for existing building components, one of the future challenges in this domain is the estimations of response factor by means of in situ measurements. This technique is based on solving the inverse heat transfer problem. Starting from the measured heat fluxes and surface temperatures by exploiting the redundancy of the measures, the response factor can be estimated. However, the main difficulty is the loss of the solution uniqueness in the inverse problems. With this

purpose some experimental activities are in progress. In particular, Figure 6.1 shows two different building components monitored during the summer of 2011 and the trends of internal and external flows registered.

In conclusion, the first part of the thesis has shown that, for massive buildings the cooling demand is mainly influenced by the average daily temperature especially with respect to the setpoint temperature. Instead, due to the high solar altitude, solar irradiation shows less relevance if there are no roof windows.

The second part of the thesis highlights the parameters to which the transmitted heat fluxes show more sensitivity. For new buildings, due to the high insulation level required by national and regional regulations, it is particularly important to know the correct thickness and conductivity of the insulation. However, for existing and poorly insulated building components, all thermo-physical properties have to be estimated with reasonable accuracy.

Appendix

Appendix A

Rank of historical series

Table A.1: Rank of Trento historical series

Trento												
RANK	JAN	FEB	MAR	APR	MAY	JUN	JUL	AUG	SEP	OCT	NOV	DEC
1	2009	1992	2010	2008	1996	1991	2001	1997	1986	2002	1992	1988
2	2004	2010	2008	1993	1998	1993	1998	2004	2002	1991	1986	1999
3	2003	1988	2000	2004	1993	1998	2008	2010	1990	1991	1991	1993
4	1993	1990	1989	2005	2006	2011	1988	1990	1994	1999	1987	1990
5	2010	2000	2007	1987	2008	1994	1993	1988	1991	2005	1984	2009
6	1998	1996	2004	2006	2010	2007	2004	1995	1998	1995	1999	1992
7	1991	1989	2011	1984	1992	1986	1987	1986	2005	1994	1989	2004
8	1992	1994	1990	1999	1986	1987	1997	2001	1992	2006	1995	2010
9	2011	2011	1993	2002	1994	2008	1991	1985	1996	2007	1993	1987
10	1986	1991	2006	1985	1995	1997	2009	1998	1989	2010	1997	1994
11	1994	1997	1988	1992	2007	1984	1990	1993	2004	1984	2001	2005
12	1995	1999	1992	1995	1997	1990	1995	2005	1985	1996	2009	1984
13	1999	2009	2005	1996	2005	1996	1996	2007	2008	1998	1985	1989
14	2007	2007	2003	2003	1991	1988	2002	1987	2010	1993	2010	1996
15	1997	1993	1995	1990	2002	1985	1985	1991	1987	1986	1990	2003
16	2008	2008	2002	1994	1989	1995	2011	2006	2001	1988	2005	1985
17	1990	1986	2009	1988	1990	2002	1994	1994	2006	1987	1996	1997
18	2006	1995	1996	2009	1987	1989	1999	1996	2009	1997	2004	2006
19	2000	2006	1986	1991	2004	2005	2005	2008	1997	2001	1988	2007
20	1987	1985	1998	1998	1985	2003	1986	2002	2007	2004	2007	1986
21	1989	2005	1987	2010	2003	2009	1992	2009	1999	1992	2006	1995
22	1988	1998	1984	2000	1988	1992	2007	2011	1995	2008	1994	1991
23	2002	2002	1994	1997	1999	2010	2006	1984	1984	2009	2002	2001
24	2005	1987	1997	1986	2009	2006	1989	1989	1993	1989	1998	1998
25	1996	2003	1991	2007	2011	1999	2010	1992	2011	1985	2000	2002
26	1984	1984	1985	1989	1984	2000	1984	1999	1988	2000	2003	2000
27	1985	2001	1999	2011	2000	2001	2000	2000	2000	2003	2008	2008
28	2001	2004	2001	2001	2001	2004	2003	2003	2003	2011	2011	2011

Table A.2: *Rank of Palermo historical series*

Palermo												
RANK	JAN	FEB	MAR	APR	MAY	JUN	JUL	AUG	SEP	OCT	NOV	DEC
1	2004	2004	2006	2007	2007	2004	2005	2004	2005	2006	2007	2004
2	2003	2006	2002	2002	2006	2002	2009	2010	2004	2009	2009	2005
3	2010	2007	2009	2009	2005	2005	2006	2007	2009	2007	2008	2006
4	2005	2005	2004	2005	2008	2007	2010	2009	2006	2008	2010	2008
5	2009	2009	2010	2004	2002	2008	2007	2006	2007	2002	2005	2003
6	2002	2010	2007	2003	2003	2009	2003	2005	2002	2005	2002	2002
7	2007	2003	2003	2010	2009	2010	2008	2008	2010	2010	2006	2007
8	2006	2002	2005	2006	2010	2003	2004	2002	2003	2003	2004	2009
9	2008	2008	2008	2008	2004	2006	2002	2003	2008	2004	2003	2010

Appendix B

Model responses for Factorial Method

Table B.1: *Building cooling response for FM in Milan*

CASE	MONTH	Z1	Z2	Z3	Z4	Z5	Z6	Z7	Z8
600	JUN	440.80	568.50	445.60	572.00	451.40	579.10	456.10	582.60
	JUL	479.60	604.60	484.90	609.20	493.70	618.60	499.10	623.20
	AUG	447.50	568.50	451.20	572.10	476.10	597.30	479.80	600.90
	SEP	472.60	556.00	478.00	560.30	519.90	603.90	525.40	608.30
620	JUN	577.60	719.20	580.70	721.50	582.60	721.70	585.80	724.60
	JUL	603.40	743.30	607.00	746.70	626.70	765.90	630.40	769.40
	AUG	460.20	595.40	462.70	598.00	484.80	620.00	487.20	622.50
	SEP	351.80	441.90	356.10	445.30	389.30	480.30	393.50	483.60
900	JUN	368.40	541.60	369.20	541.60	378.50	552.00	379.20	552.00
	JUL	395.90	571.90	396.70	571.90	408.70	585.20	409.50	585.10
	AUG	367.60	541.20	368.30	541.20	395.10	569.50	395.70	569.60
	SEP	314.70	446.80	316.40	447.70	359.20	493.40	360.80	494.30
920	JUN	525.60	699.90	525.80	700.00	526.00	700.30	526.20	700.30
	JUL	540.80	718.60	541.10	718.60	561.00	739.20	561.40	739.20
	AUG	401.80	576.20	402.20	576.30	425.50	600.40	425.90	600.40
	SEP	222.30	352.80	223.80	353.90	257.40	389.50	258.80	390.60

Table B.2: *Building cooling response for FM in Palermo*

CASE	MONTH	Z1	Z2	Z3	Z4	Z5	Z6	Z7	Z8
600	JUN	396.90	515.10	403.00	520.40	393.10	511.10	399.20	516.50
	JUL	585.70	757.70	591.60	760.10	578.20	749.90	584.10	752.40
	AUG	676.10	854.10	680.80	854.80	688.00	865.70	692.80	866.40
	SEP	544.50	655.20	550.10	660.70	581.90	693.20	587.50	698.60
620	JUN	734.30	870.40	739.20	874.40	765.30	901.60	770.20	905.60
	JUL	949.50	1,126.00	954.50	1,129.00	978.60	1,156.00	983.60	1,158.00
	AUG	913.80	1,095.00	918.00	1,096.00	952.40	1,134.00	956.60	1,135.00
	SEP	506.60	625.10	511.40	629.90	544.30	663.40	549.10	668.20
900	JUN	306.20	475.10	307.30	475.10	301.50	470.40	302.60	470.40
	JUL	547.90	753.40	547.90	753.60	539.40	745.40	539.40	745.60
	AUG	646.60	852.80	646.60	852.80	657.50	864.10	657.50	864.10
	SEP	443.00	610.60	443.70	610.60	479.30	647.90	479.90	647.90
920	JUN	666.50	840.80	666.80	840.80	696.90	871.50	697.20	871.60
	JUL	918.10	1,123.00	918.10	1,123.00	946.40	1,152.00	946.40	1,152.00
	AUG	889.90	1,096.00	889.90	1,096.00	927.90	1,134.00	927.90	1,134.00
	SEP	421.00	587.50	421.80	587.50	457.80	625.40	458.50	625.40

Table B.3: *Building loss utilization factors for FM in Milan*

CASE	MONTH	Z1	Z2	Z3	Z4	Z5	Z6	Z7	Z8
600	JUN	0.74	0.75	0.72	0.71	0.73	0.74	0.72	0.70
	JUL	0.70	0.70	0.68	0.66	0.69	0.69	0.68	0.65
	AUG	0.73	0.78	0.71	0.75	0.72	0.78	0.71	0.75
	SEP	0.63	0.66	0.62	0.65	0.63	0.66	0.62	0.65
620	JUN	0.82	0.84	0.81	0.81	0.80	0.81	0.79	0.78
	JUL	0.78	0.77	0.77	0.74	0.77	0.75	0.76	0.72
	AUG	0.80	0.84	0.79	0.82	0.79	0.83	0.79	0.81
	SEP	0.67	0.70	0.66	0.69	0.67	0.70	0.66	0.69
900	JUN	1.00	1.01	1.00	1.01	1.00	1.01	1.00	1.01
	JUL	0.99	1.00	0.99	1.00	0.99	1.00	0.99	1.00

(Continued on next page)

(Continued from previous page)

	AUG	0.99	1.00	0.99	1.00	0.99	1.00	0.99	1.00
	SEP	0.95	0.98	0.95	0.98	0.96	0.99	0.95	0.98
920	JUN	1.00	1.01	1.00	1.01	1.00	1.00	1.00	1.01
	JUL	1.00	1.00	1.00	1.00	1.00	1.00	1.00	1.00
	AUG	0.99	1.00	0.99	1.00	0.99	1.00	0.99	1.00
	SEP	0.94	0.97	0.94	0.97	0.95	0.97	0.94	0.97

Table B.4: *Building loss utilization factors for FM in Palermo*

CASE	MONTH	Z1	Z2	Z3	Z4	Z5	Z6	Z7	Z8
600	JUN	0.63	0.56	0.61	0.50	0.63	0.55	0.61	0.49
	JUL	0.30	1.01	0.18	1.03	0.27	1.01	0.15	1.03
	AUG	0.38	1.00	0.27	1.01	0.38	1.00	0.27	1.00
	SEP	0.63	0.62	0.61	0.58	0.63	0.61	0.61	0.57
620	JUN	0.75	0.70	0.73	0.65	0.74	0.68	0.73	0.64
	JUL	0.41	1.00	0.31	1.02	0.41	1.01	0.31	1.02
	AUG	0.48	0.99	0.39	1.00	0.47	0.99	0.38	1.00
	SEP	0.67	0.65	0.66	0.61	0.67	0.65	0.66	0.61
900	JUN	0.98	0.99	0.97	1.00	0.97	0.99	0.97	0.99
	JUL	1.00	1.00	1.00	1.00	0.99	1.00	0.99	1.00
	AUG	1.01	0.99	1.00	0.99	1.01	1.00	1.01	1.00
	SEP	0.98	1.00	0.98	1.00	0.99	1.00	0.98	1.00
920	JUN	1.00	1.01	1.00	1.00	1.00	1.00	1.00	1.00
	JUL	1.01	1.00	1.01	0.99	1.00	1.00	1.00	1.00
	AUG	0.99	1.00	1.02	1.00	1.01	1.00	1.02	1.00
	SEP	0.98	1.00	0.98	1.00	0.98	1.00	0.98	1.00

Appendix C

Mean and Standard deviations of model predictions

Table C.1: Mean and Std Dev. for Le test case due to expanded clay properties perturbations

	Trento				Palermo			
	Heat Losses		Heat Gains		Heat Losses		Heat Gains	
	Mean	Std. D.	Mean	Std. D.	Mean	Std. D.	Mean	Std. D.
<i>Perturbation of Specific Mass</i>								
Jan	-14275.0	1.096	0.0	0.000	-5579.1	1.288	0.0	0.000
Feb	-11252.0	0.325	0.0	0.000	-3962.4	0.520	575.7	12.218
Mar	-7975.0	1.215	0.0	0.000	-2618.5	19.694	0.0	0.000
Apr	-4140.5	4.580	0.0	0.000	-515.3	10.635	628.8	39.397
May	-3818.5	8.795	0.0	0.000	-2.4	0.713	8985.2	27.836
Jun	-628.3	11.195	229.3	16.141	0.0	0.000	4980.5	5.058
Jul	-97.6	8.604	588.4	22.000	0.0	0.000	9208.6	0.675
Aug	-152.0	7.022	746.3	26.001	0.0	0.000	6402.9	0.234
Sep	-1041.4	13.638	1415.2	7.906	-27.0	2.015	3914.5	6.127
Oct	-6142.4	2.686	0.0	0.000	-233.6	7.371	502.1	27.757
Nov	-10637.0	0.863	0.0	0.000	-1012.0	23.232	8225.8	13.118
Dec	-14637.0	0.659	0.0	0.000	-3269.3	4.047	0.0	0.000

(Continued on next page)

(Continued from previous page)

<i>Perturbation of Specific Heat</i>								
Jan	-14274.0	2.574	0.0	0.000	-5580.4	5.510	0.0	0.022
Feb	-11251.0	0.399	0.0	0.000	-3963.7	4.629	579.6	27.713
Mar	-7974.6	2.138	0.0	0.002	-2624.5	44.479	0.0	0.728
Apr	-4142.8	12.620	0.0	0.005	-524.2	32.947	642.6	87.924
May	-3821.3	19.714	0.0	0.020	-2.8	2.163	8995.0	66.632
Jun	-632.6	27.331	235.3	37.983	0.0	0.082	4984.3	16.072
Jul	-101.1	20.988	597.6	52.590	0.0	0.000	9208.4	1.392
Aug	-155.0	16.381	754.2	57.424	0.0	0.000	6402.7	0.712
Sep	-1046.1	32.419	1418.7	18.351	-27.9	4.930	3918.8	17.319
Oct	-6144.5	7.392	0.0	0.000	-237.4	18.342	513.9	63.847
Nov	-10637.0	2.051	0.0	0.000	-1020.3	53.969	8232.5	31.607
Dec	-14637.0	1.326	0.0	0.000	-3273.5	13.093	0.0	0.022
<i>Perturbation of Conductivity</i>								
Jan	-14267.0	1342.000	0.0	0.000	-5576.1	526.340	0.0	0.000
Feb	-11245.0	1058.600	0.0	0.000	-3960.2	372.770	575.8	68.224
Mar	-7970.4	749.060	0.0	0.000	-2617.6	269.090	0.0	0.000
Apr	-4138.3	394.800	0.0	0.000	-515.9	59.855	630.2	104.360
May	-3816.7	369.440	0.0	0.000	-2.4	1.022	8981.0	877.580
Jun	-628.3	72.086	229.7	40.258	0.0	0.000	4978.1	474.080
Jul	-97.9	19.081	589.0	80.503	0.0	0.000	9203.4	865.740
Aug	-152.3	22.297	746.8	100.190	0.0	0.000	6399.3	602.380
Sep	-1041.2	113.780	1414.9	142.190	-27.0	4.845	3912.7	374.940
Oct	-6139.2	580.770	0.0	0.000	-233.9	30.294	503.2	78.807
Nov	-10631.0	1001.700	0.0	0.000	-1012.3	121.980	8222.0	788.530
Dec	-14629.0	1377.800	0.0	0.000	-3267.9	311.490	0.0	0.000
<i>Perturbation of Thickness</i>								
Jan	-14285.0	384.090	0.0	0.000	-5583.1	151.190	0.0	0.000

(Continued on next page)

(Continued from previous page)

Feb	-11260.0	303.240	0.0	0.000	-3965.2	106.650	575.7	24.312
Mar	-7981.0	214.090	0.0	0.000	-2619.9	84.760	0.0	0.000
Apr	-4143.3	114.720	0.0	0.000	-514.4	20.771	627.6	45.501
May	-3821.0	109.200	0.0	0.000	-2.3	0.564	8990.9	262.080
Jun	-628.2	24.759	228.8	17.655	0.0	0.000	4983.8	137.690
Jul	-97.3	8.792	587.7	31.414	0.0	0.000	9215.4	247.770
Aug	-151.7	9.114	745.9	38.826	0.0	0.000	6407.7	172.540
Sep	-1041.7	37.800	1415.7	43.608	-26.9	2.111	3916.8	109.520
Oct	-6146.6	167.350	0.0	0.000	-233.3	11.471	500.8	33.227
Nov	-10644.0	287.300	0.0	0.000	-1011.6	43.854	8230.9	231.050
Dec	-14648.0	394.930	0.0	0.000	-3271.1	90.427	0.0	0.000

Table C.2: Mean and Std Dev. for Sw test case due to stone properties perturbations

	Trento				Palermo			
	Heat Losses		Heat Gains		Heat Losses		Heat Gains	
	Mean	Std. D.	Mean	Std. D.	Mean	Std. D.	Mean	Std. D.
<i>Perturbation of Specific Mass</i>								
Jan	-31244.0	1.944	0.0	0.000	-12058.0	41.497	0.0	0.010
Feb	-24785.0	1.724	0.0	0.000	-8534.7	21.432	114.7	13.167
Mar	-12596.0	33.252	0.0	0.519	-6066.8	67.521	0.0	0.011
Apr	-8158.3	53.005	0.0	0.039	-1832.8	55.431	223.2	18.458
May	-9075.3	28.878	0.0	0.025	-7.8	0.907	8823.6	65.611
Jun	-1082.6	15.955	5277.2	37.541	0.0	0.000	6751.0	24.353
Jul	-33.9	11.433	3355.9	44.208	0.0	0.000	15114.0	1.139
Aug	-256.6	7.962	3002.3	57.062	0.0	0.000	12152.0	0.643
Sep	-1394.7	62.510	827.9	40.628	-44.6	5.548	6120.4	27.015
Oct	-11186.0	46.239	0.0	0.088	-424.5	10.134	1916.2	69.465
Nov	-23075.0	1.477	0.0	0.000	-2079.4	46.868	9833.3	47.468
Dec	-32400.0	1.955	0.0	0.000	-6253.6	52.370	0.0	0.047

(Continued on next page)

(Continued from previous page)

<i>Perturbation of Specific Heat</i>								
Jan	-31243.0	3.710	0.0	0.000	-12065.0	68.561	0.0	1.502
Feb	-24785.0	2.447	0.0	0.000	-8540.7	39.469	116.3	21.680
Mar	-12602.0	58.426	0.5	4.205	-6079.0	110.700	0.0	1.542
Apr	-8166.8	85.074	0.0	1.113	-1844.9	93.117	228.1	35.856
May	-9081.6	46.118	0.0	0.557	-8.5	3.120	8842.1	116.190
Jun	-1085.8	26.449	5287.6	69.983	0.0	0.078	6758.0	44.725
Jul	-37.1	21.289	3368.1	80.694	0.0	0.000	15114.0	1.629
Aug	-258.7	14.664	3014.5	98.869	0.0	0.000	12151.0	1.087
Sep	-1406.6	103.730	835.3	68.186	-45.6	8.472	6126.3	44.602
Oct	-11196.0	79.168	0.1	2.463	-427.8	21.459	1931.8	118.260
Nov	-23075.0	2.418	0.0	0.000	-2092.0	83.100	9845.3	82.961
Dec	-32401.0	3.452	0.0	0.000	-6266.0	88.514	0.0	1.648
<i>Perturbation of Conductivity</i>								
Jan	-31213.0	2439.700	0.0	0.000	-12042.0	968.220	0.0	0.000
Feb	-24759.0	1934.500	0.0	0.000	-8523.2	678.130	114.0	17.958
Mar	-12581.0	1003.900	0.0	0.000	-6054.9	516.150	0.0	0.000
Apr	-8146.1	671.210	0.0	0.000	-1825.6	177.960	221.0	28.485
May	-9063.3	727.100	0.0	0.000	-7.5	0.636	8806.7	726.890
Jun	-1080.1	95.259	5267.8	434.200	0.0	0.000	6741.3	541.360
Jul	-32.6	9.174	3347.5	287.360	0.0	0.000	15099.0	1179.600
Aug	-255.6	25.127	2994.0	269.210	0.0	0.000	12139.0	948.950
Sep	-1388.0	148.270	823.7	90.560	-44.2	7.202	6111.5	494.880
Oct	-11170.0	901.770	0.0	0.000	-422.8	38.747	1906.9	191.840
Nov	-23051.0	1802.300	0.0	0.000	-2071.8	190.180	9818.4	796.710
Dec	-32367.0	2530.200	0.0	0.000	-6242.0	520.420	0.0	0.000
<i>Perturbation of Thickness</i>								
Jan	-31363.0	1944.100	0.0	0.000	-12109.0	804.000	0.0	0.057
Feb	-24880.0	1541.700	0.0	0.000	-8570.5	558.710	116.2	24.376
Mar	-12648.0	826.570	0.1	1.215	-6097.6	464.700	0.0	0.049

(Continued on next page)

(Continued from previous page)

Apr	-8195.0	575.640	0.0	0.104	-1847.0	186.810	226.4	38.992
May	-9113.9	601.470	0.0	0.065	-8.1	1.751	8867.6	634.420
Jun	-1088.7	88.155	5303.0	378.130	0.0	0.000	6780.6	451.730
Jul	-35.8	17.742	3375.3	266.640	0.0	0.000	15172.0	939.740
Aug	-258.7	26.713	3020.5	261.020	0.0	0.000	12198.0	756.490
Sep	-1407.3	168.220	835.6	105.440	-45.4	9.702	6147.4	415.390
Oct	-11235.0	756.620	0.0	0.242	-427.6	40.363	1932.6	210.350
Nov	-23164.0	1437.500	0.0	0.000	-2094.3	191.050	9877.6	673.820
Dec	-32525.0	2017.800	0.0	0.000	-6284.8	456.990	0.0	0.129

Table C.3: Mean and Std Dev. for Mi test case due to insulation properties perturbations

	Trento				Palermo			
	Heat Losses		Heat Gains		Heat Losses		Heat Gains	
	Mean	Std. D.	Mean	Std. D.	Mean	Std. D.	Mean	Std. D.
<i>Perturbation of Specific Mass</i>								
Jan	-2902.9	0.026	0.0	0.000	-1134.1	0.068	27.3	0.049
Feb	-2305.7	0.025	0.0	0.000	-799.5	0.036	82.0	0.048
Mar	-1176.4	0.016	40.3	0.023	-582.0	0.066	56.4	0.070
Apr	-770.9	0.033	60.3	0.044	-188.4	0.075	377.3	0.107
May	-852.0	0.028	29.8	0.007	-1.1	0.009	1794.2	0.030
Jun	-106.2	0.030	1166.6	0.085	0.0	0.000	1684.8	0.014
Jul	-7.3	0.025	1212.1	0.033	0.0	0.000	2530.3	0.012
Aug	-27.3	0.029	1183.7	0.012	0.0	0.000	2254.6	0.008
Sep	-147.1	0.065	510.6	0.038	-5.3	0.000	1523.2	0.007
Oct	-1056.3	0.086	52.3	0.061	-43.9	0.043	904.3	0.034
Nov	-2146.7	0.019	0.0	0.000	-206.9	0.044	1322.3	0.019
Dec	-3014.8	0.033	0.0	0.000	-598.4	0.079	64.1	0.072
<i>Perturbation of Specific Heat</i>								
Jan	-2902.9	0.045	0.0	0.000	-1134.1	0.131	27.3	0.093

(Continued on next page)

(Continued from previous page)

Feb	-2305.7	0.048	0.0	0.000	-799.5	0.068	82.0	0.091
Mar	-1176.4	0.027	40.3	0.045	-582.0	0.127	56.4	0.134
Apr	-770.9	0.062	60.3	0.084	-188.4	0.144	377.3	0.204
May	-852.0	0.054	29.8	0.013	-1.1	0.018	1794.2	0.058
Jun	-106.2	0.058	1166.6	0.163	0.0	0.000	1684.8	0.026
Jul	-7.3	0.048	1212.1	0.064	0.0	0.000	2530.3	0.021
Aug	-27.3	0.056	1183.7	0.023	0.0	0.000	2254.6	0.011
Sep	-147.1	0.126	510.6	0.076	-5.3	0.001	1523.2	0.010
Oct	-1056.3	0.171	52.3	0.123	-43.9	0.081	904.3	0.065
Nov	-2146.7	0.036	0.0	0.000	-206.9	0.087	1322.3	0.040
Dec	-3014.8	0.063	0.0	0.000	-598.4	0.150	64.1	0.136
<i>Perturbation of Conductivity</i>								
Jan	-2900.9	112.460	0.0	0.000	-1133.4	44.397	27.3	1.477
Feb	-2304.2	89.379	0.0	0.000	-798.9	31.284	82.0	3.495
Mar	-1175.6	45.978	40.3	2.008	-581.7	23.290	56.4	2.931
Apr	-770.4	30.409	60.3	2.881	-188.3	7.912	377.1	15.276
May	-851.4	33.297	29.8	1.412	-1.1	0.087	1793.0	69.604
Jun	-106.2	4.276	1165.9	45.437	0.0	0.000	1683.7	65.308
Jul	-7.3	0.462	1211.3	47.170	0.0	0.000	2528.6	98.061
Aug	-27.3	1.171	1182.9	45.953	0.0	0.000	2253.1	87.373
Sep	-147.0	6.407	510.3	20.460	-5.3	0.247	1522.2	59.067
Oct	-1055.7	41.498	52.3	2.557	-43.9	1.926	903.7	35.262
Nov	-2145.2	83.215	0.0	0.000	-206.8	8.589	1321.4	51.772
Dec	-3012.8	116.870	0.0	0.000	-598.0	23.828	64.1	3.106
<i>Perturbation of Thickness</i>								
Jan	-2912.0	163.760	0.0	0.000	-1137.8	64.768	27.5	2.235
Feb	-2313.0	130.200	0.0	0.000	-802.0	45.615	82.3	5.159
Mar	-1180.2	66.980	40.5	2.988	-584.0	34.045	56.7	4.399
Apr	-773.4	44.347	60.6	4.269	-189.1	11.646	378.6	22.410
May	-854.7	48.544	29.9	2.081	-1.1	0.144	1799.8	101.410

(Continued on next page)

(Continued from previous page)

Jun	-106.6	6.274	1170.4	66.285	0.0	0.000	1690.1	95.130
Jul	-7.4	0.710	1216.0	68.746	0.0	0.000	2538.3	142.830
Aug	-27.4	1.745	1187.4	66.943	0.0	0.000	2261.7	127.250
Sep	-147.7	9.462	512.3	29.897	-5.4	0.364	1528.0	86.025
Oct	-1059.8	60.598	52.6	3.854	-44.1	2.866	907.2	51.406
Nov	-2153.5	121.220	0.0	0.000	-207.7	12.625	1326.6	75.485
Dec	-3024.3	170.250	0.0	0.000	-600.4	34.836	64.4	4.649

Table C.4: Mean and Std Dev. for Mi test case due to clay block properties perturbations

	Trento				Palermo			
	Heat Losses		Heat Gains		Heat Losses		Heat Gains	
	Mean	Std. D.	Mean	Std. D.	Mean	Std. D.	Mean	Std. D.
<i>Perturbation of Specific Mass</i>								
Jan	-2902.8	0.370	0.0	0.000	-1134.3	3.209	27.5	2.999
Feb	-2305.7	0.187	0.0	0.000	-799.7	2.073	82.2	2.220
Mar	-1176.7	2.682	40.7	3.192	-582.5	5.066	56.8	5.152
Apr	-771.1	3.478	60.6	3.582	-188.7	4.213	377.6	4.600
May	-852.1	1.925	30.0	1.716	-1.1	0.332	1794.2	0.539
Jun	-106.3	1.163	1166.8	1.732	0.0	0.000	1684.8	0.103
Jul	-7.4	1.218	1212.2	1.345	0.0	0.000	2530.3	0.016
Aug	-27.4	0.807	1183.7	0.529	0.0	0.000	2254.6	0.049
Sep	-147.4	4.879	510.9	4.561	-5.4	0.309	1523.2	0.253
Oct	-1056.7	4.085	52.6	3.834	-44.0	1.550	904.4	1.446
Nov	-2146.7	0.157	0.0	0.000	-207.4	4.057	1322.7	3.677
Dec	-3014.8	0.305	0.0	0.000	-598.8	4.513	64.4	4.405
<i>Perturbation of Specific Heat</i>								
Jan	-2902.7	0.709	0.0	0.003	-1134.9	6.152	28.1	5.761
Feb	-2305.8	0.344	0.0	0.002	-800.2	4.176	82.8	4.460
Mar	-1177.5	5.641	41.6	6.594	-583.4	9.506	57.8	9.666

(Continued on next page)

(Continued from previous page)

Apr	-771.8	6.581	61.2	6.792	-189.4	7.949	378.4	8.674
May	-852.5	3.600	30.3	3.206	-1.2	0.615	1794.4	0.994
Jun	-106.6	2.277	1167.2	3.356	0.0	0.001	1684.8	0.187
Jul	-7.7	2.343	1212.5	2.560	0.0	0.000	2530.3	0.024
Aug	-27.6	1.556	1183.9	1.034	0.0	0.000	2254.6	0.102
Sep	-148.2	9.111	511.7	8.510	-5.5	0.628	1523.3	0.507
Oct	-1057.4	7.651	53.3	7.176	-44.3	2.853	904.7	2.649
Nov	-2146.7	0.292	0.0	0.021	-208.4	7.832	1323.7	7.120
Dec	-3014.9	0.556	0.0	0.000	-599.6	8.441	65.2	8.247
<i>Perturbation of Conductivity</i>								
Jan	-2888.2	135.130	0.0	0.000	-1128.7	58.724	27.4	6.657
Feb	-2294.1	108.240	0.0	0.000	-795.8	40.967	82.0	7.759
Mar	-1171.1	59.467	40.9	7.516	-579.7	35.999	56.7	11.711
Apr	-767.3	42.018	60.3	9.072	-187.7	16.224	375.7	25.775
May	-847.9	43.170	29.8	4.353	-1.2	0.608	1785.3	84.856
Jun	-105.9	7.021	1161.1	57.701	0.0	0.000	1676.3	79.027
Jul	-7.4	2.506	1206.1	59.052	0.0	0.000	2517.6	118.390
Aug	-27.3	2.682	1177.8	56.229	0.0	0.000	2243.2	105.400
Sep	-146.7	15.384	508.4	31.708	-5.4	0.820	1515.5	71.716
Oct	-1051.4	56.618	52.4	9.274	-43.9	4.645	900.0	44.634
Nov	-2135.9	100.740	0.0	0.002	-206.7	16.561	1316.4	67.920
Dec	-2999.6	141.640	0.0	0.000	-595.9	35.822	64.3	10.746
<i>Perturbation of Thickness</i>								
Jan	-2903.0	19.371	0.0	0.000	-1134.2	9.642	27.4	2.028
Feb	-2305.8	15.702	0.0	0.000	-799.6	6.663	82.1	1.914
Mar	-1176.5	9.521	40.4	2.186	-582.2	7.060	56.6	3.567
Apr	-771.0	7.352	60.4	2.622	-188.5	3.899	377.4	5.428
May	-852.1	6.946	29.9	1.255	-1.1	0.218	1794.3	12.465
Jun	-106.3	1.439	1166.8	8.976	0.0	0.000	1684.9	11.450
Jul	-7.4	0.810	1212.2	9.031	0.0	0.000	2530.4	17.095

(Continued on next page)

(Continued from previous page)

Aug	-27.4	0.694	1183.8	8.324	0.0	0.000	2254.7	15.202
Sep	-147.2	4.019	510.7	6.265	-5.3	0.216	1523.3	10.433
Oct	-1056.6	9.677	52.4	2.731	-43.9	1.275	904.4	7.019
Nov	-2146.8	14.606	0.0	0.000	-207.1	3.873	1322.5	11.157
Dec	-3014.9	20.569	0.0	0.000	-598.6	6.844	64.2	3.166

Table C.5: Mean and Std Dev. for Me test case due to insulation properties perturbations

	Trento				Palermo			
	Heat Losses		Heat Gains		Heat Losses		Heat Gains	
	Mean	Std. D.	Mean	Std. D.	Mean	Std. D.	Mean	Std. D.
<i>Perturbation of Specific Mass</i>								
Jan	-2902.7	0.397	0.0	0.000	-1134.9	3.257	28.0	3.050
Feb	-2305.8	0.179	0.0	0.000	-800.0	2.125	82.6	2.280
Mar	-1177.2	2.774	41.3	3.300	-583.4	5.156	57.8	5.246
Apr	-771.8	3.527	61.3	3.639	-189.5	4.268	378.4	4.662
May	-852.5	1.957	30.3	1.748	-1.2	0.344	1794.3	0.544
Jun	-106.6	1.196	1167.1	1.771	0.0	0.000	1684.8	0.096
Jul	-7.7	1.240	1212.5	1.360	0.0	0.000	2530.3	0.034
Aug	-27.6	0.826	1183.8	0.537	0.0	0.000	2254.6	0.068
Sep	-148.3	4.947	511.8	4.621	-5.4	0.321	1523.2	0.253
Oct	-1057.5	4.143	53.3	3.892	-44.3	1.580	904.7	1.468
Nov	-2146.7	0.148	0.0	0.000	-208.1	4.170	1323.4	3.777
Dec	-3014.8	0.294	0.0	0.000	-599.6	4.586	65.3	4.481
<i>Perturbation of Specific Heat</i>								
Jan	-2902.7	0.737	0.0	0.003	-1135.5	6.259	28.6	5.867
Feb	-2305.8	0.341	0.0	0.003	-800.6	4.289	83.2	4.582
Mar	-1178.1	5.838	42.3	6.812	-584.3	9.657	58.7	9.822
Apr	-772.4	6.688	61.9	6.910	-190.2	8.076	379.2	8.813
May	-852.8	3.657	30.6	3.260	-1.3	0.632	1794.4	1.008

(Continued on next page)

(Continued from previous page)

Jun	-106.9	2.337	1167.5	3.434	0.0	0.001	1684.8	0.183
Jul	-7.9	2.393	1212.7	2.603	0.0	0.000	2530.3	0.042
Aug	-27.8	1.596	1184.0	1.061	0.0	0.000	2254.5	0.118
Sep	-149.2	9.243	512.5	8.629	-5.5	0.644	1523.3	0.512
Oct	-1058.1	7.756	54.0	7.276	-44.6	2.913	905.0	2.700
Nov	-2146.7	0.288	0.0	0.023	-209.1	8.032	1324.3	7.303
Dec	-3014.9	0.550	0.0	0.000	-600.4	8.573	66.1	8.380
<i>Perturbation of Conductivity</i>								
Jan	-2888.1	135.080	0.0	0.000	-1129.3	58.943	28.0	6.877
Feb	-2294.1	108.240	0.0	0.000	-796.2	41.144	82.4	7.959
Mar	-1171.7	59.743	41.5	7.854	-580.6	36.338	57.7	12.065
Apr	-767.9	42.245	61.0	9.321	-188.5	16.501	376.6	26.075
May	-848.2	43.295	30.2	4.470	-1.3	0.637	1785.3	84.888
Jun	-106.1	7.118	1161.4	57.832	0.0	0.000	1676.3	79.025
Jul	-7.7	2.598	1206.4	59.138	0.0	0.000	2517.5	118.380
Aug	-27.5	2.746	1177.9	56.267	0.0	0.000	2243.2	105.390
Sep	-147.7	15.700	509.2	31.996	-5.4	0.850	1515.6	71.730
Oct	-1052.2	56.872	53.1	9.520	-44.2	4.763	900.2	44.737
Nov	-2135.9	100.740	0.0	0.003	-207.4	16.905	1317.1	68.225
Dec	-2999.6	141.640	0.0	0.000	-596.7	36.123	65.1	11.050
<i>Perturbation of Thickness</i>								
Jan	-2902.9	19.355	0.0	0.000	-1134.8	9.680	27.9	2.067
Feb	-2305.9	15.698	0.0	0.000	-799.9	6.703	82.5	1.960
Mar	-1177.0	9.592	41.0	2.270	-583.2	7.155	57.5	3.665
Apr	-771.7	7.404	61.1	2.680	-189.3	3.956	378.3	5.491
May	-852.4	6.980	30.2	1.288	-1.2	0.229	1794.4	12.474
Jun	-106.5	1.468	1167.1	9.012	0.0	0.000	1684.9	11.447
Jul	-7.6	0.829	1212.5	9.047	0.0	0.000	2530.4	17.087
Aug	-27.5	0.713	1183.9	8.335	0.0	0.000	2254.7	15.194
Sep	-148.1	4.090	511.6	6.329	-5.4	0.227	1523.3	10.437

(Continued on next page)

(Continued from previous page)

Oct	-1057.3	9.746	53.1	2.800	-44.2	1.300	904.7	7.039
Nov	-2146.8	14.601	0.0	0.000	-207.9	3.973	1323.2	11.247
Dec	-3015.0	20.564	0.0	0.000	-599.4	6.917	65.0	3.240

Appendix D

Adimensional fractiles of model predictions

The adimensional fractiles af are defined as the ratio of the fractile to the expected values:

$$af_{1\%} = \frac{f_{1\%}}{E\{x\}}$$

$$af_{99\%} = \frac{f_{99\%}}{E\{x\}}$$

Table D.1: *Adimensional fractiles for Le case due to expanded clay properties perturbations*

		Heat losses				Heat gains					
		Palermo		Trento		Palermo		Trento			
		$af_{1\%}$	$af_{99\%}$	$af_{1\%}$	$af_{99\%}$	$af_{1\%}$	$af_{99\%}$	$af_{1\%}$	$af_{99\%}$		
Specific Mass	JAN	1.00	1.00	1.00	1.00					MAR	Specific Mass
	FEB	1.00	1.00	1.00	1.00	0.89	1.18			APR	
	MAR	1.02	0.99	1.00	1.00	0.99	1.01			MAY	
	APR	1.08	0.98	1.00	1.00	1.00	1.00	0.87	1.21	JUN	
	MAY			1.01	1.00	1.00	1.00	0.94	1.12	JUL	
	SEP	1.25	0.88	1.04	0.98	1.00	1.00	0.94	1.10	AUG	
	OCT	1.10	0.95	1.00	1.00	1.00	1.01	0.99	1.02	SEP	
	NOV	1.07	0.96	1.00	1.00	0.91	1.17			OCT	
	DEC	1.01	1.00	1.00	1.00	0.00	0.00	0.00	0.00	NOV	
	Specific Heat	JAN	1.00	1.00	1.00	1.00					
FEB		1.01	1.00	1.00	1.00	0.83	1.50			APR	
MAR		1.06	0.98	1.00	1.00	0.99	1.03			MAY	
APR		1.28	0.97	1.01	1.00	1.00	1.01	0.80	1.60	JUN	
MAY				1.02	0.99	1.00	1.00	0.90	1.33	JUL	
SEP		1.69	0.80	1.11	0.96	1.00	1.00	0.89	1.26	AUG	
OCT		1.31	0.93	1.01	1.00	1.00	1.02	0.99	1.05	SEP	
NOV		1.19	0.93	1.00	1.00	0.86	1.47			OCT	
DEC		1.02	1.00	1.00	1.00	0.00	0.00	0.00	0.00	NOV	

(Continued on next page)

(Continued from previous page)

Conductivity	JAN	1.22	0.78	1.22	0.78					MAR	Conductivity
	FEB	1.22	0.78	1.22	0.78	0.66	1.43			APR	
	MAR	1.24	0.76	1.22	0.78	0.77	1.23			MAY	
	APR	1.31	0.76	1.22	0.78	0.78	1.22	0.64	1.46	JUN	
	MAY			1.22	0.77	0.78	1.22	0.71	1.35	JUL	
	SEP	1.51	0.65	1.26	0.75	0.78	1.22	0.71	1.33	AUG	
	OCT	1.34	0.73	1.22	0.78	0.78	1.22	0.77	1.24	SEP	
	NOV	1.30	0.73	1.22	0.78	0.69	1.42			OCT	
	DEC	1.22	0.78	1.22	0.78	0.00	0.00	0.00	0.00	NOV	
	Thickness	JAN	1.07	0.94	1.00	1.00					
FEB		1.07	0.94	1.00	1.00	0.86	1.20			APR	
MAR		1.08	0.93	1.00	1.00	0.94	1.07			MAY	
APR		1.12	0.93	1.00	1.00	0.94	1.07	0.87	1.21	JUN	
MAY				1.01	1.00	0.94	1.07	0.94	1.12	JUL	
SEP		1.23	0.85	1.04	0.98	0.94	1.07	0.94	1.10	AUG	
OCT		1.13	0.90	1.00	1.00	0.94	1.07	0.99	1.02	SEP	
NOV		1.11	0.91	1.00	1.00	0.87	1.19			OCT	
DEC		1.07	0.94	1.00	1.00	0.00	0.00	0.00	0.00	NOV	

Table D.2: Adimensional fractiles for S_w case due to stone properties perturbations

		Heat losses				Heat gains					
		Palermo		Trento		Palermo		Trento			
		$af_{1\%}$	$af_{99\%}$	$af_{1\%}$	$af_{99\%}$	$af_{1\%}$	$af_{99\%}$	$af_{1\%}$	$af_{99\%}$		
Specific Mass	JAN	1.01	0.99	1.00	1.00					MAR	Specific Mass
	FEB	1.01	1.00	1.00	1.00	0.88	1.29			APR	
	MAR	1.03	0.98	1.01	1.00	0.99	1.03			MAY	
	APR	1.10	0.96	1.02	0.99	1.00	1.01	0.99	1.02	JUN	
	MAY			1.01	1.00	1.00	1.00	0.98	1.05	JUL	
	SEP	1.36	0.81	1.14	0.93	1.00	1.00	0.97	1.06	AUG	
	OCT	1.09	0.97	1.01	0.99	0.99	1.01	0.92	1.16	SEP	
	NOV	1.08	0.97	1.00	1.00	0.95	1.12			OCT	
	DEC	1.03	0.99	1.00	1.00	0.00	0.00	0.00	0.00	NOV	
	Specific Heat	JAN	1.02	0.99	1.00	1.00					
FEB		1.02	1.00	1.00	1.00	0.84	1.64			APR	
MAR		1.06	0.98	1.02	0.99	0.99	1.05			MAY	
APR		1.19	0.94	1.03	0.99	0.99	1.03	0.99	1.05	JUN	
MAY				1.02	0.99	1.00	1.00	0.98	1.09	JUL	
SEP		1.62	0.80	1.27	0.91	1.00	1.00	0.96	1.12	AUG	
OCT		1.22	0.96	1.03	0.99	0.99	1.03	0.89	1.29	SEP	
NOV		1.16	0.96	1.00	1.00	0.93	1.23			OCT	
DEC		1.05	0.99	1.00	1.00	0.00	0.00	0.00	0.00	NOV	
Conductivity		JAN	1.18	0.81	1.18	0.81					MAR
	FEB	1.18	0.81	1.18	0.81	0.72	1.32			APR	
	MAR	1.20	0.80	1.18	0.81	0.81	1.19			MAY	
	APR	1.23	0.78	1.19	0.80	0.81	1.18	0.81	1.19	JUN	
	MAY			1.18	0.81	0.81	1.18	0.80	1.20	JUL	
	SEP	1.39	0.67	1.26	0.76	0.81	1.18	0.79	1.21	AUG	
	OCT	1.21	0.79	1.18	0.81	0.81	1.18	0.75	1.26	SEP	
	NOV	1.22	0.79	1.18	0.81	0.77	1.24			OCT	
	DEC	1.19	0.80	1.18	0.81	0.00	0.00	0.00	0.00	NOV	

(Continued on next page)

(Continued from previous page)

Thickness	JAN	1.18	0.87	1.17	0.88					MAR	Thickness
	FEB	1.18	0.87	1.17	0.88	0.74	1.61			APR	
	MAR	1.22	0.86	1.18	0.87	0.87	1.21			MAY	
	APR	1.31	0.83	1.19	0.86	0.87	1.19	0.87	1.20	JUN	
	MAY			1.18	0.87	0.88	1.17	0.86	1.24	JUL	
	SEP	1.66	0.70	1.37	0.80	0.88	1.17	0.84	1.26	AUG	
	OCT	1.31	0.84	1.19	0.87	0.87	1.19	0.78	1.39	SEP	
	NOV	1.28	0.85	1.17	0.88	0.82	1.34			OCT	
	DEC	1.21	0.86	1.17	0.88	0.00	0.00	0.00	0.00	NOV	

Table D.3: Adimensional fractiles for Me case due to clay block properties perturbations

		Heat losses				Heat gains					
		Palermo		Trento		Palermo		Trento			
		$af_{1\%}$	$af_{99\%}$	$af_{1\%}$	$af_{99\%}$	$af_{1\%}$	$af_{99\%}$	$af_{1\%}$	$af_{99\%}$		
Specific Mass	JAN	1.01	0.99	1.00	1.00	0.83	1.25	0.86	1.25	MAR	Specific Mass
	FEB	1.01	1.00	1.00	1.00	0.98	1.03	0.89	1.16	APR	
	MAR	1.02	0.98	1.01	1.00	1.00	1.00	0.89	1.16	MAY	
	APR	1.06	0.96	1.01	0.99	1.00	1.00	1.00	1.00	JUN	
	MAY			1.01	1.00	1.00	1.00	1.00	1.00	JUL	
	SEP			1.09	0.94	1.00	1.00	1.00	1.00	AUG	
	OCT	1.10	0.93	1.01	0.99	1.00	1.00	0.98	1.02	SEP	
	NOV	1.06	0.97	1.00	1.00	1.00	1.00	0.86	1.20	OCT	
	DEC	1.02	0.99	1.00	1.00	0.00	0.00	0.00	0.00	NOV	
	Specific Heat	JAN	1.02	0.99	1.00	1.00	0.73	1.54	0.79	1.60	
FEB		1.02	0.99	1.00	1.00	0.96	1.07	0.82	1.36	APR	
MAR		1.05	0.97	1.02	0.99	1.00	1.00	0.83	1.34	MAY	
APR		1.13	0.93	1.03	0.99	1.00	1.00	1.00	1.01	JUN	
MAY				1.01	0.99	1.00	1.00	1.00	1.01	JUL	
SEP				1.19	0.90	1.00	1.00	1.00	1.00	AUG	
OCT		1.21	0.91	1.02	0.99	1.00	1.00	0.97	1.05	SEP	
NOV		1.13	0.95	1.00	1.00	1.00	1.01	0.77	1.42	OCT	
DEC		1.04	0.98	1.00	1.00	0.00	0.00	0.00	0.00	NOV	
Conductivity		JAN	1.10	0.85	1.08	0.86	0.54	1.51	0.63	1.54	MAR
	FEB	1.10	0.85	1.08	0.86	0.82	1.14	0.65	1.36	APR	
	MAR	1.12	0.83	1.10	0.86	0.86	1.08	0.66	1.35	MAY	
	APR	1.19	0.78	1.10	0.85	0.86	1.08	0.86	1.09	JUN	
	MAY			1.09	0.85	0.86	1.08	0.86	1.09	JUL	
	SEP			1.24	0.74	0.86	1.08	0.86	1.08	AUG	
	OCT	1.25	0.77	1.10	0.85	0.86	1.08	0.83	1.12	SEP	
	NOV	1.18	0.80	1.08	0.86	0.86	1.09	0.60	1.42	OCT	
	DEC	1.12	0.84	1.08	0.86	0.00	0.00	0.00	0.00	NOV	
	Thickness	JAN	1.02	0.98	1.02	0.98	0.87	1.17	0.89	1.15	MAR
FEB		1.02	0.98	1.02	0.98	0.97	1.04	0.91	1.11	APR	
MAR		1.03	0.97	1.02	0.98	0.98	1.02	0.91	1.11	MAY	
APR		1.05	0.95	1.02	0.98	0.98	1.02	0.98	1.02	JUN	
MAY				1.02	0.98	0.98	1.02	0.98	1.02	JUL	
SEP				1.07	0.94	0.98	1.02	0.98	1.02	AUG	
OCT		1.07	0.94	1.02	0.98	0.98	1.02	0.97	1.03	SEP	
NOV		1.05	0.96	1.02	0.98	0.98	1.02	0.89	1.14	OCT	

(Continued on next page)

(Continued from previous page)

	DEC	1.03	0.97	1.02	0.98	0.00	0.00	0.00	0.00	NOV	
--	-----	------	------	------	------	------	------	------	------	-----	--

Table D.4: Adimensional fractiles for Me case due to insulation properties perturbations

		Heat losses				Heat gains					
		Palermo		Trento		Palermo		Trento			
		af _{1%}	af _{99%}								
Specific Mass	JAN	1.00	1.00	1.00	1.00	1.00	1.00	1.00	1.00	MAR	Specific Mass
	FEB	1.00	1.00	1.00	1.00	1.00	1.00	1.00	1.00	APR	
	MAR	1.00	1.00	1.00	1.00	1.00	1.00	1.00	1.00	MAY	
	APR	1.00	1.00	1.00	1.00	1.00	1.00	1.00	1.00	JUN	
	MAY			1.00	1.00	1.00	1.00	1.00	1.00	JUL	
	SEP			1.00	1.00	1.00	1.00	1.00	1.00	AUG	
	OCT	1.00	1.00	1.00	1.00	1.00	1.00	1.00	1.00	SEP	
	NOV	1.00	1.00	1.00	1.00	1.00	1.00	1.00	1.00	OCT	
	DEC	1.00	1.00	1.00	1.00	0.00	0.00	0.00	0.00	NOV	
Specific Heat	JAN	1.00	1.00	1.00	1.00	0.99	0.99	1.00	1.00	MAR	Specific Heat
	FEB	1.00	1.00	1.00	1.00	1.00	1.00	1.00	1.00	APR	
	MAR	1.00	1.00	1.00	1.00	1.00	1.00	1.00	1.00	MAY	
	APR	1.00	1.00	1.00	1.00	1.00	1.00	1.00	1.00	JUN	
	MAY			1.00	1.00	1.00	1.00	1.00	1.00	JUL	
	SEP			1.00	1.00	1.00	1.00	1.00	1.00	AUG	
	OCT	1.01	1.00	1.00	1.00	1.00	1.00	1.00	1.00	SEP	
	NOV	1.00	1.00	1.00	1.00	1.00	1.00	0.99	1.01	OCT	
	DEC	1.00	1.00	1.00	1.00	0.00	0.00	0.00	0.00	NOV	
Conductivity	JAN	1.09	0.91	1.09	0.91	0.88	1.12	0.88	1.11	MAR	Conductivity
	FEB	1.09	0.91	1.09	0.91	0.90	1.09	0.89	1.11	APR	
	MAR	1.09	0.90	1.09	0.91	0.91	1.09	0.89	1.11	MAY	
	APR	1.09	0.90	1.09	0.90	0.91	1.09	0.91	1.09	JUN	
	MAY			1.09	0.91	0.91	1.09	0.91	1.09	JUL	
	SEP			1.10	0.90	0.91	1.09	0.91	1.09	AUG	
	OCT	1.10	0.90	1.09	0.91	0.91	1.09	0.90	1.09	SEP	
	NOV	1.09	0.90	1.09	0.91	0.91	1.09	0.88	1.11	OCT	
	DEC	1.09	0.90	1.09	0.91	0.00	0.00	0.00	0.00	NOV	
Thickness	JAN	1.15	0.88	1.15	0.89	0.85	1.21	0.86	1.21	MAR	Thickness
	FEB	1.15	0.88	1.15	0.89	0.88	1.16	0.86	1.19	APR	
	MAR	1.16	0.88	1.15	0.88	0.89	1.15	0.86	1.19	MAY	
	APR	1.17	0.88	1.15	0.88	0.89	1.15	0.88	1.15	JUN	
	MAY			1.15	0.88	0.89	1.15	0.88	1.15	JUL	
	SEP			1.17	0.87	0.89	1.15	0.89	1.15	AUG	
	OCT	1.18	0.87	1.15	0.88	0.89	1.15	0.88	1.16	SEP	
	NOV	1.16	0.88	1.15	0.89	0.88	1.15	0.86	1.20	OCT	
	DEC	1.15	0.88	1.15	0.89	0.00	0.00	0.00	0.00	NOV	

Table D.5: *Adimensional fractiles for Mi case due to clay block properties perturbations*

		Heat losses				Heat gains					
		Palermo		Trento		Palermo		Trento			
		$af_{1\%}$	$af_{99\%}$	$af_{1\%}$	$af_{99\%}$	$af_{1\%}$	$af_{99\%}$	$af_{1\%}$	$af_{99\%}$		
Specific Mass	JAN	1.01	0.99	1.00	1.00	0.81	1.23	0.85	1.22	MAR	Specific Mass
	FEB	1.01	0.99	1.00	1.00	0.97	1.03	0.88	1.15	APR	
	MAR	1.02	0.98	1.01	1.00	1.00	1.00	0.88	1.15	MAY	
	APR	1.06	0.95	1.01	0.99	1.00	1.00	1.00	1.00	JUN	
	MAY			1.01	1.00	1.00	1.00	1.00	1.00	JUL	
	SEP			1.08	0.93	1.00	1.00	1.00	1.00	AUG	
	OCT	1.09	0.93	1.01	0.99	1.00	1.00	0.98	1.02	SEP	
	NOV	1.05	0.96	1.00	1.00	1.00	1.00	0.85	1.19	OCT	
	DEC	1.02	0.98	1.00	1.00	0.00	0.00	0.00	0.00	NOV	
Specific Heat	JAN	1.02	0.99	1.00	1.00	0.71	1.51	0.79	1.57	MAR	Specific Heat
	FEB	1.02	0.99	1.00	1.00	0.96	1.07	0.81	1.34	APR	
	MAR	1.05	0.97	1.02	0.99	1.00	1.00	0.82	1.32	MAY	
	APR	1.13	0.93	1.03	0.99	1.00	1.00	1.00	1.01	JUN	
	MAY			1.01	0.99	1.00	1.00	1.00	1.01	JUL	
	SEP			1.18	0.89	1.00	1.00	1.00	1.00	AUG	
	OCT	1.20	0.90	1.02	0.99	1.00	1.00	0.97	1.05	SEP	
	NOV	1.12	0.95	1.00	1.00	1.00	1.01	0.76	1.40	OCT	
	DEC	1.04	0.98	1.00	1.00	0.00	0.00	0.00	0.00	NOV	
Conductivity	JAN	1.10	0.85	1.08	0.86	0.53	1.48	0.63	1.49	MAR	Conductivity
	FEB	1.10	0.85	1.08	0.86	0.82	1.14	0.65	1.34	APR	
	MAR	1.12	0.83	1.09	0.86	0.86	1.08	0.65	1.33	MAY	
	APR	1.18	0.78	1.10	0.84	0.86	1.08	0.86	1.09	JUN	
	MAY			1.09	0.85	0.86	1.08	0.86	1.09	JUL	
	SEP			1.22	0.74	0.86	1.08	0.86	1.08	AUG	
	OCT	1.24	0.77	1.10	0.85	0.86	1.08	0.83	1.12	SEP	
	NOV	1.17	0.80	1.08	0.86	0.86	1.09	0.59	1.40	OCT	
	DEC	1.12	0.83	1.08	0.86	0.00	0.00	0.00	0.00	NOV	
Thickness	JAN	1.02	0.98	1.02	0.98	0.85	1.15	0.88	1.13	MAR	Thickness
	FEB	1.02	0.98	1.02	0.98	0.97	1.03	0.90	1.10	APR	
	MAR	1.03	0.97	1.02	0.98	0.98	1.02	0.90	1.10	MAY	
	APR	1.05	0.95	1.02	0.98	0.98	1.02	0.98	1.02	JUN	
	MAY			1.02	0.98	0.98	1.02	0.98	1.02	JUL	
	SEP			1.06	0.94	0.98	1.02	0.98	1.02	AUG	
	OCT	1.07	0.93	1.02	0.98	0.98	1.02	0.97	1.03	SEP	
	NOV	1.05	0.96	1.02	0.98	0.98	1.02	0.88	1.12	OCT	
	DEC	1.03	0.97	1.02	0.98	0.00	0.00	0.00	0.00	NOV	

Table D.6: *Adimensional fractiles for Mi case due to insulation properties perturbations*

		Heat losses				Heat gains					
		Palermo		Trento		Palermo		Trento			
		$af_{1\%}$	$af_{99\%}$	$af_{1\%}$	$af_{99\%}$	$af_{1\%}$	$af_{99\%}$	$af_{1\%}$	$af_{99\%}$		
	JAN	1.00	1.00	1.00	1.00	0.98	0.99	0.99	0.99	MAR	
	FEB	1.00	1.00	1.00	1.00	1.00	1.00	0.99	0.99	APR	
	MAR	1.00	1.00	1.00	1.00	1.00	1.00	0.99	0.99	MAY	

(Continued on next page)

Specific Mass

Specific Mass

(Continued from previous page)

	APR	1.00	0.99	1.00	1.00	1.00	1.00	1.00	1.00	JUN	
	MAY			1.00	1.00	1.00	1.00	1.00	1.00	JUL	
	SEP			0.99	0.99	1.00	1.00	1.00	1.00	AUG	
	OCT	1.00	0.99	1.00	1.00	1.00	1.00	1.00	1.00	SEP	
	NOV	1.00	1.00	1.00	1.00	1.00	1.00	0.98	0.99	OCT	
	DEC	1.00	1.00	1.00	1.00	0.00	0.00	0.00	0.00	NOV	
Specific Heat	JAN	1.00	1.00	1.00	1.00	0.98	0.99	0.98	0.99	MAR	Specific Heat
	FEB	1.00	1.00	1.00	1.00	1.00	1.00	0.99	0.99	APR	
	MAR	1.00	1.00	1.00	1.00	1.00	1.00	0.99	0.99	MAY	
	APR	1.00	0.99	1.00	1.00	1.00	1.00	1.00	1.00	JUN	
	MAY			1.00	1.00	1.00	1.00	1.00	1.00	JUL	
	SEP			1.00	1.00	1.00	1.00	1.00	1.00	AUG	
	OCT	1.00	0.99	1.00	1.00	1.00	1.00	1.00	1.00	SEP	
	NOV	1.00	1.00	1.00	1.00	1.00	1.00	0.98	0.99	OCT	
DEC	1.00	1.00	1.00	1.00	0.00	0.00	0.00	0.00	NOV		
Conductivity	JAN	1.09	0.91	1.09	0.91	0.86	1.10	0.87	1.10	MAR	Conductivity
	FEB	1.09	0.91	1.09	0.91	0.90	1.09	0.88	1.10	APR	
	MAR	1.09	0.90	1.09	0.91	0.91	1.09	0.88	1.10	MAY	
	APR	1.09	0.90	1.09	0.90	0.91	1.09	0.91	1.09	JUN	
	MAY			1.09	0.91	0.91	1.09	0.91	1.09	JUL	
	SEP			1.09	0.89	0.91	1.09	0.91	1.09	AUG	
	OCT	1.09	0.89	1.09	0.90	0.91	1.09	0.90	1.09	SEP	
	NOV	1.09	0.90	1.09	0.91	0.91	1.09	0.87	1.10	OCT	
DEC	1.09	0.90	1.09	0.91	0.00	0.00	0.00	0.00	NOV		
Thickness	JAN	1.15	0.88	1.15	0.89	0.84	1.19	0.84	1.19	MAR	Thickness
	FEB	1.15	0.88	1.15	0.89	0.88	1.16	0.85	1.18	APR	
	MAR	1.15	0.88	1.15	0.88	0.89	1.15	0.85	1.18	MAY	
	APR	1.16	0.87	1.15	0.88	0.89	1.15	0.88	1.15	JUN	
	MAY			1.15	0.88	0.89	1.15	0.88	1.15	JUL	
	SEP			1.17	0.87	0.89	1.15	0.89	1.15	AUG	
	OCT	1.17	0.86	1.15	0.88	0.89	1.15	0.88	1.15	SEP	
	NOV	1.16	0.87	1.15	0.89	0.88	1.15	0.85	1.19	OCT	
DEC	1.15	0.88	1.15	0.89	0.00	0.00	0.00	0.00	NOV		

Bibliography

- [1] UNI 10349. Riscaldamento e raffrescamento degli edifici. dati climatici. Technical standard, UNI Ente Nazionale Italiano di Unificazione, April 1994.
- [2] EN ISO 10456:2008. Building materials and products hygrothermal properties - tabulated design values and procedures for determining declared and design thermal values. Technical standard, CEN, European Committee for Standardization, December 2007.
- [3] EN ISO 13790:2008. Energy performance of buildings - calculation of energy use for space heating and cooling. Technical standard, CEN, European Committee for Standardization, March 2008.
- [4] ANSI/ASHRAE 140-2007. Standard method of test for the evaluation of building energy analysis computer programs. Technical standard, ASHRAE, American Society of Heating, Refrigerating and Air-Conditioning Engineers, April 2007.
- [5] EN ISO 15498:2008. Precast concrete products - wood-chip concrete shuttering blocks -product properties and performance. Technical standard, CEN, European Committee for Standardization, April 2008.
- [6] EN ISO 15927-4: 2005. Hygrothermal performance of buildings - calculation and presentation of climatic data - part 4: Hourly data for assessing the annual energy use for heating and cooling, international organization for standardization, switzerland. Technical standard, ISO - International Organization for Standardization, July 2005.
- [7] EN 771-1:2011. Specification for masonry units - part 1: Clay masonry units. Technical standard, CEN, European Committee for Standardization, June 2011.
- [8] ASHRAE 90.1. Energy standard for buildings except low rise residential

- buildings. Technical report, ASHRAE - American Society of Heating, Refrigerating, and Air-Conditioning Engineers, Atlanta, Georgia, 2007.
- [9] ISO 9869:1994. Thermal insulation - building elements - in situ measurements of thermal resistance and thermal transmittance. Technical standard, ISO, International Organization for Standardization, August 1994.
- [10] R. Albatici and F. Passerini. Bioclimatic design of buildings considering heating requirements in italian climatic conditions. a simplified approach. *Building and Environment*, 46(8):1624 – 1631, 2011. ISSN 0360-1323. doi: 10.1016/j.buildenv.2011.01.028. URL <http://www.sciencedirect.com/science/article/pii/S036013231100045X>.
- [11] F. Arpino, M. Dell’Isola, V. Fernicola, G. Ficco, and L. Iacomini. Riferibilità metrologica nella misura di trasmittanza termica mediante termoflussimetri. In *65th Congresso Nazionale ATI*, pages 13–17, Domus de Maria (Cagliari), 2010. Eurografica srl.
- [12] ASHRAE. Weather year for energy calculations. Technical report, ASHRAE - American Society of Heating, Refrigerating, and Air-Conditioning Engineers, Atlanta, Georgia, 1985.
- [13] ASHRAE. *2009 ASHRAE Handbook Fundamentals*. 2009.
- [14] V. Badescu. Comment on the statistical indicators used to evaluate the accuracy of solar radiation computing models. *Solar Energy*, 40(5):479 – 480, 1988. ISSN 0038-092X. doi: 10.1016/0038-092X(88)90104-1. URL <http://www.sciencedirect.com/science/article/pii/0038092X88901041>.
- [15] P. Baggio, V. Corrado, G. Murano, and G. Riva. Definizione degli anni tipo climatici delle province del Nord Italia. *La Termotecnica*, 61(11): 46–48, 2010.
- [16] G. Beccali, M. Cellura, and V. Lo Brano. A database of Z-transform coefficients For Mediterranean building typologies. In *Building Simulation*, pages 395–402, 2001.
- [17] G. Beccali, M. Cellura, V. Lo Brano, and A. Orioli. Is the transfer function method reliable in a European building context? A theoretical analysis and a case study in the south of Italy. *Applied Thermal Engineering*, 25(1):341–357, 2005. doi: 10.1016/j.applthermaleng.2004.06.010.

- [18] J. Bilbao, M. Argimiro, J. Franco, and Ayuso A. Test reference year generation and evaluation methods in the continental mediterranean area. *Journal of Applied Meteorology*, 43:390–400, 2003.
- [19] J. Boland, L. Scott, and M. Luther. Modelling the diffuse fraction of global solar radiation on a horizontal surface. *Environmetrics*, 12(2): 103–116, 2001. ISSN 1099-095X. doi: 10.1002/1099-095X(200103)12: 2<103::AID-ENV447>3.0.CO;2-2. URL [http://dx.doi.org/10.1002/1099-095X\(200103\)12:2<103::AID-ENV447>3.0.CO;2-2](http://dx.doi.org/10.1002/1099-095X(200103)12:2<103::AID-ENV447>3.0.CO;2-2).
- [20] J.W. Bugler. The determination of hourly insolation on an inclined plane using a diffuse irradiance model based on hourly measured global horizontal insolation. *Solar Energy*, 19(5):477 – 491, 1977. ISSN 0038-092X. doi: 10.1016/0038-092X(77)90103-7. URL <http://www.sciencedirect.com/science/article/pii/0038092X77901037>.
- [21] H.S. Carslaw and J.C. Jaeger. *Conduction of heat in solids*. Oxford University Press, 1986. ISBN 978-0198533689.
- [22] J. Chandrasekaran and S. Kumar. Hourly diffuse fraction correlation at a tropical location. *Solar Energy*, 53(6):505 – 510, 1994. ISSN 0038-092X. doi: 10.1016/0038-092X(94)90130-T. URL <http://www.sciencedirect.com/science/article/pii/0038092X9490130T>.
- [23] Y. Chen and S. Wang. Frequency-domain regression method for estimating CTF models of building multilayer constructions. *Applied Mathematical Modelling*, 25:579–592, 2001.
- [24] Y. Chen and S. Wang. A new procedure for calculating periodic response factors based on frequency domain regression method. *International Journal of Thermal Sciences*, 44:382–392, 2005. doi: 10.1016/j.ijthermalsci.2004.10.005.
- [25] Y. Chen and S. Wang. Erratum to "A new procedure for calculating periodic response factors based on frequency domain regression method". *International Journal of Thermal Sciences*, 44:298195–298195, 2005. doi: 10.1016/j.ijthermalsci.2005.08.001.
- [26] Y. Chen, S. Wang, and Z. Zuo. An approach to calculate transient heat flow through multilayer spherical structures ? *International Journal of Thermal Sciences*, 42:805–812, 2003. doi: 10.1016/S1290-0729(03)00054-1.

- [27] M. A. C. Chendo and A. L. Maduekwe. Hourly global and diffuse radiation of Lagos, Nigeria -correlation with some atmospheric parameters. *Solar Energy*, 52(3):247–251, 1994.
- [28] W. Cheng, R. Ma, K. Xie, N. Liu, and Y. Huang. Simultaneous measurement of thermal properties by thermal probe using stochastic approximation method. *Applied Energy*, 88(5):1834–1840, May 2011. ISSN 03062619. doi: 10.1016/j.apenergy.2010.12.008. URL <http://linkinghub.elsevier.com/retrieve/pii/S0306261910005155>.
- [29] S. Chirarattananon, P. Rukkwansuk, P. Chaiwiwatworakul, and P. Pakdeepol. Evaluation of vertical illuminance and irradiance models against data from north Bangkok. *Building and Environment*, 42(11):3894–3904, November 2007. ISSN 03601323. doi: 10.1016/j.buildenv.2006.11.012. URL <http://linkinghub.elsevier.com/retrieve/pii/S0360132306004173>.
- [30] CISMA. "anno tipo" climatico per le province della lombardia version 2. Technical report, Comitato Termotecnico Italiano (CTI), 2010. URL <http://shop.cti2000.it/>.
- [31] V. Corrado and H.E. Mechri. Uncertainty and sensitivity analysis for building energy rating. *Journal of building physics*, 33(2):125 – 156, 2009.
- [32] D. Costola, B. Blocken, and J.L.M. Hensen. Overview of pressure coefficient data in building energy simulation and airflow network programs. *Building and Environment*, 44(10):2027–2036, October 2009. ISSN 03601323. doi: 10.1016/j.buildenv.2009.02.006. URL <http://linkinghub.elsevier.com/retrieve/pii/S0360132309000444>.
- [33] J.A. Davies and D.C. Mc Kay. Estimating solar irradiance and components. *Solar Energy*, 29(1):55 – 64, 1982. ISSN 0038-092X. doi: 10.1016/0038-092X(82)90280-8. URL <http://www.sciencedirect.com/science/article/pii/0038092X82902808>.
- [34] M. G. Davies. Wall transient heat flow using time domain analysis. *Building and Environments*, 32(5):427–446, 1997.
- [35] M. G. Davies. Calculation of wall conduction transfer coefficients by regression in the frequency domain. *Building and Environment*, 39:589 – 590, 2004. doi: 10.1016/j.buildenv.2003.10.001.
- [36] M.G. Davies. *Building Heat Transfer*. John Wiley & Sons Ltd, 2004. ISBN 0 470 84731 X.

- [37] A. de Miguel, J. Bilbao, and M Diez-Mediavilla. Solar radiation incident on tilted surfaces in Burgos, Spain: isotropic models. *Science*, 36(10): 945–951, 1995.
- [38] A. de Miguel, J. Bilbao, R. Aguiar, H.D. Kambezidis, and E. Negro. Diffuse solar irradiation model evaluation in the North Mediterranean Belt area. *Solar Energy*, 70(2):143–153, 2001. ISSN 0038092X. doi: 10.1016/S0038-092X(00)00135-3. URL <http://linkinghub.elsevier.com/retrieve/pii/S0038092X00001353>.
- [39] S. de Wit and G. Augenbroe. Analysis of uncertainty in building design evaluations and its implications. *Energy and Buildings*, 34(9):951–958, October 2002. ISSN 03787788. doi: 10.1016/S0378-7788(02)00070-1. URL <http://linkinghub.elsevier.com/retrieve/pii/S0378778802000701>.
- [40] F. Domínguez-Muñoz, B. Anderson, J. M. Cejudo-López, and A. Carrillo-Andrés. Uncertainty in the thermal conductivity of insulation materials. *Energy and Buildings*, 42(11):2159–2168, November 2010. ISSN 03787788. doi: 10.1016/j.enbuild.2010.07.006. URL <http://linkinghub.elsevier.com/retrieve/pii/S0378778810002227>.
- [41] DPR412/93. Decree of the president of the italian republic: Regolamento recante norme per la progettazione, l’installazione, l’esercizio e la manutenzione degli impianti termici degli edifici ai fini del contenimento dei consumi di energia, in attuazione dell’art. 4, comma 4, della legge 9 gennaio 1991, n. 10. Technical report, Annex A - Heating Degree Days Table, 1993.
- [42] R. Dubayah and P.M. Rich. Topographic Solar Radiation Models for GIS. *International Journal of Geographical Information System*, 9(4):405–419, 1995.
- [43] ENEA. Atlante italiano della radiazione solare. <http://www.solaritaly.enea.it>, 2006.
- [44] D. G. Erbs, S. A. Klein, and J. A. Duffie. Estimation of the diffuse radiation fraction for hourly, daily and monthly-average global radiation. *Solar Energy*, 28(4):293–302, 1982. ISSN 0038092X. doi: 10.1016/0038-092X(82)90302-4. URL <http://linkinghub.elsevier.com/retrieve/pii/0038092X82903024>.

- [45] erratum to UNI 10349. Riscaldamento e raffrescamento degli edifici. dati climatici. Internal Document 41/9, Servizio Energia - Provincia Autonoma di Trento, March 1995.
- [46] E. G. Evseev and A. I. Kudish. An assessment of a revised Olmo et al. model to predict solar global radiation on a tilted surface at Beer Sheva, Israel. *Renewable Energy*, 34(1):112–119, January 2009. ISSN 09601481. doi: 10.1016/j.renene.2008.04.012. URL <http://linkinghub.elsevier.com/retrieve/pii/S0960148108001432>.
- [47] M. H. Fatemi. Prediction of thermal conductivity detection response factors using an artificial neural network. *Journal of Chromatography A*, 897: 227–235, 2000.
- [48] R. Festa and C. F. Ratto. Proposal of a numerical procedure to select reference years. *Solar Energy*, 50(1):9–17, 1993.
- [49] A. Gasparella and G. Pernigotto. Analisi comparativa dei codici di simulazione dinamica degli edifici: un confronto tra TRNSYS e EnergyPlus. In *65th Congresso Nazionale ATI*, pages 1–9, Domus de Maria (CA), Italy, 2010. Barcello editor.
- [50] C. Giaconia and A. Orioli. On the reliability of ASHRAE conduction transfer function coefficients of walls. *Applied Thermal Engineering*, 20: 4721–3, 2000.
- [51] L. Giovannini, D. Zardi, and M. De Franceschi. Analysis of the Urban Thermal Fingerprint of the City of Trento in the Alps. *Journal of Applied Meteorology and Climatology*, 50:1145–1162, 2011. doi: 10.1175/2010JAMC2613.1.
- [52] L. Guan. Preparation of future weather data to study the impact of climate change on buildings. *Building and Environment*, 44(4):793–800, April 2009. ISSN 03601323. doi: 10.1016/j.buildenv.2008.05.021.
- [53] L. Guan, J. Yang, and J. Bell. Cross-correlations between weather variables in Australia. *Building and Environment*, 3:1054–1070, March 2007. ISSN 03601323. doi: 10.1016/j.buildenv.2006.01.010.
- [54] C.A. Gueymard. An anisotropic solar irradiance model for tilted surfaces and its comparison with selected engineering algorithms. *Solar Energy*, 38(5):367 – 386, 1987. ISSN 0038-092X. doi: 10.1016/0038-092X(87)90009-0. URL <http://www.sciencedirect.com/science/article/pii/S0038092X87900090>.

- [55] C.A. Gueymard. Direct and indirect uncertainties in the prediction of tilted irradiance for solar engineering applications. *Solar Energy*, 83(3):432–444, March 2009. ISSN 0038092X. doi: 10.1016/j.solener.2008.11.004. URL <http://linkinghub.elsevier.com/retrieve/pii/S0038092X08002983>.
- [56] C.A. Gueymard and S.M. Wilcox. Assessment of spatial and temporal variability in the US solar resource from radiometric measurements and predictions from models using ground-based or satellite data. *Solar Energy*, 85(5):1068–1084, May 2011. ISSN 0038092X. doi: 10.1016/j.solener.2011.02.030. URL <http://linkinghub.elsevier.com/retrieve/pii/S0038092X11000855>.
- [57] C.A. Gueymard, D. Myers, and K. Emery. Proposed reference irradiance spectra for solar energy systems testing. *Solar Energy*, 73(6):443 – 467, 2002. ISSN 0038-092X. doi: 10.1016/S0038-092X(03)00005-7. URL <http://www.sciencedirect.com/science/article/pii/S0038092X03000057>.
- [58] J. Haarhoff and E. Mathews. A Monte Carlo method for thermal building simulation. *Energy and Buildings*, 38(12):1395–1399, December 2006. ISSN 03787788. doi: 10.1016/j.enbuild.2006.01.009. URL <http://linkinghub.elsevier.com/retrieve/pii/S0378778806000806>.
- [59] I. Hall, R. Prairie, H. Anferon, and E. Boes. Generation of atypical meteorological year for 26 solmet stations. Technical Report SAND -78-1601, Sandia Laboratories, Albuquerque, New Mexico, 1978.
- [60] L.G. Harriman, Colliver D.G., and Quinn H. K. New weather data for energy calculations. *ASHRAE Transactions*, 41(3):31–38, 1999.
- [61] M.N.A. Hawlader. Solar diffuse, global and extraterrestrial solar radiation for singapore. *International Journal of Ambient Energy*, 5(1):31 – 37, 1984.
- [62] J.E. Hay and J.A. Davies. Calculation of the solar radiation incident on an inclined surface. *Proc. First Canadian Solar Radiation Data Workshop*, pages 59 – 65, 1980.
- [63] D.C. Hittle. Building loads analysis and system thermodynamics program (blast) users’ manual version 2. Technical Report E-153, U.S. Army Construction Engineering Research Laboratory, Champaign, Illinois, 1979.

- [64] D.C. Hittle and R. Bishop. An improved root-finding procedure for use in calculating transient heat flow through multilayered slabs. *International Journal of Heat and Mass Transfer*, 26(11):1685 – 1693, 1983. ISSN 0017-9310. doi: 10.1016/S0017-9310(83)80089-1. URL <http://www.sciencedirect.com/science/article/pii/S0017931083800891>.
- [65] C. Hopfe and J. Hensen. Uncertainty analysis in building performance simulation for design support. *Energy and Buildings*, 43(10):2798–2805, July 2011. ISSN 03787788. doi: 10.1016/j.enbuild.2011.06.034. URL <http://linkinghub.elsevier.com/retrieve/pii/S0378778811002830>.
- [66] C. Hopfe, C. Struck, and P. Kotek. Uncertainty analysis for building performance simulation- a comparison of four tools. In *IBPSA Building Simulation*, pages 1383–1388, Beijing (China), 2007.
- [67] H.C. Hottel and B.B. Woertz. Evaluation of flat-plate solar heat collector. *ASME Transactions*, 91(64), 1942.
- [68] S. Hyun, C. Park, and G. Augenbroe. Uncertainty and sensitivity analysis of natural ventilation in high-rise apartment buildings. In *IBPSA Building Simulation*, pages 1013–1020, Beijing (China), 2007.
- [69] C. Jacovides, F. Tymvios, V. Assimakopoulos, and N. Kaltsounides. Comparative study of various correlations in estimating hourly diffuse fraction of global solar radiation. *Renewable Energy*, 31(15):2492–2504, December 2006. ISSN 09601481. doi: 10.1016/j.renene.2005.11.009. URL <http://linkinghub.elsevier.com/retrieve/pii/S0960148105003538>.
- [70] Y. Jiang. State-space method for the calculation of air conditioning loads and the thermal behavior of the room. *ASHRAE Transactions*, 88(2): 122–138, 1982.
- [71] S. Karatasou, M. Santamouris, and V. Geros. Analysis of experimental data on diffuse solar radiation in Athens , Greece , for building applications. *International Journal of Sustainable Energy*, 23(1):37–41, 2003.
- [72] A.K. Katiyar, A. Kumar, C.K. Pandey, V.K. Katiyar, and S.H. Abdi. Correlations for the estimation of monthly mean hourly diffuse solar radiation: a time dependent approach. *International Journal of Energy and Environment*, 1(5):833–840, 2010.
- [73] E. Keeble. Availability of uk climatic data for use in simulation. BEPAC Technical Note 1, Building Research Establishment, October 1990.

- [74] T. M. Klucher. Evaluation of models to predict insolation on tilted surfaces, 1978.
- [75] W. Köppen. Die wärmezonen der erde, nach der dauer der heissen, gemäßigten und kalten zeit und nach der wirkung der wärme auf die organische welt betrachtet. 1884.
- [76] J.C. Lam and D.H.W. Li. Correlation between global solar radiation and its direct and diffuse components. *Building and Environment*, 31(6):527–535, November 1996. ISSN 03601323. doi: 10.1016/0360-1323(96)00026-1. URL <http://linkinghub.elsevier.com/retrieve/pii/0360132396000261>.
- [77] B.Y.H. Liu and R.C. Jordan. The interrelationship and characteristic distribution of direct, diffuse and total solar radiation. *Solar Energy*, 4(3):1 – 19, 1960. ISSN 0038-092X. doi: 10.1016/0038-092X(60)90062-1. URL <http://www.sciencedirect.com/science/article/pii/0038092X60900621>.
- [78] K. J. Lomas and H. Eppel. Sensitivity analysis techniques for building thermal simulation programs. *Energy and Buildings*, 19(1):21 – 44, 1992. ISSN 0378-7788. doi: 10.1016/0378-7788(92)90033-D. URL <http://www.sciencedirect.com/science/article/pii/037877889290033D>.
- [79] P. G. Loutzenhiser, H. Manz, C. Felsmann, P. A. Strachan, T. Frank, and G. Maxwell. Empirical validation of models to compute solar irradiance on inclined surfaces for building energy simulation. *Solar Energy*, 81:254–267, 2007. doi: 10.1016/j.solener.2006.03.009.
- [80] H. Lund. The reference year a set of climate data for environmental engineering. In *Second Symposium on the use of computers for environmental engineering*, pages 600–606, 1974.
- [81] H. Lund. The design reference year. In *Third IBPSA Conference*, pages 600–606, Nice - Francel, 1991.
- [82] H. Lund and S. Eidorff. Selection methods for a production of test reference year. Technical Report ES DK - 248-77, Technical University of Denmark, Copenhagen, Denmark, 1980.
- [83] C. C. Y. Ma and M. Iqbal. Statistical comparison of models for estimating solar radiation on inclined surfaces. *Solar Energy*, 31(3):313–317, 1983.

- [84] I.A. Macdonald. *Uncertainty in building simulation*. Ph.d. dissertation, University of Strathclyde, Glasgow UK, July 2002.
- [85] I.A. Macdonald. Comparison of sampling techniques on the performance of Monte-Carlo based sensitivity analysis. In *IBPSA Building Simulation*, pages 992–999, Glasgow (Scotland), 2009.
- [86] W. Marion and K. Urban. User’s manual for tmy2s (typical meteorological years). Technical Report NREL/SP-463-7668, NREL - National Renewable Energy Laboratory, Golden, Colorado, 1995.
- [87] MATLAB. *version 7.0.4 (R14)*. The MathWorks Inc., Natick, Massachusetts, 2005.
- [88] L. Mazarella. Dati climatici g. de giorgio. Technical standard, Politecnico di Milano, 1997.
- [89] H. E. Mechri and V. Corrado. Practical Applications of Uncertainty and Sensitivity Techniques in Building Energy Simulation. *Procedia - Social and Behavioral Sciences*, 2(6):7708–7709, 2010. ISSN 18770428. doi: 10.1016/j.sbspro.2010.05.190. URL <http://linkinghub.elsevier.com/retrieve/pii/S1877042810013315>.
- [90] H. E. Mechri, A. Capozzoli, and V. Corrado. USE of the ANOVA approach for sensitive building energy design. *Applied Energy*, 87(10): 3073–3083, October 2010. ISSN 03062619. doi: 10.1016/j.apenergy.2010.04.001. URL <http://linkinghub.elsevier.com/retrieve/pii/S030626191000108X>.
- [91] G.P. Mitalas and D.G. Stephenson. Room thermal response factors. *ASHRAE Transaction*, 73, 1967.
- [92] T. Muneer. Solar radiation models for Europe. *Building Services Engineering Research and Technology*, (11):153–163, November 1990.
- [93] T. Muneer. *Solar radiation and daylight models*. Oxford, 2nd edition, 2004. ISBN 0 7506 5974 2.
- [94] T. Muneer and S. Younes. The all-sky meteorological radiation model: proposed improvements. *Applied Energy*, 83(5):436–450, May 2006. ISSN 03062619. doi: 10.1016/j.apenergy.2005.04.008. URL <http://linkinghub.elsevier.com/retrieve/pii/S0306261905000589>.

- [95] T. Muneer, M. Hawas, and K. Sahili. Correlation between hourly diffuse and global radiation for New Delhi. *Energy Conversion and Management*, 24(4):265–267, 1984.
- [96] J.V. Nicholas and D.R. White. *Traceable temperatures*. John Wiley & Sons LTD, 2001. ISBN 0-471-49291-4.
- [97] A. Noorian, I. Moradi, and G. Kamali. Evaluation of 12 models to estimate hourly diffuse irradiation on inclined surfaces. *Renewable Energy*, 33(6):1406–1412, June 2008. ISSN 09601481. doi: 10.1016/j.renene.2007.06.027. URL <http://linkinghub.elsevier.com/retrieve/pii/S0960148107002509>.
- [98] G. Notton, C. Cristofari, M. Muselli, and P. Poggi. Calculation on an hourly basis of solar diffuse irradiations from global data for horizontal surfaces in Ajaccio. *Energy Conversion and Management*, 45(18-19):2849–2866, November 2004. ISSN 01968904. doi: 10.1016/j.enconman.2004.01.003. URL <http://linkinghub.elsevier.com/retrieve/pii/S0196890404000238>.
- [99] A. Oliveira, J.F; Escobedo, J.A. Machado, and J. Soares. Correlation models of diffuse solar-radiation applied to the city of São Paulo, Brazil. *Applied Energy*, 71(1):59–73, January 2002. ISSN 03062619. doi: 10.1016/S0306-2619(01)00040-X. URL <http://linkinghub.elsevier.com/retrieve/pii/S030626190100040X>.
- [100] J.F. Orgill and K.G.T. Hollands. Correlation equation for hourly diffuse radiation on a horizontal surface. *Solar Energy*, 19(4):357 – 359, 1977. ISSN 0038-092X. doi: 10.1016/0038-092X(77)90006-8. URL <http://www.sciencedirect.com/science/article/pii/0038092X77900068>.
- [101] Italian Parliament. Law n°373: Norme per il contenimento del consumo energetico per usi termici negli edifici. Technical report, 1976.
- [102] Italian Parliament. Law n°10: Norme per l’attuazione del piano energetico nazionale in materia di uso razionale dell’energia, di risparmio energetico e di sviluppo delle fonti rinnovabili di energia. Technical report, 1991.
- [103] Italian Parliament. Decree n°192/2005 modified and integrated by decree 311/2006: Attuazione della direttiva 2002/91/ce relativa al rendimento energetico nell’edilizia. Technical report, 2005.

- [104] R. Perez, R. Stewart, C. Abrogast, R. Seals, and J. Scott. An anisotropic hourly diffuse radiation model for sloping surfaces: description, performance, validation, site dependency evaluation. *Solar Energy*, 36(6):481–497, 1986.
- [105] R. Perez, P. Ineichen, R. Stewart, and D. Menicucci. A new simplified version of the Perez diffuse irradiance model for tilted surfaces. *Solar Energy*, 39(3):221.231, 1987.
- [106] R. Perez, P. Ineichen, and R. Seals. Modeling daylight availability and irradiance components from direct and global irradiance. *Solar Energy*, 44(5):271–289, 1990.
- [107] D. Pissimanis, G. Karras, V. Notaridou, and K. Gavra. The generation of a typical meteorological year for the city of athens. *Solar Energy*, 40: 405–411, 1988.
- [108] R. Posadillo and R. López Luque. Evaluation of the performance of three diffuse hourly irradiation models on tilted surfaces according to the utilizability concept. *Energy Conversion and Management*, 50(9): 2324–2330, September 2009. ISSN 01968904. doi: 10.1016/j.enconman.2009.05.014. URL <http://linkinghub.elsevier.com/retrieve/pii/S0196890409001885>.
- [109] A. Prada, G. Pernigotto, P. Baggio, and A. Gasparella. Summer load evaluation in the Italian climate: sensitivity of the loss utilization factor to the weather data. In *12th Conference of International Building Performance Simulation Association*, pages 2363–2369, Sydney, Australia, 2011. IBPSA Australia and AIRAH. URL http://www.bounceinteractive.com/bs2011/bs2011/pdf/P_1744.pdf.
- [110] A. Prada, G. Pernigotto, P. Baggio, and A. Gasparella. Summer load evaluation in the Italian climate: sensitivity of the energy performance to the weather data. In *66th Congresso Nazionale ATI*, pages 1–8, Cosenza, Italy, 2011. Barcello editor.
- [111] W. Press, S. Teukolsky, W. Vetterling, and B. Flannery. *Numerical Recipes 3rd edition: The art of scientific Computing*. Cambridge University Press, 2007.
- [112] X. Qian, Y. Chen, J. D. Spitler, and D. Fisher. Applicability of calculation methods for conduction transfer function of building constructions. *International Journal of Thermal Sciences*, 48(7):1441–1451, 2009.

- ISSN 1290-0729. doi: 10.1016/j.ijthermalsci.2008.11.006. URL <http://dx.doi.org/10.1016/j.ijthermalsci.2008.11.006>.
- [113] D. Reindl, A. Beckman, and J. A. Duffie. Evaluation of hourly tilted surface radiation models. *Solar Energy*, 45(1):9–17, 1990. ISSN 0038092X. doi: 10.1016/0038-092X(90)90061-G. URL <http://linkinghub.elsevier.com/retrieve/pii/0038092X9090061G>.
- [114] D. Reindl, A. Beckman, and J. A. Duffie. Diffuse fraction correlations. *Solar Energy*, 45(1):1–7, 1990. ISSN 0038092X. doi: 10.1016/0038-092X(90)90060-P. URL <http://linkinghub.elsevier.com/retrieve/pii/0038092X9090060P>.
- [115] J.E. Seem. *Modeling of heat transfer in buildings*. Ph.d. thesis, University of Wisconsin, Madison, Wisconsin, 1987.
- [116] I. Seng Iu. *Experimental validation of the radiant time series method for cooling load calculations*. Ph.d. dissertation, Oklahoma State University, December 2002.
- [117] A. Skartveit and J.A. Olseth. Modelling slope irradiance at high latitudes. *Solar Energy*, 36(4):333 – 344, 1986. ISSN 0038-092X. doi: 10.1016/0038-092X(86)90151-9. URL <http://www.sciencedirect.com/science/article/pii/0038092X86901519>.
- [118] A. Skartveit and J.A. Olseth. A model for the diffuse fraction of hourly global radiation. *Solar Energy*, 38(4):271–274, 1987. ISSN 0038092X. doi: 10.1016/0038-092X(87)90049-1. URL <http://linkinghub.elsevier.com/retrieve/pii/0038092X87900491>.
- [119] J. Soares, A. Oliveira, M. Boznar, P. Mlakar, J.F.; Escobedo, and J.A. Machado. Modeling hourly diffuse solar-radiation in the city of Sao Paulo using a neural-network technique. *Applied Energy*, 79(2):201–214, October 2004. ISSN 03062619. doi: 10.1016/j.apenergy.2003.11.004. URL <http://linkinghub.elsevier.com/retrieve/pii/S0306261903002381>.
- [120] J. Spencer. A comparison of methods for estimating hourly diffuse solar radiation from global solar radiation. *Solar Energy*, 29(1):19–32, 1982. ISSN 0038092X. doi: 10.1016/0038-092X(82)90277-8. URL <http://linkinghub.elsevier.com/retrieve/pii/0038092X82902778>.
- [121] D.G. Stephenson and G.P. Mitalas. Transfer function for a multi-layer slabs. *ASHRAE Transaction*, 77(ASHRAE Transaction):117–126, 1971.

- [122] T. L. Stoffel and M. D. Rymes. Production of the weather year for energy calculations version 2 (wyec2), data files. *ASHRAE Transactions*, 104: 487–497, 1998.
- [123] R.J. Stone. Improved statistical procedure for the evaluation of solar radiation estimation models. *Solar Energy*, 51(4):289 – 291, 1993. ISSN 0038-092X. doi: 10.1016/0038-092X(93)90124-7. URL <http://www.sciencedirect.com/science/article/pii/0038092X93901247>.
- [124] Y. Sun, Y. Hoe, H. Xie, M. Tan, J. Wu, and G.F. Augenbroe. Uncertainty quantification of microclimate variables in building energy simulation. In *12th Conference of International Building Performance Simulation Association*, pages 2363–2369, Sydney, Australia, 2011. IBPSA Australia and AIRAH. URL http://www.bounceinteractive.com/bs2011/bs2011/pdf/P_1744.pdf.
- [125] R.C. Temps and K.L. Coulson. Solar radiation incident upon slopes of different orientations. *Solar Energy*, 19(2):179 – 184, 1977. ISSN 0038-092X. doi: 10.1016/0038-092X(77)90056-1. URL <http://www.sciencedirect.com/science/article/pii/0038092X77900561>.
- [126] W. Tian and P. de Wilde. Uncertainty and sensitivity analysis of building performance using probabilistic climate projections: A UK case study. *Automation in Construction*, May 2011. ISSN 09265805. doi: 10.1016/j.autcon.2011.04.011. URL <http://linkinghub.elsevier.com/retrieve/pii/S0926580511000653>.
- [127] TRNSYS. *version 16 (2007)*. University of Wisconsin, Madison, Wisconsin, 2007.
- [128] Test Reference Year TRY. Tape reference manual, td-9706. Technical report, National Climatic Data Center, U.S. Department of Commerce., Asheville, North Carolina, 1976.
- [129] M. K. Urbikain and M. G. Davies. One-dimensional solutions to Fourier’s equation and measures of heat transmission through walls : The role of wall decay times. *Building and environment*, 43:1433–1445, 2008. doi: 10.1016/j.buildenv.2007.07.001.
- [130] H.A.L. Van Dijk and C.A.M. Arkesteijn. Windows and space heating requirements; parameter studies leading to a simplified calculation method. IEA, the Netherlands National Report on Activities within Step 5 TPD

- 712.003, TNO Institute of Applied Physics, Princetonlaan 6, NL-3584 CB Utrecht, December 1987.
- [131] S. Wang and Y. Chen. A novel and simple building load calculation model for building and system dynamic simulation. *Applied Thermal Engineering*, 21, 2001.
- [132] S. Wang and Y. Chen. A simple procedure for calculating thermal response factors and conduction transfer functions of multilayer walls. *Applied Thermal Engineering*, 22:333–338, 2002.
- [133] S. Wang and Y. Chen. Transient heat flow calculation for multilayer constructions using a frequency-domain regression method. *Building and Environment*, 38:45 – 61, 2003.
- [134] S. Wilcox and W. Marion. User’s manual for tmy3 data sets. Technical Report NREL/TP-581-43156, NREL - National Renewable Energy Laboratory, Golden, Colorado, 2008.
- [135] J. Xu, P. B. Luh, W. E. Blankson, R. Jerdonek, and K. Shaikh. An optimization-based approach for facility energy management with uncertainties. *HVAC&R research*, 11(April):215–237, 2005.
- [136] X. Xu and S. Wang. A simple time domain calculation method for transient heat transfer models. *Energy and Buildings*, 40:1682–1690, 2008. doi: 10.1016/j.enbuild.2008.02.029.
- [137] Y.F. Yildiz and Z. D. Arsan. Identification of the building parameters that influence heating and cooling energy loads for apartment buildings in hot-humid climates. *Energy*, 36(7):4287–4296, July 2011. ISSN 03605442. doi: 10.1016/j.energy.2011.04.013. URL <http://linkinghub.elsevier.com/retrieve/pii/S0360544211002623>.